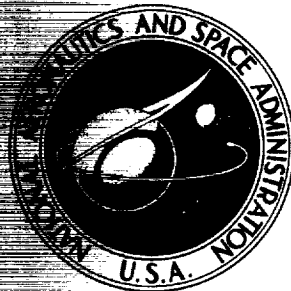NASA TECHNICAL
MEMORANDUM

NASA TM X-3106

NASA TM X-3106

CASE FILE COPY

REAL-TIME SIMULATION OF THE TF30-P-3 TURBOFAN ENGINE USING A HYBRID COMPUTER
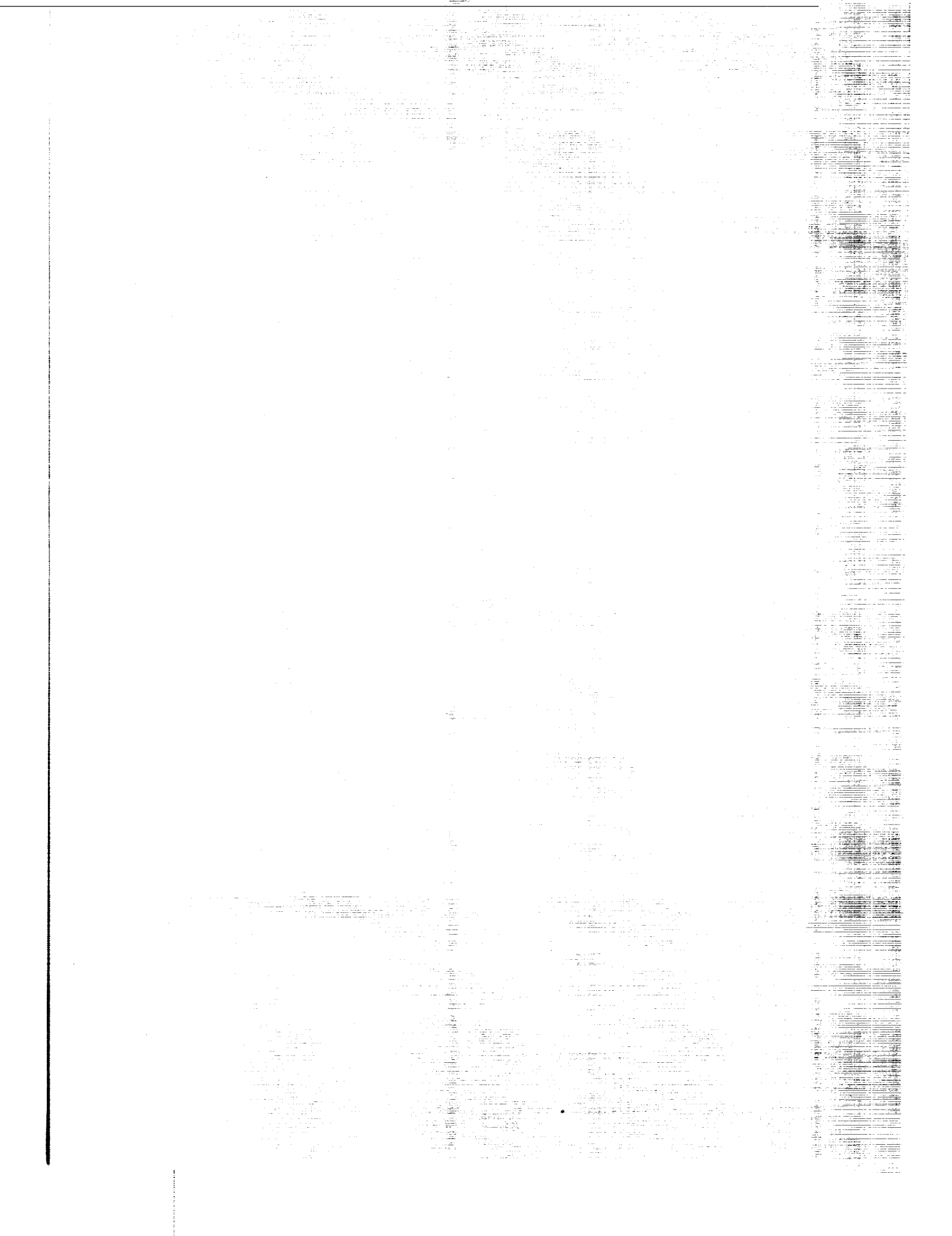
by John R. Szuch and William M. Bruton

Lewis Research Center
Cleveland, Ohio 44135

NATIONAL AERONAUTICS AND SPACE ADMINISTRATION • WASHINGTON, D. C. • OCTOBER 1974

1. Report No. NASA TM X-3106	2. Government Accession No.	3. Recipient's Catalog No.
4. Title and Subtitle REAL-TIME SIMULATION OF THE TF30-P-3 TURBOFAN ENGINE USING A HYBRID COMPUTER		5. Report Date OCTOBER 1974
		6. Performing Organization Code
7. Author(s) John R. Szuch and William M. Bruton		8. Performing Organization Report No. E-7904
		10. Work Unit No. 501-24
9. Performing Organization Name and Address Lewis Research Center National Aeronautics and Space Administration Cleveland, Ohio 44135		11. Contract or Grant No.
		13. Type of Report and Period Covered Technical Memorandum
12. Sponsoring Agency Name and Address National Aeronautics and Space Administration Washington, D.C. 20546		14. Sponsoring Agency Code

15. Supplementary Notes

16. Abstract

A real-time, hybrid-computer simulation of the TF30-P-3 turbofan engine has been developed. The simulation is primarily analog in nature but uses the digital portion of the hybrid computer to perform bivariate function generation associated with the performance of the engine's rotating components. FORTRAN listings and analog patching diagrams are provided in the report. The hybrid simulation was controlled by a digital computer programmed to simulate the engine's standard hydromechanical control. Both steady-state and dynamic data obtained from the digitally controlled engine simulation are presented. Hybrid simulation data are compared with data obtained from a digital simulation provided by the engine manufacturer. The comparisons indicate that the real-time hybrid simulation adequately matches the baseline digital simulation.

17. Key Words (Suggested by Author(s)) Simulation Real-time Hybrid computer Transient Turbofan Dynamics	18. Distribution Statement Unclassified - unlimited Category 28		
19. Security Classif. (of this report) Unclassified	20. Security Classif. (of this page) Unclassified	21. No. of Pages 103	22. Price* $4.50

* For sale by the National Technical Information Service, Springfield, Virginia 22151

CONTENTS

REAL-TIME SIMULATION OF THE TF30-P-3 TURBOFAN ENGINE

USING A HYBRID COMPUTER

by John R. Szuch and William M. Bruton

Lewis Research Center

SUMMARY

This report describes the development of a real-time hybrid-computer simulation of the Pratt & Whitney TF30-P-3 augmented turbofan engine. The simulation is intended to support research programs involving this engine.

The simulation is primarily analog in nature but does use the digital portion of the hybrid computer to perform bivariate function generation associated with modeling the performance of the engine's rotating components. The digital portion of the engine simulation requires about 10 000 words of core storage. The digital sampling interval is about 4.6 milliseconds and does allow real-time simulation of engine dynamics. Approximately 185 amplifiers and 85 multipliers are required to perform the analog calculations. FORTRAN listings and analog patching diagrams are provided in appendixes to this report.

The hybrid simulation was controlled by a general-purpose digital computer programmed to simulate the standard TF30-P-3 hydromechanical fuel and variable geometry controls. Both steady-state and dynamic data obtained from the digitally controlled engine simulation are presented. Hybrid simulation data are compared with data obtained from a digital simulation provided by the engine manufacturer. These comparisons indicate that the real-time hybrid simulation does adequately match the baseline digital simulation. The real-time simulation should, therefore, provide a valuable analytical tool for research studies involving the TF30-P-3 turbofan engine.

INTRODUCTION

Aircraft propulsion systems have become steadily more complex. With engines and inlets operating at higher levels of performance, propulsion system controls have also necessarily increased in complexity. In order to obtain maximum performance for all

flight conditions, digital control systems (ref. 1) are being considered for inlets and engines. The use of a digital computer, with its logic and memory capabilities, would provide maximum flexibility and versatility to propulsion control systems.

The development of controls for aircraft propulsion systems is facilitated by an ability to predict engine performance accurately over a wide range of operation. Computer programs for analyzing steady-state and dynamic performance of turbojet and turbofan engines have previously been developed (refs. 2 to 8). Some of these engine simulations have been expanded to include the simulation of engine controls.

In the development of digital controls for turbojet and turbofan engines, both computer simulations and experimental testing will be required to evaluate new control laws. The experimental tests can be more efficiently planned and executed if the digital control software can be tested and "debugged" by using the engine simulation. This imposes another requirement on the engine simulation. That is, the simulation must operate in "real time." The real-time requirement exists because timing and sequencing are extremely important in the development of digital control software. Also, the effects of digital sampling intervals on engine performance (ref. 9) can be predicted by using a real-time simulation.

Turbojet and turbofan engines can be simulated by using either analog (ref. 6), digital (refs. 2 to 5), or hybrid (refs. 7 and 8) computers. The real-time simulation requirement, however, limits the possible choices to the analog and hybrid computers. A purely analog simulation of a turbofan engine requires a large amount of computing equipment. Much of this equipment is needed to perform the bivariate function generation associated with modeling the engine's fan, compressor (or compressors), and turbine (or turbines). Unfortunately, analog function generation is often plagued by a lack of precision and repeatability. The precision and memory capabilities of the hybrid's own digital computer can be used to perform the required function generation, thus reducing the required amount of analog computing equipment.

This report describes the development of a real-time hybrid-computer simulation of the Pratt & Whitney TF30-P-3 augmented turbofan engine. The simulation is intended to support research programs involving this engine. The hybrid simulation was patterned after the engine manufacturer's digital simulation of the TF30-P-3 engine and was implemented on the Lewis Research Center's Electronic Associates, Inc., (EAI) Model 690 Hybrid Computing System and two EAI Model 231-R Analog Computers.

The TF30-P-3 hybrid-computer simulation was controlled by a general-purpose digital control computer (ref. 10) programmed to simulate the standard TF30-P-3 hydromechanical fuel and variable geometry controls. This digital control system was developed for on-line control of airbreathing engines during experimental testing.

Both steady-state and dynamic data obtained from the digitally controlled simulation are presented for a full range of power settings. Data were obtained at both sea level and simulated altitude conditions. Hybrid simulation data are compared with data ob-

2

tained from the engine manufacturer's digital simulation. FORTRAN listing and analog patching diagrams are provided. This information should prove useful in the development of similar engine simulations.

ENGINE DESCRIPTION

The Pratt & Whitney TF30-P-3 engine (fig. 1) is an axial, mixed-flow, augmented, twin-spool, low-bypass-ratio turbofan. A single inlet is used for both the fan airflow and the engine core airflow. Airflow leaving the fan is separated into two flow streams: one stream passing through the engine core, and the other stream passing through the annular fan duct. A nine-stage low-pressure compressor includes the core portion of the three-stage fan and is connected by a through-shaft to the three-stage low-pressure turbine. A seven-stage high-pressure compressor is connected by a hollow shaft to the single-stage high-pressure turbine. A seventh-stage compressor bleed system discharges air into the fan duct at flight Mach numbers above 1.75. A 12th-stage bleed automatically discharges air into the fan duct for compressor surge control. Cooling of high-pressure and low-pressure turbine blades is accomplished by using 16th-stage compressor bleed air.

The TF30-P-3 combustor is located between the discharge of the high-pressure compressor and the inlet of the high-pressure turbine. The combustor section consists of an annular diffuser and eight combustion chambers. Each combustion chamber contains four dual-orifice fuel spray nozzles. The main fuel control meters fuel to the combustor as a function of the power lever angle PLA, the high-pressure-compressor speed N_H, the fan inlet total pressure P_2 and temperature T_2, and the high-pressure-compressor discharge static pressure $P_{s,3}$. (All symbols are defined in appendix A.) In the combustor, airflow from the compressors reacts with the injected fuel, producing high-energy gas to run the turbines.

The engine core and fan duct flow streams combine in an augmentor and are discharged through a variable-area convergent nozzle. The augmentor consists of a diffuser section and a combustion chamber. The fuel is introduced into the combustion chamber through spray rings which are arranged into five separate zones. The augmentor fuel control meters fuel to the five zones as a function of PLA, N_H, T_2, $P_{s,3}$, the nozzle area A_N, and the turbine discharge total pressure P_6. The hydraulically actuated nozzle is adjusted to maintain a scheduled ratio of $P_{s,3}/P_6$ during augmentor operation.

ENGINE MODEL

The first step in developing an engine simulation is the formulation of an analytical model. This model, in equation form, represents the functional relations that exist between engine variables such as pressures, temperatures, and flows. In the case of the TF30-P-3 hybrid-computer simulation, the engine model should be capable of accurately predicting both steady-state and dynamic performance of the engine. Wide-range performance maps for the engine's rotating components should be included in the simulation for steady-state accuracy. Factors such as fluid momentum, mass and energy storage, and rotor inertias should be included to provide the desired transient capability.

Wherever possible, the TF30-P-3 model was patterned after the engine manufacturer's baseline digital simulation of the TF30-P-3 engine. The following sections describe the various elements which comprise the TF30-P-3 hybrid-computer simulation. Figure 2 illustrates the flow of calculations in the hybrid simulation and should help the reader in understanding the relations of the individual elements in the engine model.

Inlet

The real-time, hybrid-computer simulation of the TF30-P-3 engine does not include a dynamic simulation of an inlet. However, a steady-state representation of a typical inlet recovery is included in the simulation. The following equations are used in the hybrid simulation to calculate the total pressure P_2 and total temperature T_2 at the fan inlet from the values of P_0, T_0, and M_0 for a specified flight condition:

$$(T/T)_I = 1 + 0.2 M_0^2 \tag{1}$$

$$(P/P)_I = (T/T)_I^{3.5} \tag{2}$$

$$\eta_I = \begin{cases} 1.0 & \text{if } M_0 \le 1.0 \\ 1.0 - 0.075(M_0 - 1)^{1.35} & \text{if } M_0 > 1.0 \end{cases} \tag{3}$$

$$T_2 = (T/T)_I T_0 \tag{4}$$

$$P_2 = (P/P)_I P_0 \eta_I \tag{5}$$

4

There are basically two methods that can be used to model multistage fans and compressors. One method is to represent multistage fans and compressors with individual stage models (i. e., to compute pressure and temperature rises across each stage). This technique is referred to as stage stacking (ref. 6), but it requires a large computing facility when used in a total engine simulation. The method used in the real-time, hybrid-computer simulation involves the use of overall component performance maps. Interstage gas dynamics were not considered.

The TF30-P-3 three-stage fan was modeled with separate performance maps for the fan hub (core) and tip (duct) sections. Separate maps were required because of the radial pressure gradient which exists at the fan discharge at high rotor speeds.

Overall fan performance for the hub and tip sections is described by a pair of bivariate functions. In the baseline digital simulation, the fan tip pressure ratio and fan corrected speed were selected as independent variables and used to compute the total fan corrected airflow and the fan tip adiabatic efficiency. The same pair of independent variables were used to compute the fan hub pressure ratio and fan hub adiabatic efficiency.

To obtain the fan discharge temperature from efficiency requires additional calculations (including exponentiation). Because of the real-time requirement and equipment limitations, it was necessary to minimize the function generation and algebraic computations associated with modeling the fan (and compressors). Data obtained from the baseline simulation indicated that the fan hub and tip efficiency maps could be eliminated and the corresponding temperature ratios calculated as linear functions of the pressure ratios. In the TF30-P-3 hybrid-computer simulation, the fan model is described by the following equations:

$$(\dot{w}_c)_{FAN} = f_1\left[\left(\frac{P_{1.3}}{P_2}\right), \left(\frac{N_L}{\sqrt{\theta_2}}\right)\right] \tag{6}$$

$$\dot{w}_2 = \frac{(\dot{w}_c)_{FAN}\delta_2}{\sqrt{\theta_2}} \tag{7}$$

$$(P/P)_{FID} = f_2\left[\left(\frac{P_{1.3}}{P_2}\right), \left(\frac{N_L}{\sqrt{\theta_2}}\right)\right] \tag{8}$$

$$P_{2.1} = P_2(P/P)_{FID} \tag{9}$$

$$(T/T)_{FOD} = 0.7210 + 0.2796\left(\frac{P_{1.3}}{P_2}\right) \tag{10}$$

$$(\dot{w}T)_{1.3'} = \frac{c_{p,1.3'}}{c_{p,1.3}}(\dot{w}_2 - \dot{w}_{2.1})T_2(T/T)_{FOD} + \frac{c_{p,2.2}}{c_{p,1.3}}\dot{w}_{BL7}T_{2.2} + \frac{c_{p,3}}{c_{p,1.3}}\dot{w}_{BL12}T_3 \tag{11}$$

$$(T/T)_{FID} = 0.7588 + 0.2412(P/P)_{FID} \tag{12}$$

$$T_{2.1} = T_2(T/T)_{FID} \tag{13}$$

Figure 3 contains plots of the bivariate functions representing the performance of the fan (eqs. (6) and (8)). The pressure ratios, corrected speed, and corrected airflow have been normalized by their design values. Equation (11) indicates that the 7th- and 12th-stage bleeds are assumed to enter the fan duct immediately behind the fan. The primed station designation (e.g., 1.3') refers to the entrance to the mixing volume.

Low-Pressure Compressor

Overall performance data are used to describe the TF30-P-3 low-pressure compressor (4th to 9th stages). The compressor corrected airflow and corrected speed were selected as the independent variables and were used to compute the compressor pressure ratio. As in the case of the fan, compressor temperature ratio was calculated from a linear function of pressure ratio, thus eliminating the need for generating the bivariate efficiency function. In order to better match the temperature ratio - pressure ratio relation over the range of operation, two linear functions were used for different ranges of pressure ratio.

The modeling of the low-pressure compressor was complicated by the effect of the 7th-stage bleed on the overall compressor performance. Based on information obtained from the digital simulation, the effect of the bleed on performance was represented by a shift in the compressor corrected speed used in the pressure ratio determination. The effect of bleed on efficiency (and hence, temperature ratio) was neglected in both the baseline digital and real-time hybrid simulations.

In order to compute the low-pressure-compressor corrected airflow with the 7th-stage bleed open, the following procedure was used: First, the corrected speed shift for a fully open bleed was determined from a function of the actual corrected speed. Linear interpolation was then used to determine the speed shift for a partially open

bleed. Finally, the pressure ratio was calculated from a bivariate function of the corrected airflow and shifted corrected speed.

The 7th-stage bleed flow was assumed to be proportional to the low-pressure-compressor inlet airflow and was assumed to leave the core stream at the compressor exit (station 2.2).

The TF30-P-3 low-pressure-compressor model is described by the following equations in the hybrid-computer simulation:

$$(P/P)_{LC} = f_3\left[\left(\frac{\dot{w}_{2.1}\sqrt{\theta_{2.1}}}{\delta_{2.1}}\right), \left(N_c\right)_{LC,M}\right] \tag{14}$$

$$P_{2.2'} = P_{2.1}(P/P)_{LC} \tag{15}$$

$$\left(N_c\right)_{LC,M} = \frac{N_L}{\sqrt{\theta_{2.1}}} + XBL7\, f_9\left[\frac{N_L}{\sqrt{\theta_{2.1}}}\right] \tag{16}$$

$$(T/T)_{LC} = \begin{cases} 0.84 + 0.1989(P/P)_{LC} & \text{if } (P/P)_{LC} > 1.16 \\ \\ 0.515 + 0.4689(P/P)_{LC} & \text{if } (P/P)_{LC} \le 1.16 \end{cases} \tag{17}$$

$$T_{2.2'} = T_{2.1}(T/T)_{LC} \tag{18}$$

$$\dot{w}_{BL7} = 0.06\, XBL7\, \dot{w}_{2.1} \tag{19}$$

Figure 4(a) contains a plot of the bivariate function representing the low-pressure-compressor performance (eq. (14)) with the 7th-stage bleed closed. Figure 4(b) contains a plot of the corrected speed shift for the 7th-stage bleed fully open. The low-pressure-compressor map variables have been normalized by their design-point values.

High-Pressure Compressor

The mathematical treatment of the high-pressure compressor (10th to 16th stages) was quite similar to that of the low-pressure compressor. The basic difference was in the treatment of the 12th-stage bleed and its effect on the overall compressor performance. Based on information obtained from the digital simulation, the effect of the bleed

was represented by a shift in the compressor corrected flow used in the pressure ratio determination. The 12th-stage bleed flow was assumed to leave the core stream at the compressor exit (station 3). The cooling bleeds for the high- and low-pressure turbines are also extracted at the high-pressure-compressor exit. These bleed flows were assumed to be proportional to the high-pressure-compressor inlet airflow.

The high-pressure-compressor temperature ratio was calculated from a linear function of pressure ratio. Data from the digital simulation indicated that the slope and intercept of the function were sensitive to the bleed. Therefore, the slope and intercept were assumed to be linear functions of the percent of fully open bleed. The TF30-P-3 high-pressure-compressor model is described by the following equations in the hybrid simulation:

$$(P/P)_{HC} = f_4 \left[\left(\dot{w}_c \right)_{HC,M}, \frac{N_H}{\sqrt{\theta_{2.2}}} \right] \tag{20}$$

$$P_{3'} = P_{2.2}(P/P)_{HC} \tag{21}$$

$$\left(\dot{w}_c \right)_{HC,M} = \frac{\dot{w}_{2.2}\sqrt{\theta_{2.2}}}{\delta_{2.2}} - XBL12 \, f_{10}\left[\frac{N_H}{\sqrt{\theta_{2.2}}} \right] \tag{22}$$

$$(T/T)_{HC} = (1.0322 - 0.185 \, XBL12) + (0.12588 + 0.08032 \, XBL12)(P/P)_{HC} \tag{23}$$

$$T_{3'} = T_{2.2}(T/T)_{HC} \tag{24}$$

$$\dot{w}_{BL12} = 0.055 \, XBL12 \, \dot{w}_{2.2} \tag{25}$$

$$\dot{w}_{BLHT} = 0.04744 \, \dot{w}_{2.2} \tag{26}$$

$$\dot{w}_{BLLT} = 0.01985 \, \dot{w}_{2.2} \tag{27}$$

Figure 5(a) contains a plot of the normalized bivariate function representing the high-pressure-compressor performance (eq. (20)). This plot represents the closed-bleed performance of the high-pressure compressor (XBL12 = 0). Figure 5(b) contains a plot of the normalized corrected flow shift for the 12th-stage bleed fully open.

8

In the baseline digital simulation, overall turbine performance is represented by a set of bivariate functions. For each turbine, pressure ratio and a speed parameter $N/\sqrt{T}$ were used as independent variables to determine the turbine flow parameter $\dot{w}\sqrt{T}/P$ and enthalpy drop parameter $\Delta h/T$. Based on previous simulation experience, the digital program map outputs were normalized by the speed parameter for use in the hybrid simulation models. The TF30-P-3 turbine models are described by the following equations in the hybrid simulation:

$$(\text{fp})_{HT} = f_5\left[\left(\frac{P_{4.1}}{P_4}\right), \left(\frac{N_H}{\sqrt{T_4}}\right)\right] \tag{28}$$

$$\dot{w}_4 = \frac{(\text{fp})_{HT}P_4 N_H}{T_4} \tag{29}$$

$$(\text{hp})_{HT} = f_7\left[\left(\frac{P_{4.1}}{P_4}\right), \left(\frac{N_H}{\sqrt{T_4}}\right)\right] \tag{30}$$

$$(\Delta h)_{HT} = (\text{hp})_{HT}\sqrt{T_4}\,N_4 \tag{31}$$

$$(\dot{w}T)_{4.1'} = \dot{w}_4\left[\frac{c_{p,4}}{c_{p,4.1}}T_4 - \frac{(\Delta h)_{HT}}{c_{p,4.1}}\right] + \dot{w}_{BLHT}\left[\frac{c_{p,3}}{c_{p,4.1}}T_3 - \frac{K_{BWHT}(\Delta h)_{HT}}{c_{p,4.1}}\right] \tag{32}$$

$$(\text{fp})_{LT} = f_6\left[\left(\frac{P_5}{P_{4.1}}\right), \left(\frac{N_L}{\sqrt{T_{4.1}}}\right)\right] \tag{33}$$

$$\dot{w}_{4.1} = \frac{(\text{fp})_{LT}P_{4.1}N_L}{T_{4.1}} \tag{34}$$

$$(\text{hp})_{LT} = f_8\left[\left(\frac{P_5}{P_{4.1}}\right), \left(\frac{N_L}{\sqrt{T_{4.1}}}\right)\right] \tag{35}$$

$$(\Delta h)_{LT} = (hp)_{LT} \sqrt{T_{4.1}} \, N_L \qquad (36)$$

$$(\dot{w}T)_5 = \dot{w}_{4.1}\left[\frac{c_{p,4.1}}{c_{p,5}} T_{4.1} - \frac{(\Delta h)_{LT}}{c_{p,5}}\right] + \dot{w}_{BLLT}\left[\frac{c_{p,3}}{c_{p,5}} T_3 - \frac{K_{BWLT}(\Delta h)_{LT}}{c_{p,5}}\right] \qquad (37)$$

Figures 6 and 7 contain plots of the normalized bivariate functions representing the high-pressure- and low-pressure-turbine performance (eqs. (28), (30), (34), and (35)). The constants K_{BWHT} and K_{BWLT} appearing in equations (32) and (37) denote the fractions of the cooling bleed flows that are assumed to do turbine work.

Combustor, Augmentor, and Duct

The performance of the combustor can be represented by a total pressure loss due to friction and a temperature rise resulting from the heat release from the burned fuel. The ratio of the total pressure loss to the combustor inlet pressure P_3 was assumed to be proportional to the square of the compressible flow parameter $\dot{w}\sqrt{T}/P$ at the combustor inlet. The following equation is used in the hybrid simulation to calculate the resulting combustor exit pressure:

$$P_{4'} = P_3 - \frac{K_B \dot{w}_3^2 T_3}{P_3} = P_3 - \frac{K_B \dot{w}_3^2 V_3}{R_A W_3} \qquad (38)$$

The use of the stored mass W_3 in equation (38) results in a savings in computing equipment.

The digital program makes use of a number of bivariate functions to describe the combustor efficiency and temperature rise. Data from that simulation indicated that a simple energy balance assuming constant combustion efficiency could adequately describe the steady-state temperature rise in the combustor. The following equation is used in the hybrid simulation to describe that process:

$$(\dot{w}T)_{4'} = \frac{c_{p,3}}{c_{p,4}} \dot{w}_3 T_3 + \eta_B \frac{HVF}{c_{p,4}} \dot{w}_{F4} \qquad (39)$$

The specific heats $c_{p,3}$ and $c_{p,4}$, together with the efficiency η_B and fuel heating value HVF, were assumed to be constant.

10

The TF30-P-3 augmentor was represented by two sections having separate flow streams. In the baseline digital program, a static pressure balance between the streams was assumed at the entrance to the augmentor. However, only total pressures are used in the hybrid simulation. Data from the digital simulation indicated that the total pressure ratio $P_6/P_{1.6}$ was approximately constant along selected engine operating lines. Therefore, in the hybrid simulation, the total pressure P_5 and P_6 are calculated from

$$P_5 = P_6 = K_{PR6}P_{1.6} \tag{40}$$

Each section of the augmentor was treated in the same way as the combustor. The fuel flow to the core augmentor section was supplied from two zones, and the duct augmentor section was fed from the remaining three zones. The following equations described the TF30-P-3 augmentor model:

$$P_7 = P_6 - K_{CAB}(\dot{w}_{4.1} + \dot{w}_{BLLT})^2 \frac{T_6}{P_6} \tag{41}$$

$$(\dot{w}T)_6 = (\dot{w}T)_5 \tag{42}$$

$$(\dot{w}T)_7 = \frac{c_{p,6}}{c_{p,7}}(\dot{w}T)_6 + \frac{\eta_{CAB}}{c_{p,7}} HVF\, \dot{w}_{F7} \tag{43}$$

$$T_7 = \frac{(\dot{w}T)_7}{\dot{w}_{4.1} + \dot{w}_{BLLT} + \dot{w}_{F7}} \tag{44}$$

$$P_{1.7'} = P_{1.6} - \frac{K_{DAB}\dot{w}_{1.6}^2 V_{1.6}}{R_A w_{1.6}} \tag{45}$$

$$(\dot{w}T)_{1.7'} = \frac{c_{p,1.6}}{c_{p,1.7}}\dot{w}_{1.6}T_{1.6} + \frac{\eta_{DAB}}{c_{p,1.7}} HVF\, \dot{w}_{F1.7} \tag{46}$$

As in the combustor, the specific heats and combustion efficiencies in the augmentor were assumed to be constant.

The total pressure drop in the bypass duct was modeled in the same manner as for the combustor sections. However, no temperature rise (or drop) was assumed in the

duct. The following equations describe the hybrid simulation duct model:

$$P_{1.6'} = P_{1.3} - \frac{K_D \dot{w}_{1.3}^2 V_{1.3}}{R_A w_{1.3}}$$

(47)

$$T_{1.6'} = T_{1.3}$$

(48)

Exhaust Nozzle

In order to match the analytical model used in the digital simulation, the TF30-P-3 exhaust nozzle was modeled as two separate nozzles fed by the separate core and duct augmentor sections. The sum of the physical areas of the two nozzles must equal the nozzle area set by the engine control.

The standard isentropic compressible flow equations were assumed to describe the flows through the two exhaust nozzles. Because of the assumption of an instantaneous pressure balance at the entrance to the augmentor (eq. (40)), it was possible to compute the low-pressure-turbine flow (eqs. (33) and (34)) without having to depend on volume dynamics downstream of the low-pressure turbine or resort to iterative procedures. The core augmentor equations (eqs. (41) and (44)) define the conditions at the entrance to the core exhaust nozzle and allow a direct calculation of the core nozzle area.

In the nonaugmented mode, the physical exhaust nozzle area is constant. In order to provide a degree of freedom in matching digital nonaugmented data, variable flow coefficients $C_{d,8}$ and $C_{d,1.8}$ were assumed for the core and duct nozzles, respectively. Each flow coefficient was calculated from a linear function of its corresponding nozzle pressure ratio. The slope and intercept of each flow coefficient were adjusted to best match the digital data.

During the augmented mode, the physical nozzle area was controlled so as to maintain engine variables near their military power values. Therefore, the separate nozzle pressure ratios (and hence, flow coefficients) were nearly constant over the range of augmentation. In order to provide a degree of freedom in matching digital data during augmentation, a total nozzle flow coefficient $C_{d,N}$ was calculated from a linear function of the physical nozzle area. The slope and intercept were adjusted to best match the digital data. The following equations describe the TF30-P-3 exhaust nozzle model:

$$(P/P)_{CN} = \frac{P_0}{P_7}$$

(49)

$$A_8 = \frac{K_{CN}(\dot{w}_{4.1} + \dot{w}_{BLLT} + \dot{w}_{F7})\sqrt{T_7}}{P_7 \; FN7 \; C_{d,8}} \tag{50}$$

$$FN7 = \begin{cases} 0.2588 & \text{if } (P/P)_{CN} \leq 0.53 \\[2ex] \left[P/P\right]_{CN}^{0.7143}\sqrt{1 - \left[P/P\right]_{CN}^{0.2857}} & \text{if } (P/P)_{CN} > 0.53 \end{cases} \tag{51}$$

$$C_{d,8} = 1.3625 - 0.7158(P/P)_{CN} \qquad \text{where } 0.825 \leq C_{d,8} \leq 1.0 \tag{52}$$

$$A_{1.8} = C_{d,N}A_N - A_8 \qquad \text{where } C_{d,N}A_N \geq A_{N,MIN} \tag{53}$$

$$C_{d,N} = 1.049 - 1.622 \times 10^{-4} \; A_N \tag{54}$$

$$\dot{w}_{1.7} = \frac{C_{d,1.8}A_{1.8}P_{1.7} \; FN17}{K_{DN}\sqrt{T_{1.7}}} \tag{55}$$

$$(P/P)_{DN} = \frac{P_0}{P_{1.7}} \tag{56}$$

$$FN17 = \begin{cases} 0.2588 & \text{if } (P/P)_{DN} \leq 0.53 \\[2ex] \left[P/P\right]_{DN}^{0.7143}\sqrt{1 - \left[P/P\right]_{DN}^{0.2857}} & \text{if } (P/P)_{DN} > 0.53 \end{cases} \tag{57}$$

$$C_{d,1.8} = 1.575 - 1.00(P/P)_{DN} \qquad \text{where } 0.825 \leq C_{d,1.8} \leq 1.0 \tag{58}$$

Engine Dynamics

The equations previously discussed describe the steady-state operation of the various engine components. However, a transient engine simulation must also consider the effects of fluid compressibility, fluid momentum, energy storage, and rotor inertias.

In the TF30-P-3 hybrid simulation, intercomponent volumes were assumed at engine locations where either (1) gas dynamics were considered to be important or (2) gas dynamics were required to eliminate the need for iterative solutions (fig. 3). Modified forms of the continuity, energy, and state equations (ref. 11) were written for each volume and solved for the stored mass, temperature, and pressure in the volume. When mixing of gases was not involved, a simple first-order lag form of the energy equation was used. The time constant for each lag was estimated to be equal to the ratio of the stored mass in the volume to the flow through the volume.

Because of the real-time requirement and the computing equipment limitations, gas properties such as specific heats were assumed to be constant over the range of engine operating temperatures and fuel-air ratios. Gas properties were adjusted at the engine design point (sea-level, static, standard-day, military power setting) to achieve the desired steady-state cycle balance. The following equations describe the intercomponent volume dynamics in the TF30-P-3 hybrid simulation:

$$W_{2.2} = \int_0^t (\dot{w}_{2.1} - \dot{w}_{BL7} - \dot{w}_{2.2})dt + W_{2.2,i} \qquad (59)$$

$$T_{2.2} = \frac{1}{\tau_{2.2}} \int_0^t (T_{2.2'} - T_{2.2})dt + T_{2.2,i} \qquad (60)$$

$$P_{2.2} = \frac{R_A W_{2.2} T_{2.2}}{V_{2.2}} \qquad (61)$$

$$W_3 = \int_0^t (\dot{w}_{2.2} - \dot{w}_{BL12} - \dot{w}_{BLHT} - \dot{w}_{BLLT} - \dot{w}_3)dt + W_{3,i} \qquad (62)$$

$$T_3 = \frac{1}{\tau_3} \int_0^t (T_{3'} - T_3)dt + T_{3,i} \qquad (63)$$

$$P_3 = \frac{R_A W_3 T_3}{V_3} \qquad (64)$$

$$W_4 = \int_0^t (\dot{w}_3 + \dot{w}_{F4} - \dot{w}_4)dt + W_{4,i} \qquad (65)$$

14

$$(WT)_4 = \gamma_4 \int_0^t [(\dot{w}T)_{4'} - \dot{w}_4 T_4]dt + (WT)_{4,i} \qquad (66)$$

$$T_4 = \frac{(WT)_4}{W_4} \qquad (67)$$

$$P_4 = \frac{R_A (WT)_4}{V_4} \qquad (68)$$

$$W_{4.1} = \int_0^t (\dot{w}_4 + \dot{w}_{BLHT} - \dot{w}_{4.1})dt + W_{4.1,i} \qquad (69)$$

$$(WT)_{4.1} = \gamma_{4.1} \int_0^t [(\dot{w}T)_{4.1'} - \dot{w}_{4.1} T_{4.1}]dt + (WT)_{4.1,i} \qquad (70)$$

$$T_{4.1} = \frac{(WT)_{4.1}}{W_{4.1}} \qquad (71)$$

$$P_{4.1} = \frac{R_A (WT)_{4.1}}{V_{4.1}} \qquad (72)$$

$$W_{1.3} = \int_0^t (\dot{w}_2 - \dot{w}_{2.1} + \dot{w}_{BL7} + \dot{w}_{BL12} - \dot{w}_{1.3})dt + W_{1.3,i} \qquad (73)$$

$$(WT)_{1.3} = \gamma_{1.3} \int_0^t [(\dot{w}T)_{1.3'} - \dot{w}_{1.3} T_{1.3}]dt + (WT)_{1.3,i} \qquad (74)$$

$$T_{1.3} = \frac{(WT)_{1.3}}{W_{1.3}} \qquad (75)$$

$$P_{1.3} = \frac{R_A (WT)_{1.3}}{V_{1.3}} \qquad (76)$$

15

$$W_{1.6} = \int_0^t (\dot{w}_{1.3} - \dot{w}_{1.6})dt + W_{1.6,i} \qquad (77)$$

$$T_{1.6} = \frac{1}{\tau_{1.6}} \int_0^t (T_{1.3} - T_{1.6})dt + T_{1.6,i} \qquad (78)$$

$$P_{1.6} = \frac{R_A W_{1.6} T_{1.6}}{V_{1.6}} \qquad (79)$$

$$W_{1.7} = \int_0^t (\dot{w}_{1.6} + \dot{w}_{F1.7} - \dot{w}_{1.7})dt + W_{1.7,i} \qquad (80)$$

$$(WT)_{1.7} = \gamma_{1.7} \int_0^t [(\dot{w}T)_{1.7'} - \dot{w}_{1.7} T_{1.7}]dt + (WT)_{1.7,i} \qquad (81)$$

$$T_{1.7} = \frac{(WT)_{1.7}}{W_{1.7}} \qquad (82)$$

$$P_{1.7} = \frac{R_A (WT)_{1.7}}{V_{1.7}} \qquad (83)$$

The effects of fluid momentum on the TF30-P-3 engine dynamics were also included in the hybrid simulation. While these effects are primarily high frequency in nature, their inclusion in the simulation also serves to eliminate algebraic or iterative loops. The momentum equation was solved for the flow through (1) the combined fan core and low-pressure compressor, (2) the high-pressure compressor, (3) the combustor, (4) the fan duct, and (5) the duct augmentor. The following equations describe the TF30-P-3 flow dynamics:

$$\dot{w}_{2.1} = \left(\frac{Ag_c}{l}\right)_{FID+LC} \int_0^t (P_{2.2'} - P_{2.2})dt + \dot{w}_{2.1,i} \qquad (84)$$

$$\dot{w}_{2.2} = \left(\frac{Ag_c}{l}\right)_{HC} \int_0^t (P_{3'} - P_3)dt + \dot{w}_{2.2,i} \qquad (85)$$

$$\dot{w}_3 = \left(\frac{Ag_c}{l}\right)_B \int_0^t (P_{4'} - P_4)dt + \dot{w}_{3,i} \tag{86}$$

$$\dot{w}_{1.3} = \left(\frac{Ag_c}{l}\right)_D \int_0^t (P_{1.6'} - P_{1.6})dt + \dot{w}_{1.3,i} \tag{87}$$

$$\dot{w}_{1.6} = \left(\frac{Ag_c}{l}\right)_{DAB} \int_0^t (P_{1.7'} - P_{1.7})dt + \dot{w}_{1.6,i} \tag{88}$$

Probably the most significant factors in governing the transient behavior of a turbofan engine are the rotor moments of inertia. The rotor speeds were computed by using the conservation of angular momentum. The following equations are used in the TF30-P-3 hybrid simulation to compute the rotor speeds:

$$(NQ)_{HT} = \frac{30J}{\pi} (\Delta h)_{HT}(\dot{w}_4 + K_{BWHT}\dot{w}_{BLHT}) \tag{89}$$

$$(NQ)_{HC} = \frac{30J}{\pi} \dot{w}_{2.2}(c_{p,3'}T_{3'} - c_{p,2.2}T_{2.2}) \tag{90}$$

$$N_H = \frac{30}{\pi I_H} \int_0^t \left[\frac{(NQ)_{HT} - (NQ)_{HC}}{N_H}\right] dt + N_{H,i} \tag{91}$$

$$(NQ)_{LT} = \frac{30J}{\pi} (\Delta h)_{LT}(\dot{w}_{4.1} + K_{BWLT}\dot{w}_{BLLT}) \tag{92}$$

$$(NQ)_{FID+LC} = \frac{30J}{\pi} \dot{w}_{2.1}(c_{p,2.2'}T_{2.2'} - c_{p,2}T_2) \tag{93}$$

$$(NQ)_{FOD} = \frac{30J}{\pi} (\dot{w}_2 - \dot{w}_{2.1})(c_{p,1.3'}T_{1.3'} - c_{p,2}T_2) \tag{94}$$

$$N_L = \frac{30}{\pi I_L} \int_0^t \frac{(NQ)_{LT} - (NQ)_{FID+LC} - (NQ)_{FOD}}{N_L} dt + N_{L,i} \tag{95}$$

HYBRID SIMULATION

The equations describing the TF30-P-3 mathematical model were implemented by using the Lewis Research Center's Analog and Hybrid Computing Facility. The Lewis EAI Model 690 Hybrid Computing System consists of an EAI 640 Digital Computer, an EAI 693 Hybrid Interface Unit, and an EAI 680 Analog Computer. Two EAI 231-R Analog Computers were also used in this simulation.

The bulk of the calculations were performed on an EAI 680 and two 231-R Analog Computers. The analog computers perform all the operations characteristic of analog machines (i.e., summing, integration with respect to time, multiplication, attenuation, univariate function generation, etc.). The use of peripheral equipment such as x-y plotters and strip-chart recorders allows continuous monitoring by the user of computed variables. All the required analog computers can be tied together by means of a Centralized Trunk System to allow the transmittal of information between analog consoles.

The 640 Digital Computer was used primarily to perform the bivariate function generation associated with fan, compressor, and turbine performance. The digital computer also provided teletypewriter output listings of selected engine variables. In order to minimize the core storage requirements and digital cycle time, scaled-fraction variables and arithmetic routines were used in the digital program. Scaled-fraction variables are limited to values between ±1. The use of scaled fractions necessitates the scaling of digital variables in the same manner as the analog variables are scaled.

Figure 8 illustrates the split of the computational load between the various computers used in the TF30-P-3 real-time simulation. The split of the computational load was based on the computing equipment complement of each console and a desire to minimize trunking. The control inputs to the TF30-P-3 simulation (i.e., $\dot{w}_{F4}$, $\dot{w}_{F7}$, $\dot{w}_{F1.7}$, XBL7, XBL12, and A_N) were provided by an independent digital computer representation of the TF30-P-3 hydromechanical control system. That control simulation was implemented on the Lewis SEL 810B computer and is described in a separate report (ref. 10).

Digital Program

MAIN digital program. - The MAIN digital program performs the following tasks in the TF30-P-3 hybrid simulation: (1) reads unscaled component performance data and map scale-factor data by means of paper tape, performs the required map scaling, and stores the scaled map data in the MAP2 COMMON block which is shared with the bivariate function interpolation routine; (2) computes fan inlet conditions P_2 and T_2 from equations (1) to (5) and sets potentiometers on the analog to values corresponding to P_2,

18

T_2, and P_0; (3) accepts map input data from the analog by means of the analog-to-digital converters (ADC's); (4) performs the required function generation by means of calls to the bivariate function interpolation routine MAP2 (discussed in a separate section); (5) outputs map values to the analog by means of the digital-to-analog converters (DAC's); (6) provides teletype listing (if desired) of selected engine variables in both engineering and SI units. Additional ADC's are used to input analog data when obtaining teletype listings.

Appendix B contains a FORTRAN listing of the MAIN digital program and a detailed discussion of its operation. Appendix C contains a description of the required format for digital input data (component performance data). Samples of the digital data format are also provided.

MAP2 function routine. - Because of the nature of the fan and compressor performance maps (figs. 3, 4(a), and 5(a)), rectilinear interpolation cannot be used to generate these functions. Therefore, a radial-interpolation, bivariate-function-generation routine, MAP2, was developed at the Lewis Research Center for generating this type of function. The MAP2 routine is based on the MAPFUN routine described in reference 12. The MAP2 routine uses scaled-fraction arithmetic routines to minimize core storage requirements and execution time. Because of its favorable qualities, MAP2 was also used to perform the bivariate function generation associated with the turbine performance, although rectilinear interpolation could have been used.

Appendix D contains a FORTRAN listing of the MAP2-MAP2L function generation routine and a detailed discussion of its operation. Also included in appendix D is an assembly language listing of MAP2-MAP2L. The assembly language version was used in the real-time simulation of the TF30-P-3 engine to further reduce the execution time and core storage requirements.

The digital program (with assembly language MAP2-MAP2L) required approximately 10 000 words of core storage. The resulting digital sampling interval (with steady analog inputs) was 4.65 milliseconds.

Analog Program

The analog portion of the TF30-P-3 hybrid simulation performs all the required computations except the bivariate function generation previously discussed. The analog computation load is split between the 680 Analog Computer and two 231-R Analog Computers. The 680 Analog Computer also serves as the interface between the engine simulation and the SEL 810B digital control simulation. Approximately 185 amplifiers and 85 multipliers were required to perform the analog calculations.

Appendix E contains the analog patching diagrams for the TF30-P-3 hybrid simulation. For the most part, conventional analog techniques were used to implement the

engine model. Scale factors are not shown on the analog diagrams. Appendix E also contains a list of the scale factors and a list of the potentiometer settings at the design point. The following sections describe two features of the analog portion of the simulation.

Digital-to-analog multiplier interface. - One of the factors in determining the size (number of consoles) of an analog simulation is the complement of multipliers on each machine. On the 680 Analog Computer, a total of 24 multiuse multipliers are available. These multipliers may be used to multiply, divide, square, or take the square root. As a supplement to the multipliers, the 680 also has six digital-to-analog multipliers (DAM's) which allow a digitally supplied variable to be multiplied by an analog variable with the product appearing on the analog console. Each additional product is obtained at the cost of two DAC channels which may not be used as conventional DAC's. Appendix E contains a list of the products obtained with the DAM feature in the TF30-P-3 real-time simulation.

Analog function generation. - In order to decrease the digital sampling interval, the univariate function generation associated with the low- and high-pressure-compressor bleeds (figs. 4(b) and 5(b)) was performed on the 680 Analog Computer. Two 10-segment, variable-diode function generators (VDFG's) were used. The map input variables $(N_c)_{LC, M}$ and $(\dot{w}_c)_{HC, M}$ were computed on the analog from equations (16) and (22), respectively, and transmitted to the digital by ADC's.

Two 10-segment, fixed-diode function generators (FDFG's) were used on the 231-R Analog Computers to calculate the core and duct nozzle compressible flow functions FN7 and FN17. These functions (eqs. (51) and (57)) assume a constant specific-heat ratio γ of 1.4.

RESULTS AND DISCUSSION

Steady State

The TF30-P-3 hybrid simulation with digital control was evaluated over a range of steady-state operating conditions. The purpose of the steady-state evaluation was to test the various curve fits and assumptions in the hybrid model.

With the simulation operating at the sea-level, standard-day, static, military power point, excursions along the operating line were made by ramping the PLA signal to a desired power setting. After the transient settled out, a steady-state listing of selected variables was obtained at the teletype. Table I contains the teletype data for the sea-level, static operating line for power settings of 15° (idle). 70°, and 120° (full augmentation).

Figure 9 contains plots of a number of the hybrid-computer-simulated engine variables over the range of power settings. For comparison, the corresponding values obtained from the baseline digital program were also plotted. In order to better match the digital data at the very low power settings, the 12th-stage bleed opening (XBL12) was limited to 70 percent of its fully open value (table I(a)).

Figure 9 shows good agreement between hybrid and digital data at PLA's above 30°. Below 30°, discrepancies occurred in the sensitivities of rotor speeds and compressor discharge pressure to the power lever angle. For power lever angles below 30°, the hybrid-computer-simulated fuel flow exceeded the baseline digital value. This resulted in discrepancies in rotor speeds, temperatures, and so forth, for this range of power lever angles. However, because of the nature of the control design, errors in the engine variables can also cause errors in control outputs such as fuel flow. The observed differences in fuel flow, rotor speeds, and compressor discharge pressure were probably due to inaccuracies in the engine model at the low power settings.

Since almost all the previously discussed assumptions were based on sea-level, static, operating-line data, it was decided to evaluate the steady-state performance of the hybrid simulation at a different flight condition. The steady-state data acquisition was repeated for a 6.096-kilometer (20 000-ft), Mach 1.2 flight condition. For this flight condition, the 12th-stage bleed was closed for the entire operating line, and its effect on the compressor performance need not be considered. The fan inlet conditions for this flight condition were computed by the digital program and were $P_2 = 11.205$ N/cm^2 (16.252 psia) and $T_2 = 320.25$ K (576.45^o R). Table II and figure 10 contain the teletype listings and comparison plots for this flight condition.

For this flight condition, excellent agreement between hybrid and digital data was observed at the low power settings. Some discrepancies were observed in the range of power lever angles between 45° and 69°. Some unexplained irregularities were observed in the digital values of $P_{s,3}$, T_4, $\dot{w}_2$, and N_L in this range of power settings. In general, however, the same basic trends were observed in both the hybrid and digital data.

Other discrepancies were observed in the augmentation range of PLA between 110° and 120°. In the digital model, the nozzle area reached its maximum value only at a PLA of 120°, while in the hybrid model the area was near its maximum at 110°. This contributes to the observed differences in augmentor fuel flow since these control outputs are correlated in the digital control.

The general agreement of hybrid and digital data shown in figures 9 and 10 substantiates the assumptions of (1) constant combustor efficiency, (2) linear pressure ratio - temperature ratio relations, and (3) pressure-sensitive flow coefficients for the core and duct nozzles. The agreement of hybrid and digital data also substantiates the fan and compressor models used in the real-time simulation.

The observed discrepancies at low power settings can be compensated for by manipulation of the compressor bleeds (if applicable). Perhaps a more satisfactory solution to

the problem of matching steady-state data at low power settings is to implement variable specific heats c_p at the compressor discharge stations. Experience with similar simulations indicates that linear c_p-T relations, used only in the load torque calculations (eqs. (90) and (93)) have strong effects on the speed split at low power settings and can be "tuned" to match low-power-setting data. This problem is eliminated completely in the simulation described in reference 7, where all fluid properties are assumed to be variable. Unfortunately, the necessary computing equipment and computing time were not available to do this in this simulation.

The use of digitally implemented bivariate functions in the hybrid simulation did result in a better wide-range match of steady-state data than previously obtained by the authors in all-analog simulations.

Transients

The TF30-P-3 hybrid simulation with digital control was evaluated for power lever slams (rapid increases) and chops (rapid decreases) between idle and military power settings and also between military power and full-augmentation power settings. Transients were run only for sea-level, standard-day, static conditions. Data obtained with the hybrid simulation were compared with the corresponding baseline digital data. The power lever angle signal was ramped from its initial value to its final value at a rate corresponding to 125 degrees per second. Selected analog variables were recorded by using strip-chart recorders. Details of the TF30-P-3 control simulation are contained in reference 13.

The simulation was operated at the idle power setting (PLA = 15°). Table I(a) lists steady-state values for selected engine variables at that operating point. The power lever angle was then ramped to a value (67°) slightly below the military power setting (69°). The 2° margin in power lever angle was chosen so as not to inadvertently initiate augmentation.

Figure 11 shows the response of selected engine variables to this throttle slam. Also shown are the corresponding baseline digital simulation variables. The power lever angle reached its final value in approximately 0.4 second. Significant increases in the combustor fuel flow (commanded by the digital control) were not seen until about 0.7 second into the transient.

The digital simulation of the fuel control (ref. 13) includes a secondary fuel manifold fill-drain calculation. The filling of the manifold was initiated when the commanded fuel flow reached 0.1260 kilogram per second, which is approximately equal to the sea-level, static, idle fuel flow. The manifold was filled when the commanded fuel flow reached 0.1638 kilogram per second. When the manifold was filled, the commanded fuel flow reached the engine without the lag associated with the fill dynamics. Figure 11 in-

dicates that the manifold filling took 0.7 second in the hybrid simulation and 1.0 second in the digital simulation. This time difference was a result of the fuel flow differences caused by the discrepancies in the engine models at the low power settings.

Comparison with digital data indicates that the hybrid simulation variables responded more rapidly to the PLA slam. The differences in the T_4, $P_{s,3}$, and N_H responses were caused by the differences in fuel flow supplied by the control.

The 12th-stage bleed doors which are open at the idle condition are closed during the acceleration when the low-pressure-compressor discharge static pressure exceeds $1.481 P_2 + 6.254 \text{ N/cm}^2$. Figure 11 shows that the hybrid simulation bleed doors closed approximately 0.6 second before the digital simulation bleed doors. This was due to the faster response of $P_{s,2.2}$ in the hybrid simulation.

The nozzle area was at its maximum value at the static, idle condition. It was reduced to its minimum value (fig. 11(e)) by the digital control at a rate consistent with the baseline digital simulation.

The hybrid simulation was operated at the $PLA = 67^\circ$ condition. A throttle slam was then run with the PLA signal ramped to 120° at the same 125-degree-per-second rate. Table I(c) lists steady-state engine variables at the full-augmentation condition. Figure 12 shows the resulting response of selected engine variables to this throttle slam. Also shown are the corresponding baseline digital variables. The fuel flows to the five augmentor zones are metered as functions of PLA, N_H, T_2, and $P_{s,3}$. The nozzle area is increased by the digital control so as to maintain a scheduled ratio of $P_{s,3}/P_6$ during the augmentor operation. This maintains all engine variables upstream of the augmentor approximately constant at their military power values.

Figure 12 indicates that the timings of the zone fuel flow initiations in the hybrid and digital simulations are in general agreement. Differences of 0.1 to 0.2 second were observed, except for zone 4. Zone 4 fuel flow came on about 0.5 second early apparently because of an incorrect hold calculation in the simulated augmentor control. This hold was intended to represent the time required to fill the zone 4 manifold.

Figure 12(h) shows agreement between the nozzle area responses. The same 0.1- to 0.2-second delay for the digital response was observed. The agreement in the area responses indicates that the augmentor inlet and high-pressure-compressor discharge pressure dynamics are approximately the same in the hybrid and digital simulations.

Figures 13 and 14 contain the hybrid and baseline digital engine responses to throttle chops from $PLA = 120^\circ$ to $PLA = 67^\circ$ and from $PLA = 67^\circ$ to $PLA = 15^\circ$, respectively. Figure 13 shows agreement between the hybrid and baseline digital results for full augmentation to military chop. The timings of zone fuel flow shutoffs and the magnitudes of the selected engine variables are in agreement. Figure 13(i) does show slightly less damping in the hybrid simulation's response of P_6.

Figure 14 shows excellent agreement between the hybrid and baseline digital results for the military-to-idle chop. The response of fuel flow (and hence, $P_{s,3}$ and T_4) agrees since the line fill problem that existed for the corresponding acceleration does not exist at the start of the deceleration. This results in excellent agreement in the opening of the 12th-stage bleed when $P_{s,2.2} = 1.543 \, P_2 + 6.495 \, \text{N/cm}^2$. The response of the temperature T_4 to the throttle chops and slams was obtained by decreasing the gain of the $(WT)_4$ integrator (eq. (66)) by a factor of 25. This was necessary to match the baseline digital response and was an attempt to represent heat-transfer effects in the combustor. These effects were considered in the baseline digital program but were not included in the hybrid model.

Frequency Responses

A comparison of the hybrid and baseline digital engine dynamics (independent of the control) can be accomplished by opening the loops between the engine and the engine control. This was done with the hybrid simulation at the sea-level, static, PLA = 50° operating point. A constant combustor fuel flow was supplied to the engine with the 12th-stage bleed closed and the nozzle area at its minimum value. A sinusoidal fuel flow signal was superimposed on the constant fuel flow signal, resulting in sinusoidal oscillations in engine variables such as rotor speeds and pressures. The amplitude of the driving signal was ±10 percent of the constant input fuel flow. Both the driving signal and a selected output signal were input to an analog transfer function analyzer which calculated the amplitude ratio of and the phase angle between the two signals.

Figures 15 to 17 contain the frequency responses of the high-pressure-rotor speed, the high-pressure-compressor discharge static pressure, and the core augmentor inlet pressure, respectively, to fuel flow perturbations. Also plotted are the results from a similar procedure using the baseline digital simulation and a digital transfer function analyzer. The digital transfer function analyzer could not perform adequately above 1.3 hertz because of low signal levels. The analog transfer function analyzer had provisions for increasing the signal levels at the higher frequencies, allowing analysis to 10 hertz.

Figure 15 shows general agreement between the hybrid and digital responses of N_H. Since the low-frequency dynamics are caused primarily by rotor inertia, agreement in the dynamics indicates that the rotor dynamics have been adequately modeled in the hybrid simulation. The observed difference in the steady-state gain (normalizing factor) would seem to indicate a discrepancy in the steady-state engine models. However, the steady-state digital data presented in figures 9(a) and (b) show a sensitivity

24

$$\frac{\Delta N_H}{\Delta \dot{w}_{F4}} = \frac{\Delta N_H / \Delta PLA}{\Delta \dot{w}_{F4} / \Delta PLA}$$

of 0.992 rpm/(kg/hr), which is close to the value obtained from the hybrid simulation data. Therefore, errors in the digital analyzer results are suspected.

Figure 16 shows the frequency response of the high-pressure-compressor discharge static pressure. Significant differences were observed in both the steady-state gain and the dynamics. The hybrid data show a break frequency around 2 hertz with higher order dynamics above 1 hertz. The higher frequency dynamics may be attributable to the inclusion of combustor momentum effects in the combustor. The digital response is flat with increasing phase lag, characteristic of a dead time. A study of the transient response of $P_{s,3}$ to the PLA chop from 67° to 15° (fig. 14) shows a lag rather than a dead time between $P_{s,3}$ and $\dot{w}_{F4}$. Again, errors in the digital analysis are suspected.

Figure 17 compares the hybrid and digital responses of P_6 to the $\dot{w}_{F4}$ oscillations. Agreement in the steady-state gain was observed. The dynamics were in general agreement in the low-frequency range. However, the hybrid data show a resonant condition at about 3 hertz. The digital data indicate a similar condition above 1 hertz, but the inability of the digital analyzer to function above 1.3 hertz prevented a real comparison in that frequency range. The observed resonant condition may be attributable to duct dynamics since the pressure P_6 is assumed to be proportional to the duct augmentor pressure $P_{1.6}$.

CONCLUDING REMARKS

A real-time hybrid simulation of the TF30-P-3 turbofan engine has been developed. The simulation is primarily analog in nature but does use the digital portion of the hybrid computer to perform bivariate function generation associated with modeling the performance of the engine's rotating components. The digital sampling interval is approximately 4.6 milliseconds and does allow real-time simulation without compensation for the phase lag caused by the digital sample-and-hold process.

The hybrid simulation was based on the engine model used in a baseline digital simulation provided by the engine manufacturer. Differences between the hybrid and digital models were dictated by the real-time requirement. The hybrid model assumes constant fluid properties and combustor efficiencies to minimize analog equipment requirements. The hybrid model also includes momentum effects in the compressors and combustors which allow the use of flow as an input to the compressor performance maps without the need for iteration.

Results from the hybrid and digital simulations were compared. These comparisons indicated that the real-time hybrid simulation does adequately match the baseline digital

simulation for both steady-state and dynamic conditions. Discrepancies at low power settings did result in faster hybrid responses for accelerations from idle to military power. These discrepancies could be minimized by considering the effects of variable specific heats on the engine balance at low power settings.

The real-time hybrid simulation provides a valuable analytical tool for research studies involving the TF30-P-3 turbofan engine. In particular, digital controls may be developed and tested on the simulation prior to actual engine testing. Transient data obtained with the hybrid simulation and a digital control are presented. These data indicate that the simulation does provide a realistic test vehicle for the control. In fact, the generation of the data presented did result in the discovery of a number of ''bugs'' in the control which might otherwise have gone undetected.

Lewis Research Center,
    National Aeronautics and Space Administration,
        Cleveland, Ohio, July 8, 1974,
            501-24.

APPENDIX A

SYMBOLS

A cross-sectional area, cm^2 (in.^{2})

C_d nozzle flow coefficient

c_p specific heat, J/kg-K (Btu/lbm-^{O}R)

dt   time increment, sec

FN7   core nozzle flow function

FN17   duct nozzle flow function

f_i general function, $i = 1, 10$

fp   flow parameter, kg-K-cm^2/N-rpm-sec (lbm-^{O}R-in.^{2}/lbf-rpm-sec)

g_c gravitational conversion factor, 100 cm-kg/N-sec^2 (386.3 lbm-in./lbf-sec^2)

HVF   heating value of fuel, J/kg (Btu/lbm)

Δh enthalpy drop, J/kg (Btu/lbm)

hp   enthalpy drop parameter, J/kg-$K^{1/2}$-rpm (Btu/lbm-^{O}R$^{1/2}$-rpm)

I polar moment of inertia, N-cm-sec^2 (in.-lbf-sec^2)

J work conversion factor, 100 N-cm/J (9339.6 in.-lbf/Btu)

K constant (appropriate units)

l length, cm (in.)

M Mach number

m   second function map index, $m = 7$ to 12

N rotor speed, rpm

n   first function map index, $m = 1$ to 6

P total pressure, N/cm^2 (psia)

P/P   pressure ratio

PLA   power lever angle, deg

Q torque, N-cm (in.-lbf)

R_A gas constant of air, N-cm/kg-K (in.-lbf/lbm-^{O}R)

T total temperature, K (^{O}R)

T/T   temperature ratio

V	volume, cm^3 (in.^{3})
W	stored mass, kg (lbm)
$\dot{w}$	mass flow rate, kg/sec (lbm/sec)
XBL7	fraction of 7th-stage bleed
XBL12	fraction of 12th-stage bleed
$X\underline{I}$	ADC channel I input, I = 0, 23
XSC	scale factor on x map input
x	x input to bivariate map (normalized by design-point value)
x_j	array of x inputs for j^{th} value of y input, j = 1, 8
$Y\underline{I}$	DAC channel I input, I = 0, 23
YSC	scale factor of y map input
y	y input to bivariate map (normalized by design-point value)
ZSC(1)	scale factor on first function of x and y
ZSC(2)	scale factor on second function of x and y
z_1	first function of x and y (normalized by design-point value)
z_2	second function of x and y (normalized by design-point value)
z_{1j}	array of first function outputs for j^{th} value of y, j = 1, 8
z_{2j}	array of second function outputs for j^{th} value of y, j = 1, 8
γ	specific-heat ratio
δ	total pressure (normalized by sea-level value)
η	efficiency
θ	total temperature (normalized by standard-day value)
τ	time constant, sec

Subscripts:

B	combustor
BLHT	high-pressure-turbine bleed
BLLT	low-pressure-turbine bleed
BL7	7th-stage bleed
BL12	12th-stage bleed
BWHT	portion of high-pressure-turbine bleed doing work

28

BWLT	portion of low-pressure-turbine bleed doing work
CAB	core augmentor
CN	core nozzle
c	corrected to inlet conditions
D	duct
DN	duct nozzle
F	fuel
FAN	total fan
FID	fan hub section
FID+LC	fan hub and low-pressure compressor
FZ1	augmentor zone 1
FZ2	augmentor zone 2
FZ3	augmentor zone 3
FZ4	augmentor zone 4
FZ5	augmentor zone 5
FOD	fan tip section
H	high speed
HC	high-pressure compressor
HT	high-pressure turbine
I	inlet
i	initial condition
L	low speed
LC	low-pressure compressor
LT	low-pressure turbine
M	map
MIN	minimum value
N	total nozzle
PR6	core-duct pressure ratio
s	static
0	ambient

1.3	fan tip discharge
1.6	duct augmentor inlet
1.7	duct nozzle inlet
1.8	duct nozzle throat
2	fan inlet
2.1	fan hub discharge
2.2	low-pressure-compressor discharge
3	high-pressure-compressor discharge
4	high-pressure-turbine inlet
4.1	low-pressure-turbine inlet
5	low-pressure-turbine discharge
6	core augmentor inlet
7	core nozzle inlet
8	core nozzle throat

Superscript:

( )'   inlet to mixing station

FORTRAN symbols - MAIN program:

AN	total nozzle area, in.^{2}
ANSI	total nozzle area, m^2
ETAI	inlet efficiency
I	integer
IERR	error flag for linkage routines
IX	array containing number of points per curve for each map pair
J	integer
JX	map scaling index
JY	array containing number of curves for each map pair
JZ1	map scaling index
JZ2	map scaling index
KX	array containing x out-of-range counts for each map pair
KY	array containing y out-of-range counts for each map pair

30

M	integer
MAP2	bivariate function (first function)
MAP2L	bivariate function (second function)
MM	function relay address
M0	Mach number
N	map index
NCV	number of curves for map being read in
NTBL	number of data points for map being read in
NX	number of points per curve for map being read in
NY	number of curves for map being read in
PADR	array of addresses of digitally set potentiometers
PLA	power lever angle, deg
PS22	low-pressure-compressor discharge static pressure, psia
PS22SI	low-pressure-compressor discharge static pressure, N/cm^2
PS3	high-pressure-compressor discharge static pressure, psia
PS3SI	high-pressure-compressor discharge static pressure, N/cm^2
PVAL	array of settings for digitally set potentiometers
P0	ambient pressure, psia
P0SI	ambient pressure, N/cm^2
P2	fan inlet pressure, psia
P2Q0	inlet pressure ratio
P2SI	fan inlet pressure, N/cm^2
P3Q22	high-pressure-compressor pressure ratio
QRBADS	linkage routine for reading ADC's
QSHYIN	linkage routine for console selection
QSRUN	linkage routine for setting logic mode
QSSECF	linkage routine for setting time scale
QSTDA	linkage routine for transferring DAC contents
QWBDAS	linkage routine for loading DAC registers
QWFRL	linkage routine for setting function relays

QWPR	linkage routine for setting potentiometers
SENSW	logical array for testing sense switches
T0	ambient temperature, ^{O}R
T0SI	ambient temperature, K
T2	fan inlet temperature, ^{O}R
T2Q0	inlet temperature ratio
T2SI	fan inlet temperature, K
T22	low-pressure-compressor discharge temperature, ^{O}R
T22SI	low-pressure-compressor discharge temperature, K
T3	high-pressure-compressor discharge temperature, ^{O}R
T3SI	high-pressure-compressor discharge temperature, K
T4	high-pressure-turbine inlet temperature, ^{O}R
T4SI	high-pressure-turbine inlet temperature, K
T6	core augmentor inlet temperature, ^{O}R
T6SI	core augmentor inlet temperature, K
VALS	array containing unscaled, normalized map data
V$\underline{I}$	potentiometer settings, I = 1, 3
WA2	fan airflow, lbm/sec
WA2SI	fan airflow, kg/sec
WAR2	fan corrected airflow, lbm/sec
WAR22M	low-pressure-compressor map corrected airflow, lbm/sec
WF4	combustor fuel flow, lbm/sec
WF4SI	combustor fuel flow, kg/sec
WF7	core augmentor fuel flow, lbm/sec
WF7SI	core augmentor fuel flow, kg/sec
WF17	duct augmentor fuel flow, lbm/sec
WF17SI	duct augmentor fuel flow, kg/sec
WR22SI	low-pressure-compressor corrected airflow, kg/sec
X$\underline{I}$	ADC input variables, I = 0, 23
XNH	high-pressure-rotor speed, rpm

32

XNL	low-pressure-rotor speed, rpm
XNLR2	fan corrected speed, rpm
XSC	scale factor for x breakpoints on map being read in
XVALS	array containing scaled x breakpoints for each map pair
YI	array containing DAC initial conditions
Y$\underline{I}$	DAC output variables, I = 0, 23
YSC	scale factor for y breakpoints on map being read in
YVALS	array containing scaled y breakpoints for each map pair
ZSC(1)	scale factor for first function in map pair being read in
ZSC(2)	scale factor for second function in map pair being read in
ZVALS	array containing scaled map outputs for each map pair

FORTRAN symbols - MAP2 (MAP2L) function routine:

I	index for x breakpoints
IX	array of last search indices for x breakpoints
J	index for y curves
JY	array of last search indices for y curves
KX	array of x out-of-range counts
KY	array of y out-of-range counts
MAP2	bivariate function (first function)
MAP2L	bivariate function (second function)
N	map index
NX	array of number of points per curve
NXP	number of points per curve for map being read
NY	array of number of curves per map
NYC	number of curves for map being read
XFRAC	fractional location of XIN between XLO and XHI
XHI	$(I + 1)^{th}$ breakpoint on inferred YIN curve
XIN	x input to map
XLO	I^{th} breakpoint on inferred YIN curve
XVALS	array of scaled x breakpoints for each map pair

YIN   y input to map

YINCR   fractional location of YIN between J^{th} and $(J + 1)^{th}$ curves

YVALS   array of scaled y breakpoints for each map pair

ZL   map output for XLO, YIN inputs

ZR   map output for XHI, YIN inputs

ZVALS   array of scaled map outputs for each map pair

APPENDIX B

MAIN DIGITAL PROGRAM - DESCRIPTION AND FORTRAN LISTING

Description

The primary function of the MAIN digital program is to read the bivariate function input variables on the ADC channels, to call the function generation routine MAP2, and to transfer updated function output variables to the analog computer through the DAC channels.

The MAIN digital program and the function generation routine MAP2 are capable of handling as many as six pairs of bivariate functions, with each function described by as many as eight curves and 10 points per curve. A COMMON block MAP2 is shared by the MAIN digital program and MAP2 (see FORTRAN listings). This COMMON block contains arrays for function data XVALS, YVALS, and ZVALS; search indices IX and JY; argument dimensions NX and NY; and out-of-range counters KX and KY.

The MAIN digital program reads the unscaled, but normalized, component performance data and associated scale factors and stores the data in the VALS array. Appendix C contains samples of the required format for reading the data. The data in the VALS array are divided by the appropriate scale factor; and the results are stored in the XVALS, YVALS, and ZVALS arrays. The search indices and out-of-range counters are initialized, and the argument dimensions are stored in the NX and NY arrays. The functions of the search indices and out-of-range counters are discussed in appendix D.

After scaling and storing the component performance data, the MAIN digital program reads scaled-fraction DAC initial-condition data. These data are stored in the YI array. By initializing the DAC's with specified values, the user can check the analog portion of the simulation prior to entering the digital computation loop. Appendix C contains a sample of the required format for the DAC initial condition data. Unused DAC's are initialized to zero.

Table III lists the scaled variables and associated DAC channels which are transmitted to the EAI 680 Analog Computer by the MAIN digital program. Since the desired initial condition corresponds to the engine design point, the initial values of the scaled map outputs should be equal to the inverse of the map output scale factors.

After initializing the DAC's, the MAIN digital program reads, from the teletype, unscaled values for the variables P_0, T_0, and M_0. The program calculates analog potentiometer settings corresponding to the variables P_2, T_2, and P_0 for the specified flight condition. The analog portion of the simulation is discussed in appendix E. The potentiometers to be set by the digital computer are specified as input data by means of paper tape. The format used for this data input is illustrated in appendix C.

The main computation loop in the MAIN digital program starts at statement 30. At this point, the required analog data are read from the appropriate ADC's and stored in the locations specified by the arguments used in the call to the QRBADS linkage routine. These arguments indicate that a total of 10 ADC's are to be read, starting with ADC0. The contents of these ADC's are to be stored sequentially in the locations reserved for the variables listed in the SCALED FRACTION declaration, starting with the variable X0.

Table IV lists the ADC's and the associated scaled input variables received from the EAI 680 Analog Computer. The scale factors associated with the map inputs are equal to the products of the design-point values and the XSC (or YSC) scale factors specified with the map data. For example, at the design point, ADC channel 5 receives a scaled signal equal to 1.0/1.9045, or 0.52507.

The MAIN digital program then calls the function generation routine MAP2 with the appropriate input variables. The calling statement is of the form:

$$z_1 = MAP2(n, x, y)$$

The scaled map output values returned by MAP2 are transferred through the DAC channels to the analog computer. For certain of the functions, another called statement $z_2 = MAP2L(m)$ is used. The reason for using a different calling statement is discussed in appendix D.

After the DAC variables in table III are transferred, a sense switch on the 640 control console is tested to determine if additional data are to be input from the analog. If the sense switch is depressed (analog should be in "HOLD" mode), the ADC channels listed in table V are read. Before teletype listing, the variables to be listed are unscaled to allow listing with both engineering and SI units. After teletype listing, the program returns to statement 30, where updated ADC's are read.

FORTRAN Listing


```
      DIMENSION VALS(248),ZSC(2),PADR(3),PVAL(3)
C*****ADC VARIABLES
      SCALED FRACTION X0,X1,X2,X3,X4,X5,X6,X7,X8,X9,X10,X11,X12,X13,
     1 X14,X15,X16,X17,X18,X19,X20,X21,X22,X23
C*****DAC VARIABLES
      SCALED FRACTION Y4,Y5,Y6,Y7,Y8,Y9,Y10,Y11
C*****OTHER VARIABLES
      SCALED FRACTION XVALS(10,8,6),YVALS(8,6),ZVALS(10,8,12),YI(24),
     1 MAP2,MAP2L,V1,V2,V3,SSQRT
      COMMON/MAPS/XVALS,YVALS,ZVALS,IX(6),JY(6),NX(6),NY(6),KX(6),KY(6)
      LOGICAL SENSW
      REAL M0
```

```
C*****INPUT REAL COMPONENT MAP DATA AND SCALE FACTORS
      TYPE 1
    1 FORMAT(/3X,54HPLACE DATA TAPE FOR MAPS NO. 1-8 IN HSPTR. THEN R-S-
     1R./)
      PAUSE
      DO 10   N=1,4
      READ(4,3) XSC,YSC,ZSC(1)
    3 FORMAT(4F11.4)
      IF(N-4)   4,5,5
    4 NCV=8
      GO TO 6
    5 NCV=7
    6 NTBL=17*NCV
      READ(4,7)(VALS(I),I=1,NCV)
    7 FORMAT(8F8.2)
      J=NCV+1
      READ(4,8)(VALS(I),I=J,NTBL)
    8 FORMAT(8F8.4)
C*****SCALE COMPONENT MAP DATA
      DO 9   J=1,NCV
      DO 9   I=1,8
      YVALS(J,N)=VALS(J)/YSC
      JX=NCV+2*((J-1)*8+I)-1
      XVALS(I,J,N)=VALS(JX)/XSC
    9 ZVALS(I,J,N)=VALS(JX+1)/ZSC(1)
      IX(N)=1
      JY(N)=1
      NX(N)=8
      NY(N)=NCV
      KX(N)=0
      KY(N)=0
   10 CONTINUE
      NCV=8
      NTBL=NCV*31
      DO 13   N=5,6
      READ(4,3) XSC,YSC,ZSC(1),ZSC(2)
      READ(4,11)(VALS(I),I=1,NCV)
      J=NCV+1
      READ(4,11)(VALS(I),I=J,NTBL)
   11 FORMAT(10F7.4)
      DO 12   J=1,NCV
      YVALS(J,N)=VALS(J)/YSC
      DO 12   I=1,10
      JX=NCV+30*(J-1)+I
      XVALS(I,J,N)=VALS(JX)/XSC
      JZ1=JX+10
      ZVALS(I,J,N)=VALS(JZ1)/ZSC(1)
      JZ2=JX+20
      ZVALS(I,J,N+2)=VALS(JZ2)/ZSC(2)
   12 CONTINUE
      IX(N)=1
      JY(N)=1
      NX(N)=10
      NY(N)=NCV
   13 CONTINUE
C*****INITIALIZE DACS
      TYPE 14
   14 FORMAT(/3X,64HPLACE DATA TAPE FOR DAC INITIAL CONDITIONS IN HSPTR.
```

```
     1 THEN R-S-R./)
       PAUSE
       READ(4,15)(YI(I),I=1,24)
    15 FORMAT(5S8)
C*****INITIALIZE ANALOG CONSOLE
       CALL QSHYIN(IERR,680)
       CALL QSRUN(IERR)
       CALL QSSECF(IERR)
       DO 200 M=1,24
       MM=5*M-1
       CALL QWFRL(MM,.FALSE.,IERR)
   200 CONTINUE
C*****TRANSFER INITIAL DAC VALUES
       CALL QWBDAS(YI,0,24,IERR)
       CALL QSTDA
C*****SPECIFY OPERATING CONDITIONS FOR ENGINE
       TYPE 16
    16 FORMAT(/3X,33HTYPE DESIRED VALUES FOR P0,T0,M0./)
       ACCEPT 17,P0,T0,M0
    17 FORMAT(F7.3,F8.3,F5.2)
       T2Q0=(1.+.2*M0*M0)
       P2Q0=T2Q0**3.5
       ETAI=1.0
       IF(M0.LE.1.)  GO TO 18
       ETAI=1.0-.075*(M0-1.0)**1.35
    18 T2=T2Q0*T0
       P2=P2Q0*P0*ETAI
       P0SI=P0*.68948
       T0SI=T0*.55555
       P2SI=P2*.68948
       T2SI=T2*.55555
       TYPE 19,P2,T2
    19 FORMAT(/3X,5HP2 = ,F7.3,7H, T2 = ,F8.3/)
       V1=P2/40.
       V2=T2/1000.
       V3=P0/40.
   ****SET POTS WHICH ARE SENSITIVE TO OPERATING CONDITIONS
       TYPE 20
    20 FORMAT(/3X,55HPLACE DATA TAPE FOR POT ADDRESSES IN HSPTR. THEN R-S
      1-R./)
       PAUSE
       READ(4,22)(PADR(I),I=1,3)
    22 FORMAT(8A5)
       PVAL(1)=V1
       PVAL(2)=V2
       PVAL(3)=V3
       DO 25   I=1,3
       DO 23   J=1,3
       CALL QWPR(PADR(I),PVAL(I),IERR)
       IF(IERR.EQ.1)  GO TO 25
    23 CONTINUE
       TYPE 24,PADR(I),IERR
    24 FORMAT(3X,A4,9H   IERR = ,I1/)
       PAUSE
    25 CONTINUE
       TYPE 26
    26 FORMAT(3X,55HSLAVE CONSOLES 4 AND 5 TO CONSOLE 1. MANUALLY GO TO I
      1C.)
```

```
          TYPE 29
   29 FORMAT(/3X,44HPROCEED TO DYNAMIC PART OF PROGRAM BY R-S-R./)
          PAUSE
C*****READ ADC VALUES AND GENERATE MAP OUTPUTS
   30 CALL QRBADS(X0,0,10,IERR)
          Y7=MAP2(1,X0,X1)
          Y4=MAP2(2,X0,X1)
          Y5=MAP2(3,X2,X3)
          Y6=MAP2(4,X4,X5)
   32 Y8=MAP2(5,X6,X7)
          Y9=MAP2L(7)
   34 Y10=MAP2(6,X8,X9)
          Y11=MAP2L(8)
C*****TRANSFER UPDATED DAC VALUES TO ANALOG
   35 CALL QWBDAS(Y4,4,8,IERR)
          CALL QSTDA
C*****OUTPUT UNSCALED DATA AT TELETYPE IF DESIRED
          IF(.NOT.SENSW(1))  GO TO 30
          CALL QRBADS(X10,10,14,IERR)
          WF4=X10
          WF4=WF4*3.
          WF4SI=WF4*.45359
          WF7=X18
          WF7=WF7*6.
          WF7SI=WF7*.45359
          WF17=X15
          WF17=WF17*8.
          WF17SI=WF17*.45359
          AN=X13
          AN=AN*1600.
          ANSI=AN*.00064516
          PS22=X14
          PS22=PS22*150.
          PS22SI=PS22*.68948
          PS3=X11
          PS3=PS3*400.
          PS3SI=PS3*.68948
          T22=X16
          T22=T22*1500.
          T22SI=T22*.55555
          T3=X17
          T3=T3*2000.
          T3SI=T3*.55555
          T4=X12
          T4=T4*4000.
          T4SI=T4*.55555
          T6=X19
          T6=T6*2000.
          T6SI=T6*.55555
          WAR2=Y7
          WAR2=WAR2*250.
          WA2=(WAR2*P2*1.5497)/SQRT(T2)
          WA2SI=WA2*.45359
          XNLR2=X1
          XNLR2=XNLR2*20000.
          XNL=.04391*XNLR2*SQRT(T2)
          WAR22M=X4
          WAR22M=WAR22M*40.
```

```
       WR22SI=WAR22M*.45359
       P3Q22=Y6
       P3Q22=P3Q22*5.
       XNH=X20
       XNH=XNH*20000.
       PLA=X23
       PLA=PLA*150.
       TYPE 99
  99 FORMAT(18X,36HTF30-P3 SIMULATION STEADY-STATE DATA//)
       TYPE 100,P0SI,P0
 100 FORMAT(5X,9HP0        = ,F7.3,9X,7HN/SQ CM,7X,2H( ,F7.3,9X,8HPSIA     )
     1)
       TYPE 101,T0SI,T0
 101 FORMAT(5X,9HT0        = ,F7.2,9X,7HK        ,7X,2H( ,F7.2,9X,8HR       )
     1)
       TYPE 102,M0
 102 FORMAT(5X,9HM0        = ,F7.4)
       TYPE 103,P2SI,P2
 103 FORMAT(5X,9HP2        = ,F7.3,9X,7HN/SQ CM,7X,2H( ,F7.3,9X,8HPSIA     )
     1)
       TYPE 104,T2SI,T2
 104 FORMAT(5X,9HT2        = ,F7.2,9X,7HK        ,7X,2H( ,F7.2,9X,8HR       )
     1)
       TYPE 105,PLA
 105 FORMAT(5X,9HPLA       = ,F7.2,9X,3HDEG)
       TYPE 106,WF4SI,WF4
 106 FORMAT(5X,9HWF4       = ,F7.4,9X,7HKG/SEC ,7X,2H( ,F7.4,9X,8HLBM/SEC)
     1)
       TYPE 107,WF7SI,WF7
 107 FORMAT(5X,9HWF7       = ,F7.4,9X,7HKG/SEC ,7X,2H( ,D7.4,9X,8HLBM/SEC)
     1)
       TYPE 108,WF17SI,WF17
 108 FORMAT(5X,9HWF17      = ,F7.4,9X,7HKG/SEC ,7X,2H( ,F7.4,9X,8HLBM/SEC)
     1)
       TYPE 109,X21
 109 FORMAT(5X,9HXBL7      = ,S7)
       TYPE 110,X22
 110 FORMAT(5X,9HXBL12     = ,S7)
       TYPE 111,ANSI,AN
 111 FORMAT(5X,9HAN        = ,F7.5,9X,7HSQ M    ,7X,2H( ,F7.1,9X,8HSQ IN  )
     1)
       TYPE 112,XNH
 112 FORMAT(5X,9HXNH       = ,F7.0,9X,3HRPM)
       TYPE 113,XNL
 113 FORMAT(5X,9HXNL       = ,F7.0,9X,3HRPM)
       TYPE 114,PS22SI,PS22
 114 FORMAT(5X,9HPS22      = ,F7.3,9X,7HN/SQ CM,7X,2H( ,F7.3,9X,8HPSIA     )
     1)
       TYPE 115,PS3SI,PS3
 115 FORMAT(5X,9HPS3       = ,F7.2,9X,7HN/SQ CM,7X,2H( ,F7.2,9X,8HPSIA     )
     1)
       TYPE 116,WA2SI,WA2
 116 FORMAT(5X,9HWA2       = ,F7.2,9X,7HKG/SEC ,7X,2H( ,F7.2,9X,8HLBM/SEC)
     1)
       TYPE 117,T22SI,T22
 117 FORMAT(5X,9HT22       = ,F7.2,9X,7HK        ,7X,2H( ,F7.2,9X,8HR       )
     1)
       TYPE 118,T3SI,T3
```

```
 118 FORMAT(5X,9HT3        = ,F7.1,9X,7HK          ,7X,2H(  ,F7.1,9X,8HR          )
    1)
    TYPE 119,T4SI,T4
 119 FORMAT(5X,9HT4        = ,F7.1,9X,7HK          ,7X,2H(  ,F7.1,9X,8HR          )
    1)
    TYPE 120,T6SI,T6
 120 FORMAT(5X,9HT6        = ,F7.1,9X,7HK          ,7X,2H(  ,F7.1,9X,8HR          )
    1)
    TYPE 121,WR22SI,WAR22M
 121 FORMAT(5X,9HWAR22M = ,F7.3,9X,7HKG/SEC ,7X,2H(  ,F7.3,9X,8HLBM/SEC)
    1)
    TYPE 122,P3Q22
 122 FORMAT(5X,9HP3Q22  = ,F7.4)
    GO TO 30
    END
```

APPENDIX C

DIGITAL INPUT DATA

In the MAIN digital program, each map or set of component performance data is stored with an identifying map number in the XVALS, YVALS, and ZVALS arrays. The map numbers are required when calling the MAP2 routine to allow the location of the appropriate blocks of stored data. Table VI contains a list of the map numbers for the TF30-P-3 component performance data.

A basic requirement for the MAP2 data is that each curve of a given function must have the same number of breakpoints. However, different maps may have different numbers of curves or breakpoints per curve. In the TF30-P-3 simulation, the fan and compressor maps are represented by eight points per curve, while the turbine maps require 10 points per curve. All maps have eight curves except the high-pressure turbine, which has seven curves.

Tables VII to XII illustrate the format used to input the component performance data. Tables VII to X contain the data for maps 1 to 4, respectively. In the TF30-P-3 simulation, all component performance data are normalized by the sea-level, static, $PLA = 69^O$ value of the corresponding variable. Although normalized, the input data may exceed unity. In order to use the scaled-fraction function routine MAP2, these data must be scaled in the MAIN digital program. Therefore, the first line of data for each map contains scale factors XSC, YSC, and ZSC(1) which are used to scale the already normalized data. The second line of data contains the normalized y values. The remaining lines of data contain the x and z_1 pairs for each of the ascending values of y. For example, the third line of data contains the normalized values of the first four x and z_1 pairs for the lowest value of y. The fourth line of data contains the normalized map outputs corresponding to the last four x and z_1 for the lowest value of y. The x breakpoints can be different for each of the curves.

Tables XI and XII contain the data for map pairs (5,7) and (6,8), respectively. For convenience, data for pairs of maps describing the performance of a particular component are combined. In order to use the MAP2L feature described in appendix D, breakpoints for both maps in the pair must be common. For each map pair, the first line of data contains scale factors XSC, YSC, ZSC(1), and ZSC(2). The last scale factor is used to scale the second map output z_2. The second line of data contains the normalized y values. The remaining lines of data contain the x, z_1, and z_2 values for each of the ascending values of y. For the case of map pairs, the x, z_1, and z_2 data are separated with a whole line used for each.

The MAIN digital program accepts (by means of paper tape) the scaled-fraction initial conditions for all 24 (numbered 0 to 23) of the DAC's. The first five lines of data

42

shown in table XIII illustrate the format used to input these data. The last line of data in table XIII illustrates the format used to input the addresses of analog potentiometers to be set by the MAIN digital program for specified flight conditions.

APPENDIX D

MAP2 FUNCTION GENERATION ROUTINE - DESCRIPTION AND FORTRAN

AND ASSEMBLY LANGUAGE LISTINGS

Description

MAP2 is a function generation routine developed for the EAI 640 Digital Computer for handling a special type of function of two variables. This special type of function contains curves (constant y values) which are not defined over the same range of the x variable. Examples of such functions are fan and compressor performance maps for turbofan engines. Normal rectilinear interpolation cannot be used for these functions so a special interpolation scheme is used in MAP2.

MAP2 can accommodate six pairs of independent input variables and twelve function output variables. That is, in addition to the six independent bivariate functions, six additional functions can be generated. However, these additional functions each must have arguments and argument breakpoints common to one of the six independent functions. This feature is useful in modeling fans, compressors, and turbines whose performance is usually described by pairs of bivariate functions.

In order to reduce storage requirements and execution time, MAP2 was designed to use scaled-fraction arithmetic and scaled-fraction data. The tables of function data, map input and output variables, and the routine MAP2 itself must be declared as scaled fractions in any program or subroutine which loads the function tables or calls MAP2.

The arrays IX and JY containing the search indices are initialized to 1 in the calling program. These search indices are updated during each execution of MAP2 and are used to speed up the table search for subsequent calls to MAP2. Details of the table search and interpolation scheme are discussed in reference 12.

The arrays KX and KY containing the out-of-range counters for each function are initialized to zero in the calling program. These counters keep track of the number of consecutive times an argument exceeds the range of the input data for its respective map. A limited number of out-of-range calls to MAP2 are allowed in order to permit short-duration increases in map inputs (caused by noise, etc.) without problem interruption. If the out-of-range count reaches 25 for either map input, the program is interrupted and subroutine MOOR (map out of range) is called. In the TF30-P-3 simulation, MOOR places the analog computer in "HOLD," prints an error message at the teletype, and pauses to await the user's corrective action. The maximum allowable out-of-range count and the action taken by MOOR are arbitrary and may be modified for a particular simulation.

44

As previously discussed, six additional functions can be accommodated by MAP2 if they have arguments and argument breakpoints common to one of the original six functions. This feature reduces the storage requirements for the input data arrays XVALS and YVALS. In addition, the execution time can be reduced by skipping the table search and going directly to the interpolation calculations.

Both FORTRAN and assembly language versions of MAP2 have been developed. These may be used interchangeably. However, for the digital sampling interval lengths required for real-time engine simulation, the assembly language version must be used. Both versions have been written in such a way that overflows are not possible if the scaled-fraction data have been loaded correctly.

In order to handle the additional functions for which the table search can be skipped, an additional entry point, MAP2L, was added to the assembly language version. The calling statement for these functions requires only the map number m. Since the FORTRAN compiler for the EAI 640 Digital Computer does not allow multiple-entry-point subprograms, a separate subprogram, MAP2L, was written.

FORTRAN Listings

```
      SCALED FRACTION FUNCTION MAP2(N,XIN,YIN)
      SCALED FRACTION XIN,YIN,YINCR,XHI,XLO,XFRAC,ZL,ZR,Y1,Y2,
    1 MAP2,XVALS(12,8,6),YVALS(8,6),ZVALS(10,8,12)
      COMMON/MAPS/XVALS,YVALS,ZVALS,IX(6),JY(6),NX(6),NY(6),KX(6),KY(6)
C.....IF ENTRY IS FROM MAP2L LOCK UP OUTPUT ONLY.
      IF(N.GT.6) GO TO 400
      NYC=NY(N)
      NXP=NX(N)
      I=IX(N)
      J=JY(N)
  100 Y1=YIN-YVALS(J,N)
      IF(Y1.GT..00000S) GO TO 110
      IF(Y1.EQ..00000S) GO TO 120
      IF(J.LE.1) GO TO 140
      J=J-1
      GO TO 100
  110 Y2=YIN-YVALS(J+1,N)
      IF(Y2.LT..00000S) GO TO 180
      IF(Y2.EQ..00000S) GO TO 130
      J=J+1
      IF(J.GE.NYC) GO TO 150
      Y1=Y2
      GO TO 110
  120 YINCR=.00000S
      GO TO 190
  130 YINCR=.99999S
      GO TO 190
  140 YINCR=.00000S
      GO TO 160
  150 YINCR=.99999S
```

```
        J=J-1
  160 IF(KY(N).GE.25) GO TO 500
        KY(N)=KY(N)+1
        GO TO 200
  180 YINCR=Y1/(Y1-Y2)
  190 KY(N)=0
  200 XLO=XVALS(I,J,N)+YINCR*(XVALS(I,J+1,N)-XVALS(I,J,N))
        IF(XIN.GT.XLO) GO TO 210
        IF(XIN.EQ.XLO) GO TO 220
        IF(I.LE.1) GO TO 240
        I=I-1
        GO TO 200
  210 XHI=XVALS(I+1,J,N)+YINCR*(XVALS(I+1,J+1,N)-XVALS(I+1,J,N))
        IF(XIN.LT.XHI) GO TO 280
        IF(XIN.EQ.XHI) GO TO 230
        I=I+1
        IF(I.GE.NXP) GO TO 250
        XLO=XHI
        GO TO 210
  220 XFRAC=.00000S
        GO TO 290
  230 XFRAC=.99999S
        GO TO 290
  240 XFRAC=.00000S
        GO TO 260
  250 XFRAC=.99999S
        I=I-1
  260 IF(KX(N).GE.25) GO TO 500
        KX(N)=KX(N)+1
        GO TO 300
  280 XFRAC=(XIN-XLO)/(XHI-XLO)
  290 KX(N)=0
  300 IX(N)=I
        JY(N)=J
  400 ZR=ZVALS(I+1,J,N)+YINCR*(ZVALS(I+1,J+1,N)-ZVALS(I+1,J,N))
        ZL=ZVALS(I,J,N)+YINCR*(ZVALS(I,J+1,N)-ZVALS(I,J,N))
        MAP2=ZL+XFRAC*(ZR-ZL)
        RETURN
  500 CALL MOOR(N,XIN,YIN)
        RETURN
        END




        SCALED FRACTION FUNCTION MAP2L(N)
        SCALED FRACTION MAP2,MAP2L,XIN,YIN
C.....XIN AND YIN ARE DUMMY ARGUMENTS AND DO NOT AFFECT RESULT.
        MAP2L=MAP2(N,XIN,YIN)
        RETURN
        END
```

```
      SUBROUTINE MOOR(N,XIN,YIN)
      SCALED FRACTION XIN,YIN
C.....TEST FOR OPERATE MODE
      CALL ORAMI(ILOC)
      IF(ILOC.EQ.4) CALL OSH(IFRR)
      TYPE 600,N,XIN,YIN
  600 FORMAT(/7HMAP NO.,I3,20H INPUTS OUT OF RANGE/6HXIN = ,S7,
     1 8H  YIN = ,S7/)
      PAUSE
      IF(ILOC.EQ.4) CALL OSOP(IFRR)
      RETURN
      END
```

Assembly Language Listing

```
00001:
00002:
00003:
00004:
00005:
00006:
00007:
00008:                                       COMMON   MAPS
00009:                      00740    XVALS    BSS      480
00010:                      00760    YVALS    BSS      48
00011:                      01700    ZVALS    BSS      960
00012:                      00006    IX       BSS      6
00013:                      00006    JY       BSS      6
00014:                      00006    NX       BSS      6
00015:                      00006    NY       BSS      6
00016:                      00006    KX       BSS      6
00017:                      00006    KY       BSS      6
00018: 00000               00000             REL      0
00019:                                        NAME     MAP2,MAP2L
00020:                                        EXTERN   MOOR
00021:                     * COMPLETE FUNCTION GENERATION ENTRY POINT
00022: 00000  00000 00000  MAP2     ADR      0
00023: 00001  53777 00000           LX       *-1            SET UP RETURN
00024: 00002  22004 00004           ICX      4
00025: 00003  51361 00364           STX      RETURN
00026: 00004 141774 00000           LA       *-4            MAP NO. ADR
00027: 00005  26440                  SSN                    SET IND. BIT
00028: 00006 161334 00342           STA      TEM1
00029: 00007  57333 00342           LX,I     TEM1
00030: 00010  51334 00344           STX      N
00031: 00011  71331 00342           AOM      TEM1
00032: 00012 145330 00342           LA,I     TEM1
00033: 00013 161332 00345           STA      XIN
00034: 00014  71326 00342           AOM      TEM1
00035: 00015 145325 00342           LA,I     TEM1
00036: 00016 161330 00345           STA      YIN
00037:                     * SET MAP CONSTANTS AND YVALS ADDRESS   (X=N)
```

47

```
00038:  00017  142XXX  02747              LA,X    KY-1
00039:  00020  161333  00353              STA     YCNT
00040:  00021  142XXX  02755              LA,X    KY-1
00041:  00022  161332  00354              STA     YCNT
00042:  00023  142XXX  02741              LA,X    NY-1        CURVES/MAP
00043:  00024  161323  00347              STA     NYC         NYC=NY(N)
00044:  00025  142XXX  02733              LA,X    NX-1        POINTS/CURVE
00045:  00026  161322  00350              STA     NXP         NXP=NX(N)
00046:  00027  142XXX  02717              LA,X    IY-1
00047:  00030  161321  00351              STA     I           IOLD=IY(N)
00048:  00031  142XXX  02725              LA,X    JY-J        ACCUM=JOLD
00049:  00032  22777   00001              DCX     1           X=N-1
00050:  00033  26500                      EX·                 A=N-1, X=JOLD
00051:  00034  31300   00334              M       MAXNCV
00052:  00035  26540                      EQ
00053:  00036  161303  00341              STA     DEL         =MAXNCV*(N-1)
00054:  00037  151273  00332              A       YV
00055:  00040  161302  00342              STA     TEM1        =A,N
00056:                          *  DETERMINE  Y  INTERVAL  (Y=J=JOLD)
00057:  00041  141305  00346      LOOP1   LA      YIN
00058:  00042  177300  00342              S,IX    TEM1        Y(J,N)
00059:  00043  27412                      SMZ                 ·  ACC=Y1
00060:  00044  41012   00056              J       LOOP2
00061:  00045  27402                      SM
00062:  00046  41055   00123              J       STYINC      ACC=0
00063:  00047  26500                      EX                  ACC=J
00064:  00050  121267  00337              C       ONE
00065:  00051  27402                      SG
00066:  00052  41024   00076              J       Y2SML
00067:  00053  26500                      EX                  X=J
00068:  00054  22777   00001              DCX     1           X=J=J-1
00069:  00055  41764   00041              J       LOOP1
00070:  00056  161265  00343      LOOP2   STA     TEM2        =Y1
00071:  00057  22001   00001              ICX     1           X=J+1
00072:  00060  141256  00345              LA      YIN
00073:  00061  177251  00342              S,IX    TEM1        Y(J+1,N)
00074:  00062  27414                      SPZ                 ACC=Y2
00075:  00063  41030   00113              J       CALC1
00076:  00064  27404                      SP
00077:  00065  41007   00074              J       YEQJ1
00078:  00066  26500                      EX                  ACC=J+1
00079:  00067  121260  00347              C       NYC
00080:  00070  27404                      SL
00081:  00071  41010   00101              J       Y2BIG
00082:  00072  26500                      EX                  X=J=J+1
00083:  00073  41763   00056              J       LOOP2       ACC=Y2
00084:  00074  141244  00340      YEQJ1   LA      MAXINC      ='77777
00085:  00075  41025   00122              J       SETJ
00086:  00076  26500       Y2SML  EX                          X=J
00087:  00077  26740              CLR
00088:  00100  41004   00104              J       TYCNT
00089:  00101  26500       Y2BIG  EX                          X=J+1
00090:  00102  22777   00001              DCX     1           X=J
00091:  00103  141235  00340              LA      MAXINC      ='77777
00092:  00104  161251  00355      TYCNT   STA     YINCR
00093:  00105  141247  00354              LA      YCNT
00094:  00106  121230  00336              C       MAXCNT
00095:  00107  27404                      SL
```

48

```
00096:  00110  41164  00274          J      ABORT
00097:  00111  71243  00354          AOM    YCNT
00098:  00112  41014  00126          J      STORJ
00099:                      * CALCULATE YINCR   (X=J+1, ACC=Y2)
00100:  00113  22100              CALC1 TCA            ACC=-Y2
00101:  00114 151227  00343        A      TEM2   Y1
00102:  00115 161225  00342        STA    TEM1   =Y1-Y2
00103:  00116  26740              CLR
00104:  00117  26540              EQ
00105:  00120 141223  00343        LA     TEM2
00106:  00121  11221  00342        D      TEM1
00107:  00122  22777  00001  SETJ  DCX    1      X=J
00108:  00123 161232  00355  STYINC STA   YINCR
00109:  00124  26740              CLR
00110:  00125 161227  00354        STA    YCNT   CLEAR COUNT
00111:  00126  51224  00352  STORJ STX    J
00112:                  * SET UP XVALS AND ZVALS ADDRESSES
00113:  00127  22777  00001        DCX    1      X=J-1
00114:  00130  26500              EX
00115:  00131 151210  00341        A      DEL
00116:  00132  31203  00335        M      MAXNPT
00117:  00133  26540              EQ
00118:  00134 161206  00342        STA    TEM1   =J,N
00119:  00135 151174  00331        A      XV
00120:  00136 161222  00360        STA    XIJN   =X(0,J,N)
00121:  00137 151176  00335        A      MAXNPT
00122:  00140 161221  00361        STA    XIJIN  =X(0,J+1,N)
00123:  00141 141201  00342        LA     TEM1   =J,N
00124:  00142 151171  00333        A      ZV
00125:  00143 161217  00362        STA    ZIJN   =Z(0,J,N)
00126:  00144 151171  00335        A      MAXNPT
00127:  00145 161216  00363        STA    ZIJIN  =Z(0,J+1,N)
00128:  00146  53203  00351        LX     I
00129:                  * DETERMINE X INTERVAL   (X=I=IOLD)
00130:  00147 147212  00361  LOOP3 LA,IX  XIJIN  X(I,J+1,N)
00131:  00150 177210  00360        S,IX   XIJN   X(I,J,N)
00132:  00151  31204  00355        M      YINCR
00133:  00152 157206  00360        A,IX   XIJN   ACC=XLO
00134:  00153 121172  00345        C      XIN
00135:  00154  27412              SGE
00136:  00155  41012  00167        J      LOOP4
00137:  00156  27402              SG
00138:  00157  41031  00210        J      XLORH  X=I
00139:  00160  26500              EX            ACC=I
00140:  00161 121156  00337        C      ONE
00141:  00162  27402              SG
00142:  00163  41030  00213        J      X2SML
00143:  00164  26500              EX            X=I
00144:  00165  22777  00001        DCX    1      X=I=I-1
00145:  00166  41761  00147        J      LOOP3
00146:  00167 161167  00356  LOOP4 STA    XLO
00147:  00170  22001  00001        ICY    1      X=I+1
00148:  00171 147170  00361        LA,IX  XIJIN  X(I+1,J+1,N)
00149:  00172 177166  00360        S,IX   XIJN   X(I+1,J,N)
00150:  00173  31162  00355        M      YINCR
00151:  00174 157164  00360        A,IX   XIJN   ACC=XHI
00152:  00175 121150  00345        C      XIN
00153:  00176  27414              SLE
```

49

```
00154: 00177  41031 00230              J      CALC2
00155: 00200  27404                    SL
00156: 00201  41007 00210              J      XLORH      X=I=I+1
00157: 00202  26500                    EX                ACC=I+1
00158: 00203 121145 00350              C      NXP
00159: 00204  27404                    SL
00160: 00205  41011 00216              J      X2BIG
00161: 00206  26500                    EX                X=I=I+1
00162: 00207  41760 00167              J      LOOPA      ACC=XHI
00163:                  * XIN=XLO (X=I) OR XIN=XHI (Y=I=I+1)
00164: 00210  26740             XLORH  CLR
00165: 00211 161146 00357              STA    XFRAC
00166: 00212  41031 00243              J      RANDR
00167: 00213  26500             X2SML  EX                X=I
00168: 00214  26740                    CLR
00169: 00215  41004 00221              J      TXCNT
00170: 00216  26500             X2BIG  EX                X=I+1
00171: 00217  22777 00001              DCX    1          X=I
00172: 00220 141120 00344              LA     MAXINC     ='77777
00173: 00221 161136 00357      TXCNT   STA    XFRAC
00174: 00222 141131 00353              LA     XCNT
00175: 00223 121113 00336              C      MAXCNT
00176: 00224  27404                    SL
00177: 00225  41047 00274              J      ABORT
00178: 00226  71125 00353              AOM    XCNT
00179: 00227  41014 00243              J      RANDR
00180:                  * CALCULATE XFRAC  (X=I+1, ACC=XHI)
00181: 00230 171126 00356      CALC2   S      XLO
00182: 00231 161111 00342              STA    TEM1       =XHI-XLO
00183: 00232  26740                    CLR
00184: 00233  26540                    EQ
00185: 00234 141111 00345              LA     XIN
00186: 00235 171121 00356              S      XLO
00187: 00236  11104 00342              D      TEM1
00188: 00237 161120 00357              STA    XFRAC
00189: 00240  22777 00001              DCX    1          X=I
00190: 00241  26740                    CLR
00191: 00242 161111 00353              STA    XCNT       CLEAR COUNT
00192:                  * SET UP REENTRY CONDITIONS  (X=I)
00193: 00243  51106 00351      RANDR   STY    I
00194: 00244  26500                    EX                ACCUM = I
00195: 00245  53077 00344              LX     N          X=MAP NO.
00196: 00246 162XXX 02717              STA,X  IX-1       IX(N)=I
00197: 00247 141103 00352              LA     J
00198: 00250 162XXX 02725              STA,X  JY-1       JY(N)=J
00199: 00251 141102 00353              LA     XCNT
00200: 00252 162XXX 02747              STA,X  KX-1       KX(N)=XCNT
00201: 00253 141101 00354              LA     YCNT
00202: 00254 162XXX 02755              STA,X  KY-1       KY(N)=YCNT
00203: 00255  53074 00351              LX     I
00204:                  * CALCULATE FUNCTION OUTPUT  (Y=I)
00205: 00256 147105 00363      INTRP   LA,IX  ZIJIN      Z(I,J+1,N)
00206: 00257 177103 00362              S,IX   ZIJN       Z(I,J,N)
00207: 00260  31075 00355              M      YINCP
00208: 00261 157101 00362              A,IX   ZIJN
00209: 00262 161060 00342              STA    TEM1       =ZL
00210: 00263  22001 00001              ICX    1          X=I+1
00211: 00264 147077 00363              LA,IY  ZIJIN      Z(I+1,J+1,N)
```

```
00212:  00265  177075  00362              S,IX    ZIJN    Z(I+1,J,N)
00213:  00266   31067  00355              M       YINCR
00214:  00267  157073  00362              A,IX    ZIJN    =ZR
00215:  00270  171052  00342              S       TEM1    =ZR-ZL
00216:  00271   31066  00357              M       XFRAC
00217:  00272  151050  00342              A       TEM1    MAP OUTPUT
00218:  00273   45071  00364              J,I     RETURN
00219:                          * MAP OUT OF RANGE
00220:  00274   60XXX        ABORT    L      MOOR
00221:  00275   YYXXX  00344           ADR    N
00222:  00276   XXXXX  00345           ADR    XIN
00223:  00277   XXXXX  00346           ADR    YIN
00224:  00300   00000  00000           ADR    0
00225:  00301   45063  00364           J,I    RETURN    OUTPUT=?
00226:                          * FUNCTION LOOKUP ONLY ENTRY POINT
00227:                          * SET UP OUTPUT TABLE ADDRESSES
00228:  00302   00000  00000        MAP2L    ADR    0
00229:  00303   53777  00302              LX     *-1       SET UP RETURN
00230:  00304   22001  00001              ICX    1
00231:  00305   51057  00364              STX    RETURN
00232:  00306  141774  00302              LA     *-4       MAP NO. ADR
00233:  00307   26440                     SSN              SET IND. BIT
00234:  00310  161032  00342              STA    TEM1
00235:  00311  145031  00342              LA,I   TEM1      ACCUM=N
00236:  00312  171025  00337              S      ONE       ACC=N-1
00237:  00313   31021  00334              M      MAXNCV
00238:  00314   26540                     EQ
00239:  00315  161024  00341              STA    DEL
00240:  00316  141034  00352              LA     J
00241:  00317  171020  00337              S      ONE       ACC=J-1
00242:  00320  151021  00341              A      DEL
00243:  00321   31014  00335              M      MAXNPT
00244:  00322   26540                     EQ               ACC=J,N
00245:  00323  151010  00333              A      ZV
00246:  00324  161036  00362              STA    ZIJN      =Z(0,J,N)
00247:  00325  151010  00335              A      MAXNPT
00248:  00326  161035  00363              STA    ZIJ1N     =Z(0,J+1,N)
00249:  00327   53022  00351              LX     I
00250:  00330   41726  00256              J      INTRP
00251:                          * COMMON REFERENCES
R 00252:  00331  XXXXX  77777        XV     ADR    XVALS-1
00253:  00332  XXXXX  00737        YV     ADR    YVALS-1
00254:  00333  XXXXX  01017        ZV     ADR    ZVALS-1
00255:  00334   00010              MAXNCV DEC    8
00256:  00335   00012              MAXNPT DEC    10
00257:  00336   00031              MAXCNT DEC    25
00258:  00337   00001              ONE    OCT    1
00259:  00340   77777              MAXINC OCT    77777
00260:  00341   00000  00000        DEL    BSS    1,0
00261:  00342   00000  00000        TEM1   BSS    1,0
00262:  00343   00000  00000        TEM2   BSS    1,0
00263:  00344   00000  00000        N      BSS    1,0
00264:  00345   00000  00000        XIN    BSS    1,0
00265:  00346   00000  00000        YIN    BSS    1,0
00266:  00347   00000  00000        NYC    BSS    1,0
00267:  00350   00000  00000        NYP    BSS    1,0
00268:  00351   00000  00000        I      BSS    1,0
00269:  00352   00000  00000        J      BSS    1,0
```

51

```
00270:  00353   00000  00000    XCNT    BSS      1,0
00271:  00354   00000  00000    YCNT    BSS      1,0
00272:  00355   00000  00000    YINCR   BSS      1,0
00273:  00356   00000  00000    YLO     BSS      1,0
00274:  00357   00000  00000    YFRAC   BSS      1,0
00275:  00360   00000  00000    XIJN    BSS      1,0
00276:  00361   00000  00000    XIJIN   BSS      1,0
00277:  00362   00000  00000    ZIJN    BSS      1,0
00278:  00363   00000  00000    ZIJIN   BSS      1,0
00279:  00364   00000  00000    RETURN  BSS      1,0
00280:                  00000            END      0
```

APPENDIX E

ANALOG PROGRAM - PATCHING DIAGRAMS, POTENTIOMETER SETTINGS,

AND SCALE FACTORS

The bulk of the calculations in the real-time TF30-P-3 simulation are performed on one EAI 680 Analog Computer and two EAI 231-R Analog Computers. Figures 18 to 20 contain the analog patching diagrams for those computers.

Table XIV contains a list of potentiometer definitions and settings for the analog portion of the simulation. Table XV contains a list of scale factors for the analog variables.

The EAI 680 Analog Computer has a complement of 24 quarter-square multipliers. This complement can effectively be increased by six by using the DAM feature. Digitally generated variables may be multiplied, on the 680, by analog variables with the product available at the analog. Table XVI lists the DAM variables in the TF30-P-3 hybrid simulation. Figure 18 illustrates the role of the DAM's in the TF30-P-3 simulation.

REFERENCES

1. Bentz, Charles E.; and Zeller, John R.: Integrated Propulsion Control System Program. Paper 730359, SAE, Apr. 1973.

2. McKinney, John S.: Simulation of Turbofan Engine. Part I: Description of Method and Balancing Technique. AFAPL-TR-67-125, Air Force Aeropropulsion Lab., Air Force Systems Command (AD-825197), 1967.

3. McKinney, John S.: Simulation of Turbofan Engine, Part II: User's Manual and Computer Program Listing. AFAPL-TR-67-125, Air Force Aeropropulsion Lab., Air Force Systems Command, 1967.

4. Koenig, Robert W.; and Fishbach, Laurence H.: GENENG - Program for Calculating Design Performance for Turbojet and Turbofan Engines. NASA TN D-6552, 1972.

5. Fishbach, Laurence H.; and Koenig, Robert W.: GENENG II - A Program for Calculating Design and Off-Design Performance of Two- and Three-Spool Turbofans with as many as Three Nozzles. NASA TN D-6553, 1972.

6. Seldner, Kurt; Mihaloew, James R.; and Blaha, Ronald J.: Generalized Simulation Technique for Turbojet Engine System Analysis. NASA TN D-6610, 1972.

7. Szuch, John R.: HYDES, A Generalized Hybrid Computer Program for Studying Turbojet or Turbofan Engine Dynamics. NASA TM X-3012, 1974.

8. Szuch, John R.: Analysis of Integral Lift-Fan Engine Dynamics. NASA TM X-2691, 1973.

9. Arpasi, Dale J.; Cwynar, David S.; and Wallhagen, Robert E.: Sea-Level Evaluation of Digitally Implemented Turbojet Engine Control Functions. NASA TN D-6936, 1972.

10. Arpasi, Dale J.; Zeller, John R.; and Batterton, Peter G.: A General Purpose Digital System for On-Line Control of Airbreathing Propulsion Systems. NASA TM X-2168, 1971.

11. Shapiro, Ascher H.: The Dynamics and Thermodynamics of Compressible Fluid Flow. Vol. I., Ronald Press Co., 1953.

12. Cwynar, David S.; and Batterton, Peter G.: Digital Implementation of the TF30-P-3 Turbofan Engine Control. NASA TM X-3105, 1974.

13. Hart, Clint E.: Function Generation Subprograms for use in Digital Simulations. NASA TM X-71526, 1974.

54

(a) Power lever angle, 15°

```
PØ      =   1Ø.132   N/SQ CM      (   14.695    PSIA   )
TØ      =   288.14   K            (   518.66    R      )
MØ      =   .ØØØØ
P2      =   1Ø.132   N/SQ CM      (   14.695    PSIA   )
T2      =   288.14   K            (   518.66    R      )
PLA     =   15.Ø6    DEG
WF4     =   .126Ø    KG/SEC       (    .2779    LBM/SEC)
WF7     =   .ØØ23    KG/SEC       (    .ØØ51    LBM/SEC)
WF17    =   .ØØ66    KG/SEC       (    .Ø146    LBM/SEC)
XBL7    =   .ØØ1Ø9
XBL12   =   .686Ø3
AN      =   .654Ø    SQ M         (   1Ø13.8    SQ IN  )
XNH     =   997Ø.    RPM
XNL     =   3962.    RPM
PS22    =   12.915   N/SQ CM      (   18.731    PSIA   )
PS3     =   32.11    N/SQ CM      (   46.58     PSIA   )
WA2     =   4Ø.Ø2    KG/SEC       (   88.24     LBM/SEC)
T22     =   322.56   K            (   58Ø.62    R      )
T3      =   425.2    K            (   765.3     R      )
T4      =   755.2    K            (   1359.3    R      )
T6      =   6Ø6.1    K            (   1Ø91.Ø    R      )
WAR22M  =   1Ø.8Ø5   KG/SEC       (   23.823    LBM/SEC)
P3Q22   =   2.3632
```

(b) Power lever angle, 70°

```
PØ      =   1Ø.132   N/SQ CM      (   14.695    PSIA   )
TØ      =   288.14   K            (   518.66    R      )
MØ      =   .ØØØØ
P2      =   1Ø.132   N/SQ CM      (   14.695    PSIA   )
T2      =   288.14   K            (   518.66    R      )
PLA     =   69.98    DEG
WF4     =   .8421    KG/SEC       (   1.8566    LBM/SEC)
WF7     =   .5737    KG/SEC       (   1.2648    LBM/SEC)
WF17    =   .ØØ13    KG/SEC       (    .ØØ29    LBM/SEC)
XBL7    =   .ØØØ85
XBL12   =   .ØØØ48
AN      =   .382Ø5   SQ M         (   592.1     SQ IN  )
XNH     =   14Ø42.   RPM
XNL     =   9336.    RPM
PS22    =   53.124   N/SQ CM      (   77.Ø5Ø    PSIA   )
PS3     =   161.39   N/SQ CM      (   234.Ø8    PSIA   )
WA2     =   1Ø4.46   KG/SEC       (   23Ø.3Ø    LBM/SEC)
T22     =   5Ø4.85   K            (   9Ø8.75    R      )
T3      =   695.3    K            (   1251.7    R      )
T4      =   1276.Ø   K            (   2296.8    R      )
T6      =   8Ø7.2    K            (   1453.1    R      )
WAR22M  =   12.819   KG/SEC       (   28.261    LBM/SEC)
P3Q22   =   2.8938
```

TABLE I. - Concluded. TELETYPE OUTPUT LISTINGS FOR SEA-LEVEL,

STANDARD-DAY, STATIC OPERATING LINE -

CLOSED-LOOP CONTROL

(c) Power lever angle, 120°

```
P0      =   10.132     N/SQ CM     (  14.695     PSIA    )
T0      =   288.14     K           (  518.66     R       )
M0      =     .0000
P2      =   10.132     N/SQ CM     (  14.695     PSIA    )
T2      =   288.14     K           (  518.66     R       )
PLA     =   119.95     DEG
WF4     =    .8403     KG/SEC      (  1.8526     LBM/SEC)
WF7     =   2.1531     KG/SEC      (  4.7468     LBM/SEC)
WF17    =   2.5718     KG/SEC      (  5.6699     LBM/SEC)
XBL7    =    .00097
XBL12   =    .00036
AN      =    .65309    SQ M        (  1012.3     SQ IN   )
XNH     =   14042.     RPM
XNL     =    9338.     RPM
PS22    =   53.124     N/SQ CM     (  77.050     PSIA    )
PS3     =   161.19     N/SQ CM     (  233.78     PSIA    )
WA2     =   104.49     KG/SEC      (  230.36     LBM/SEC)
T22     =   505.16     K           (  909.30     R       )
T3      =   711.7      K           (  1281.2     R       )
T4      =   1276.0     K           (  2296.8     R       )
T6      =   811.6      K           (  1460.9     R       )
WAR22M  =   12.823     KG/SEC      (  28.271     LBM/SEC)
P3Q22   =   2.9855
```

TABLE II. - TELETYPE OUTPUT LISTINGS FOR SIMULATED

6.096-KILOMETER (20 000-FT) ALTITUDE, MACH 1.2

FLIGHT CONDITION - CLOSED-LOOP CONTROL

(a) Power lever angle, 15°

```
P0      =   4.660      N/SQ CM     (   6.760     PSIA    )
T0      =   248.64     K           (  447.56     R       )
M0      =   1.1999
P2      =   11.205     N/SQ CM     (  16.252     PSIA    )
T2      =   320.25     K           (  576.45     R       )
PLA     =   15.01      DEG
WF4     =    .2470     KG/SEC      (   .5445     LBM/SEC)
WF7     =    .0026     KG/SEC      (   .0058     LBM/SEC)
WF17    =    .0013     KG/SEC      (   .0029     LBM/SEC)
XBL7    = -.00012
XBL12   =   .00146
AN      =   .33051     SQ M        (  512.3      SQ IN   )
XNH     =   11687.     RPM
XNL     =   7029.      RPM
PS22    =   29.453     N/SQ CM     (  42.718     PSIA    )
PS3     =   69.21      N/SQ CM     (  100.39     PSIA    )
WA2     =   76.72      KG/SEC      (  169.14     LBM/SEC)
T22     =   439.24     K           (  790.64     R       )
T3      =   564.0      K           (  1015.3     R       )
T4      =   903.0      K           (  1625.4     R       )
T6      =   634.0      K           (  1141.3     R       )
WAR22M  =   11.003     KG/SEC      (  24.257     LBM/SEC)
P3Q22   =   2.2451
```

TABLE II. - Concluded. TELETYPE OUTPUT LISTINGS FOR SIMULATED

6.096-KILOMETER (20 000-FT) ALTITUDE, MACH 1.2

FLIGHT CONDITION - CLOSED-LOOP CONTROL

(b) Power lever angle, 70°

P0	=	4.660	N/SQ CM	(	6.760	PSIA	)
T0	=	248.64	K	(	447.56	R	)
M0	=	1.1999					
P2	=	11.205	N/SQ CM	(	16.252	PSIA	)
T2	=	320.25	K	(	576.45	R	)
PLA	=	69.98	DEG				
WF4	=	.7981	KG/SEC	(	1.7596	LBM/SEC)	
WF7	=	.5511	KG/SEC	(	1.2150	LBM/SEC)	
WF17	=	-.0004	KG/SEC	(	-.0009	LBM/SEC)	
XBL7	=	.00097					
XBL12	=	.00073					
AN	=	.39264	SQ M	(	608.5	SQ IN	)
XNH	=	14296.	RPM				
XNL	=	9353.	RPM				
PS22	=	53.074	N/SQ CM	(	76.977	PSIA	)
PS3	=	155.80	N/SQ CM	(	225.97	PSIA	)
WA2	=	105.21	KG/SEC	(	231.95	LBM/SEC)	
T22	=	539.34	K	(	970.82	R	)
T3	=	763.8	K	(	1375.0	R	)
T4	=	1316.4	K	(	2369.6	R	)
T6	=	843.0	K	(	1517.5	R	)
WAR22M	=	12.591	KG/SEC	(	27.758	LBM/SEC)	
P3Q22	=	2.7806					

(c) Power lever angle, 120°

P0	=	4.660	N/SQ CM	(	6.760	PSIA	)
T0	=	248.64	K	(	447.56	R	)
M0	=	1.1999					
P2	=	11.205	N/SQ CM	(	16.252	PSIA	)
T2	=	320.25	K	(	576.45	R	)
PLA	=	119.95	DEG				
WF4	=	.8011	KG/SEC	(	1.7662	LBM/SEC)	
WF7	=	1.8866	KG/SEC	(	4.1594	LBM/SEC)	
WF17	=	2.6294	KG/SEC	(	5.7968	LBM/SEC)	
XBL7	=	.00134					
XBL12	=	.00122					
AN	=	.65423	SQ M	(	1014.0	SQ IN	)
XNH	=	14299.	RPM				
XNL	=	9356.	RPM				
PS22	=	53.087	N/SQ CM	(	76.995	PSIA	)
PS3	=	155.73	N/SQ CM	(	225.87	PSIA	)
WA2	=	105.24	KG/SEC	(	232.02	LBM/SEC)	
T22	=	539.34	K	(	970.82	R	)
T3	=	763.8	K	(	1375.0	R	)
T4	=	1315.6	K	(	2368.1	R	)
T6	=	843.0	K	(	1517.5	R	)
WAR22M	=	12.577	KG/SEC	(	27.729	LBM/SEC)	
P3Q22	=	2.8193					

TABLE III. - DIGITAL-TO-ANALOG CHANNELS AND

VARIABLES FOR TF30-P-3

DAC channel	Digital variable	Engine variable
4	Y4	Fan hub pressure ratio
5	Y5	Low-pressure-compressor pressure ratio
6	Y6	High-pressure-compressor pressure ratio
7	Y7	Total fan airflow
8	Y8	High-pressure-turbine flow parameter
9	Y9	High-pressure-turbine enthalpy parameter
10	Y10	Low-pressure-turbine flow parameter
11	Y11	Low-pressure-turbine enthalpy parameter

TABLE IV. - ANALOG-TO-DIGITAL CHANNELS AND

VARIABLES FOR TF30-P-3

ADC channel	Digital variable	Engine variable
0	X0	Fan tip pressure ratio
1	X1	Corrected fan speed
2	X2	Low-pressure-compressor corrected airflow
3	X3	Bleed-shifted low-pressure-compressor corrected speed
4	X4	Bleed-shifted high-pressure-compressor corrected speed
5	X5	High-pressure-compressor corrected speed
6	X6	High-pressure-turbine pressure ratio
7	X7	High-pressure-turbine speed parameter
8	X8	Low-pressure-turbine pressure ratio
9	X9	Low-pressure-turbine speed parameter

TABLE V. - SUPPLEMENTAL ANALOG-TO-DIGITAL CHANNELS

AND VARIABLES FOR TF30-P-3

ADC channel	Digital variable	Engine variable
10	X10	Combustor fuel flow
11	X11	High-pressure-compressor discharge static pressure
12	X12	High-pressure-turbine inlet temperature
13	X13	Nozzle area
14	X14	Low-pressure-compressor discharge static pressure
15	X15	Duct augmentor fuel flow
16	X16	Low-pressure-compressor discharge temperature
17	X17	High-pressure-compressor discharge temperature
18	X18	Core augmentor fuel flow
19	X19	Core augmentor inlet temperature
20	X20	High-pressure-compressor rotor speed
21	X21	Fraction of 7th-stage bleed
22	X22	Fraction of 12th-stage bleed
23	X23	Power lever angle

TABLE VI. - COMPONENT MAP DESIGNATIONS

FOR TF30-P-3

Map index, n	Map output variable	Equation
1	Fan corrected airflow	6
2	Fan hub pressure ratio	8
3	Low-pressure-compressor pressure ratio	14
4	High-pressure-compressor pressure ratio	20
5	High-pressure-turbine flow parameter	28
6	Low-pressure-turbine flow parameter	33

Map pair index, m	Map output variable	Equation
7	High-pressure-turbine enthalpy parameter	30
8	Low-pressure-turbine enthalpy parameter	35

TABLE VII. - TF30-P-3 FAN CORRECTED AIRFLOW DATA

1.4984   2.1342   1.0816

.3201	.4268	.5335	.6402	.7470	.8537	.9604	1.0671
.0000	.5840	.3420	.4134	.4099	.3770	.4407	.3587
.4674	.3389	.4895	.3171	.5104	.2964	.5494	.2379
.0000	.6381	.3992	.4746	.4368	.4555	.4714	.4356
.5024	.4145	.5309	.3934	.5724	.3446	.5994	.2595
.0000	.6597	.4164	.5589	.5029	.5221	.5764	.4810
.6078	.4590	.6393	.3966	.6478	.3642	.6743	.2920
.0000	.7354	.4906	.6437	.5879	.6078	.6663	.5619
.7117	.4983	.7222	.4611	.7277	.4237	.7367	.3158
.0000	.7917	.5814	.7471	.6408	.7328	.7397	.6909
.8106	.6325	.8251	.5905	.8381	.5061	.8391	.3634
.0000	.8665	.6858	.8665	.7592	.8600	.8236	.8453
.8791	.8228	.9630	.7631	.9930	.6718	.9990	.4326
.0000	.9730	.7792	.9730	.9485	.9708	1.0274	.9643
1.0974	.9505	1.1503	.9236	1.2027	.8354	1.2187	.5299
.0000	1.0556	.8516	1.0556	1.0314	1.0543	1.2092	1.0513
1.2947	1.0469	1.3681	1.0331	1.4135	.9993	1.4310	.6165

TABLE VIII. - TF30-P-3 FAN HUB PRESSURE RATIO DATA

1.4984   2.1342   1.3599

.3201	.4268	.5335	.6402	.7470	.8537	.9604	1.0671
.0000	.5135	.3746	.5135	.4370	.5135	.4745	.5135
.4995	.5135	.5244	.5131	.5494	.5122	.5744	.5117
.0000	.5444	.3746	.5444	.4370	.5444	.4745	.5444
.4995	.5444	.5244	.5435	.5494	.5430	.5994	.5426
.0000	.5893	.4370	.5938	.5119	.5961	.5409	.5938
.5764	.5933	.6078	.5929	.6293	.5911	.6743	.5870
.0000	.6119	.4495	.6618	.5424	.6668	.5879	.6654
.6293	.6622	.6663	.6591	.6953	.6563	.7367	.6504
.0000	.6210	.5089	.7116	.5814	.7234	.6408	.7302
.6928	.7348	.7807	.7411	.8106	.7425	.8391	.7434
.0000	.6663	.5269	.7892	.6858	.8204	.7592	.8304
.8236	.8372	.8791	.8417	.9260	.8454	.9990	.8522
.0000	.6799	.6078	.8585	.7792	.9106	.8646	.9342
.9485	.9551	1.0274	.9718	1.0974	.9832	1.2187	.9972
.0000	.7252	.6703	.9410	.8516	.9995	1.0314	1.0539
1.1213	1.0806	1.2092	1.1074	1.2947	1.1323	1.4310	1.1650

TABLE IX. - TF30-P-3 LOW-PRESSURE-COMPRESSOR

PRESSURE RATIO DATA

1.1915   2.4246   1.8953

.3637	.6061	.7274	.8486	.9698	.9941	1.0062	1.0547
.1747	.3980	.3136	.3942	.3336	.3931	.3786	.3881
.4011	.3824	.4394	.3592	.4559	.3429	.5640	.1895
.2939	.5496	.4400	.5344	.4648	.5314	.5115	.5163
.5344	.5049	.5784	.4746	.5956	.4526	.7022	.1895
.3971	.6937	.5608	.6671	.5891	.6626	.6378	.6379
.6603	.6209	.7066	.5815	.7254	.5549	.8579	.1895
.5004	.8263	.6965	.8165	.7333	.8150	.8069	.8013
.8320	.7789	.8606	.7088	.8698	.6679	.9214	.1895
.6514	1.0235	.8835	1.0223	.9197	1.0113	.9683	.9571
.9818	.9192	1.0009	.8244	1.0041	.7733	1.0168	.1895
.7070	1.1068	.9327	1.0765	.9591	1.0534	.9966	.9848
1.0082	.9412	1.0231	.8442	1.0244	.7896	1.0327	.1895
.7864	1.2130	.9532	1.0993	.9748	1.0701	1.0069	.9946
1.0173	.9495	1.0314	.8510	1.0319	.7952	1.0406	.1895
.9262	1.3949	1.0096	1.1614	1.0201	1.1178	1.0336	1.0204
1.0387	.9692	1.0451	.8620	1.0468	.8070	1.0517	.1895

TABLE X. - TF30-P-3 HIGH-PRESSURE-COMPRESSOR

PRESSURE RATIO DATA

1.4352		1.9845		1.7463			
.6666	.7618	.8570	.9522	1.0000	1.0475	1.0951	
.5023	.6636	.5637	.5612	.5759	.5361	.5884	.5075
.6021	.4757	.6093	.4582	.6211	.4170	.6394	.3492
.5418	.8033	.6376	.7052	.6566	.6790	.6746	.6437
.6911	.6000	.6986	.5745	.7097	.5158	.7302	.3492
.5920	.9867	.7277	.8812	.7542	.8519	.7790	.8096
.8009	.7537	.8102	.7209	.8235	.6437	.8486	.3492
.6710	1.2679	.8443	1.1072	.8777	1.0677	.9049	1.0069
.9268	.9280	.9358	.8826	.9476	.7806	.9724	.3492
.6925	1.3534	.9128	1.2235	.9534	1.1861	.9789	1.1096
.9979	1.0143	1.0050	.9608	1.0140	.8445	1.0406	.3492
.7176	1.4495	.9713	1.3381	1.0172	1.2993	1.0409	1.2078
1.0567	1.0967	1.0621	1.0356	1.0696	.9070	1.0980	.3492
.7463	1.5368	1.0323	1.4575	1.0747	1.4009	1.0965	1.2965
1.1059	1.1659	1.1087	1.0967	1.1120	.9542	1.1195	.3492

TABLE XI. - TF30-P-3 HIGH-PRESSURE-TURBINE FLOW AND

ENTHALPY PARAMETER DATA

2.1150		1.7036		1.2828		2.3539			
.8347	.8688	.9028	.9369	.9710	1.0051	1.0391	1.0732		
.2115	.4230	.6345	.8460	1.0575	1.2690	1.4805	1.6920	1.9035	2.1148
1.2155	1.2155	1.2155	1.2155	1.2071	1.1545	1.0519	.8851	.5772	.0000
1.7372	1.6737	1.5536	1.3700	1.1137	.8545	.6214	.4096	.1977	.0000
.2115	.4230	.6345	.8460	1.0575	1.2690	1.4805	1.6920	1.9035	2.1148
1.1648	1.1648	1.1648	1.1648	1.1571	1.1096	1.0070	.8466	.5580	.0000
1.6772	1.6101	1.5007	1.3241	1.0720	.8192	.6002	.3954	.1906	.0000
.2115	.4230	.6345	.8460	1.0575	1.2690	1.4805	1.6920	1.9035	2.1148
1.1186	1.1186	1.1186	1.1186	1.1103	1.0590	.9621	.8017	.5195	.0000
1.6242	1.5536	1.4477	1.2782	1.0331	.7909	.5790	.3742	.1871	.0000
.2115	.4230	.6345	.8460	1.0575	1.2690	1.4805	1.6920	1.9035	2.1148
1.0750	1.0750	1.0750	1.0750	1.0667	1.0198	.9172	.7568	.4874	.0000
1.5607	1.5042	1.3983	1.2358	.9957	.7556	.5508	.3629	.1765	.0000
.2115	.4230	.6345	.8460	1.0575	1.2690	1.4805	1.6920	1.9035	2.1148
1.0352	1.0352	1.0352	1.0352	1.0262	.9749	.8723	.7119	.4490	.0000
1.5183	1.4653	1.3594	1.1935	.9604	.7274	.5296	.3460	.1694	.0000
.2115	.4230	.6345	.8460	1.0575	1.2690	1.4805	1.6920	1.9035	2.1148
.9974	.9974	.9974	.9974	.9884	.9364	.8338	.6735	.4105	.0000
1.4477	1.4053	1.3064	1.1475	.9258	.7062	.5120	.3354	.1624	.0000
.2115	.4230	.6345	.8460	1.0575	1.2690	1.4805	1.6920	1.9035	2.1148
.9627	.9627	.9627	.9627	.9538	.8992	.7953	.6350	.3848	.0000
1.3983	1.3594	1.2688	1.1122	.8919	.6709	.4943	.3177	.1553	.0000
.2115	.4230	.6345	.8460	1.0575	1.2690	1.4805	1.6920	1.9035	2.1148
.9300	.9300	.9300	.9300	.9211	.8723	.7697	.6144	.3656	.0000
1.3594	1.3241	1.2358	1.0805	.8594	.6497	.4731	.3036	.1483	.0000

TABLE XII. - TF30-P-3 LOW-PRESSURE-TURBINE FLOW AND

ENTHALPY PARAMETER DATA

```
    3.6257     1.8518     4.6554     3.2331
 .3703   .4629   .5555   .6481   .8333   .9259  1.0185  1.1111
 .3625   .7251  1.0877  1.4503  1.8129  2.1754  2.5380  2.9006  3.2632  3.6254
2.6885  2.6885  2.6769  2.6606  2.6419  2.6070  2.5651  2.5023  2.3277   .0000
2.6737  2.4733  1.9721  1.5195  1.2340   .9699   .7436   .5011   .2521   .0000
 .3625   .7251  1.0877  1.4503  1.8129  2.1754  2.5380  2.9006  3.2632  3.6254
2.2462  2.2462  2.2346  2.2229  2.2001  2.1764  2.1345  2.0786  1.8389   .0000
2.3440  2.0950  1.6553  1.3288  1.0785   .8503   .6304   .4106   .1972   .0000
 .3625   .7251  1.0877  1.4503  1.8129  2.1754  2.5380  2.9006  3.2632  3.6254
1.8621  1.8621  1.8505  1.8342  1.8156  1.7853  1.7458  1.6876  1.3966   .0000
2.0627  1.8299  1.4775  1.1962   .9705   .7339   .5302   .3427   .1616   .0000
 .3625   .7251  1.0877  1.4503  1.8129  2.1754  2.5380  2.9006  3.2632  3.6254
1.6061  1.5945  1.5828  1.5642  1.5391  1.5083  1.4618  1.3966  1.1638   .0000
1.8687  1.6327  1.3352  1.0863   .8713   .6724   .4784   .2974   .1325   .0000
 .3625   .7251  1.0877  1.4503  1.8129  2.1754  2.5380  2.9006  3.2632  3.6254
1.2220  1.2174  1.2104  1.1918  1.1652  1.1405  1.0940  1.0242   .8379   .0000
1.5842  1.3643  1.1154   .8858   .6883   .5108   .3556   .2198   .1002   .0000
 .3625   .7251  1.0877  1.4503  1.8129  2.1754  2.5380  2.9006  3.2632  3.6254
1.0824  1.0824  1.0707  1.0591  1.0363  1.0079   .9683   .9078   .7448   .0000
1.4710  1.2609  1.0184   .8050   .6136   .4526   .3168   .1939   .0872   .0000
 .3625   .7251  1.0877  1.4503  1.8129  2.1754  2.5380  2.9006  3.2632  3.6254
 .9776   .9776   .9753   .9590   .9348   .9124   .8729   .8147   .6634   .0000
1.3417  1.1380   .9214   .7177   .5515   .4041   .2780   .1713   .0775   .0000
 .3625   .7251  1.0877  1.4503  1.8129  2.1754  2.5380  2.9006  3.2632  3.6254
 .8961   .8961   .8845   .8752   .8519   .8263   .7867   .7262   .5935   .0000
1.2835  1.0701   .8406   .6466   .4995   .3685   .2554   .1519   .0614   .0000
```

TABLE XIII. - TF30-P-3 DIGITAL-TO-ANALOG

CONVERTER INITIAL CONDITION AND

POTENTIOMETER ADDRESS DATA

```
   .00000   .00000   .00000   .00000   .73550
   .52752   .57264   .92456   .77955   .42480
   .21479   .30936   .00000   .00000   .00000
   .00000   .00000   .00000   .00000   .00000
   .00000   .00000   .00000   .00000
 P000 P060 P100
```

TABLE XIV. - POTENTIOMETER SETTINGS

(a) EAI 680 Digital Computer

Potentiometer	Definition	Setting	Potentiometer	Definition	Setting
P00	$P_2/40$	0.3674	P19	120/150	0.8000
P01	2/3	.6667	P50	1/100	.0100
P02	0.7210/2 (eq. (10))	.3605	P51	$P_{s,2.2}/P_{2.2}$	.9100
P03	0.2796 (3/2) (eq. (10))	.4194	P52	$\sqrt{15/518.69}$ 14.696/3	.8328
P05	1/3	.3333	P55	$PLA_i/150$	.4610
P06	$P_{s,3}/3P_3$	.3143	P56	$PLA_{min}/150$	.1000
P07	$P_{s,3,i}/100$	.5774	P60	$T_2/1000$	.5187
P09	$\dot{w}_{2,1,i}/200$	.6112	P61	$\sqrt{518.69/2000}$	.5092
P10	$3(Ag_c/l)_{FID+IC}/40$	.8685	P63	$\sqrt{518.69/1000}$	.7202
P11	2/3	.6667	P64	5(0.1989)/2 (eq. (17))	.4973
P12	2/3	.6667	P65	(0.84 - 0.515)/2 (eq. (17))	.1625
P13	5(0.06)/3 (eq. (19))	.1000	P67	5(0.4689 - 0.1989)/2 (eq. (17))	.6750
P14	1/25	.0400	P69	1.16/5 (eq. (17))	.2320
P15	$\dot{w}_{2,2,i}/200$	.6112	P70	$\tau_3/10$	.6555
P16	3/40	.0750	P71	$\tau_3/10$	.6555
P17	$(Ag_c/l)_{MC}/50$	.1653	P72	$T_{3,i}/1500$	.6088
P19	$\dot{w}_{F4,MAX}/3$	.5975	P73	$30R_A/V_3$	.1506
P20	0.1852/2 (eq. (23))	.0926	P74	3/8	.3750
P21	1.0322/2 (eq. (23))	.5161	P79	$XBL7_i$	0
P22	5(0.08032)/2 (eq. (23))	.2008	P81	$\sqrt{518.69/1500}$	.5880
P23	5(0.12588)/2 (eq. (23))	.3147	P85	0.7	.7000
P25	$\dot{w}_{F4,i}/3$	.5975	P88	4(0.055) (eq. (25))	.2200
P26	$\dot{w}_{F4,min}/3$	.0948	P99	$12(14.696)\sqrt{5/518.69}/27$	.6397
P27	$\dot{w}_{F4}/30$	0	P100	$P_0/40$	.3674
P31	0.7588/2 (eq. (12))	.3794	P105	1.049/10 (eq. (54))	.1094
P32	$100\sqrt{518.69/1000}/6$ (14.696)	.8184	P106	$A_{N,min}/1600$	.3223
P33	3(0.2412)/2 (eq. (12))	.3618	P107	$160(1.622\times10^{-4})$ (eq. (25))	.2060
P35	$\dot{w}_{F7,i}/6$	0	P109	$XBL12_i$	0
P36	5/6	.8333	Q02	$[(P/P)_{LC}/(P/P)_{LC,M}]/10$	.1007
P37	5/6	.8333	Q04	$[(P/P)_{FIP}/(P/P)_{FID,M}]/10$	.1002
P39	0.84/2 (eq. (17))	.4200	Q09	$A_{N,i}/1600$	.3223
P40	$\dot{w}_{F1,7,i}/8$	0	Q12	$12(Ag_c/l)_{FID+LC}/400$	.3479
P41	5/8	.6250	Q14	$W_{2,2,i}$	.6216
P42	5/8	.6250	Q19	$3(Ag_c/l)_{HC}/80$	.3106
P43	5/8	.6250	Q22	$(P/P)_{HC}/(P/P)_{HC,M}/10$	.1003
P47	1/5	.2000	Q24	$PLA/150$	.8333

TABLE XIV. - Continued. POTENTIOMETER SETTINGS

(b) EAI 231-4 Analog Computer

Potenti-ometer	Definition	Setting	Potenti-ometer	Definition	Setting
P09	$1/2$	0.5000	Q12	$\dot{w}_{1.3,i}/300$	0.3630
P10	$(Ag_c/l)_D/375$	.7224	Q15	$3c_{p,2.2}\gamma_{1.3}/10c_{p,1.3}$	.4206
P11	$3/8$	.3750	Q16	$c_{p,1.3}\gamma_{1.3}/2c_{p,1.3}$	.6980
P12	$(Ag_c/l)_D/375$	.7224	Q20	$2(Ag_c/l)_{DAB}/75$	.4014
P13	$3/8$	.3750	Q21	$3/8$	.3750
P14	$\gamma_{1.3}/2$	.6980	Q23	$1/3$	.3333
P15	$15R_A/2V_{1.3}$	.1112	Q24	$3c_{p,1.3'}$	.7177
P16	$c_{p,3}\gamma_{1.3}/60c_{p,1.3}$	.0235	Q26	$\tau_{1.6}/100$	.3732
P19	$3/4$	.7500	Q39	$1/2$	.5000
P20	$2(Ag_c/l)_{DAB}/75$	.4014	Q40	$8/150$	.0533
P21	$3/8$	.3750	Q41	$8\eta_{DAB}HVF\,\gamma_{1.7}/10^6c_{p,1.7}$	.3815
P22	$\dot{w}_{1.6,i}/300$	.3630	Q42	$3c_{p,1.6}\gamma_{1.7}/10c_{p,1.7}$	.3843
P23	$1/5$	.2000	Q43	$1/6$	.1667
P24	$3c_{p,2}$	.7176	Q47	$4/5$	.8000
P25	$\tau_{1.6}/100$	.3732	Q48	$0.825(4/5)$ (eq. (58))	.6600
P26	$10R_A/V_{1.3}$	.1482	P50	$15K_D V_{1.3}(Ag_c/l)_D/4R_A$	.1592
P27	$T_{1.6,i}/1000$	.6640	P51	$W_{1.3,i}/8$	.3746
P40	$1/5$	.2000	P52	$(WT)_{1.3,i}/6000$	.3315
P41	$6\gamma_{1.7}/50$	.1537	P54	$15K_{DAB}V_{1.6}(Ag_c/l)_{DAB}/4R_A$	.0150
P42	$1/5$	.2000	P55	$W_{1.6,i}/8$	.3665
P44	$125R_A/V_{1.7}$	.1029	P60	$0.9\sqrt{2}\,K_{CN}$	.6522
P46	$4(1.575)/50$ (eq. (58))	.1260	P61	$135\;4000\,K_{DN}/10^4$	.4325
P48	$0.8(1.0)$ (eq. (58))	.8000	P62	$W_{1.7,i}/150$	.3386
Q10	$1/16$	.0625	P63	$(WT)_{1.7,i}/10^5$	.3376
Q11	$3/20$	.1500			

TABLE XIV. - Concluded. POTENTIOMETER SETTINGS

(c) EAI 231-5 Analog Computer

Potenti-ometer	Definition	Setting	Potenti-ometer	Definition	Setting
P00	$4(Ag_c/l)_B/2000$	0.3912	Q26	$2c_{p,4}\gamma_{4.1}/5c_{p,4.1}$	0.5388
P01	$\dot{w}_{3,i}/200$	.5700	Q28	$8/15$	.5333
P05	$\tau_3/100$	.8474	Q33	$K_{BWLT}/40$	.0250
P06	$T_{3,i}/2000$	.6358	Q34	$c_{p,3}/c_{p,6}40$	.0244
P07	$1/4$	.2500	Q35	$1/40$	.0250
P08	$1/2$	.5000	Q36	$10^5 K_{CAB}/8$	.0198
P12	R_A/V_3	.1852	Q37	$6\eta_{CAB}HVF/10^6 c_{p,7}$	.3504
P15	$8\gamma_4/5$	.1677	Q38	$4c_{p,6}/10c_{p,7}$	.4000
P16	$50R_A/4V_4$	.9510	Q39	$3/100$	.0300
P17	$5/8$	.6250	Q41	$4/5$	.8000
P20	$1/2$	.5000	Q42	$0.825 (4/5)$ (eq. (52))	.6600
P25	$\gamma_{4.1}/2$	.6609	Q45	$30/\pi I_L$	.1431
P26	$R_A/15V_{4.1}$	.1396	Q46	$15/\pi I_H$	.1672
P27	$3/8$	.3750	Q47	$3/5$	.6000
P28	$K_{PR6}/10$	.1049	Q48	$4\times10^4 \pi/30J$	.4485
P30	$(N_L/\sqrt{T_{4.1}})_M/10(N_L/\sqrt{T_{4.1}})$	.1005	Q63	$1/2$	.5000
P34	$c_{p,4.1}/8c_{p,6}$	.1281	Q91	$2/5$	.4000
P40	$4(1.3625)/50$ (eq. (52))	.1090	Q92	$5c_{p,2}/2$	.5980
P45	$N_{L,i}/2\times10^4$	.9685	Q93	$2/5$	.4000
P46	$N_{H,i}/2\times10^4$	.6966	Q98	$4\times10^4 \pi/30J$	.4485
P47	$3c_{p,2.2}/5$	.1444	P50	$K_B V_3 (Ag_c/l)_B/R_A$	.2103
P48	$(0.7158)0.8$ (eq. (52))	.5728	P51	$W_{3,i}/2$	.5210
Q00	$4(Ag_c/l)_B/2000$	.3912	P54	$W_{4,i}/2$	.6725
Q01	$1/4$	.2500	P55	$(WT)_{4,i}/5000$	.6087
Q05	$3\tau_3/400$	.6356	P56	$4R_A/V_4$	.1592
Q07	$40(0.01985)$ (eq. (27))	.7940	P57	$4000\sqrt{10}/45\,000$	.2846
Q08	$20(0.04744)$ (eq. (26))	.9488	P58	$4R_A/5V_{4.1}$	.8878
Q11	$3/20$	.1500	P59	$3\gamma_{4.1}/100c_{p,4.1}$	.1550
Q15	$3\eta_B HVF \gamma_4/5\times10^4 c_{p,4}$	.4436	P60	$25W_{4.1,i}$	.6884
Q16	$8c_{p,3}\gamma_4/c_{p,4}$	.7828	P61	$(WT)_{4.1,i}/100$	.5235
Q19	$\sqrt{10}(N_H/\sqrt{T_4})_M/5(N_H/\sqrt{T_4})$	.6321	P62	0.5	.5058
Q20	$1/2$	.5000	P63	$1/10c_{p,6}$	.3927
Q21	$1/4$	.2500	P66	$3c_{p,2.2}/4$	.1824
Q23	$K_{BWHT}/20$	.0132	P67	$6/5(c_{p,3})$	.2925
Q25	$c_{p,3}\gamma_{4.1}/5c_{p,4.1}$	.2517			

TABLE XV. - SCALE FACTORS

Variable	Scale factor	Variable	Scale factor	Variable	Scale factor
P_0	27.579 N cm² (40 psia)	$T_{1.3}$	555.55 K (1000° R)	$N_L \sqrt{2.1}$	$2 \cdot 10^4$ rpm
P_2	27.579 N cm² (40 psia)	$T_{1.6}$	555.55 K (1000° R)	N_H	$2 \cdot 10^4$ rpm
$P_{1.3}$	55.158 N cm² (80 psia)	$T_{1.7}$	2222.2 K (4000° R)	$N_H \sqrt{2.2/T_4}$	$2 \cdot 10^4$ rpm
$P_{1.3} P_2$	3	$\dot{w}_2$	272.15 kg sec (600 lbm, sec)	$N_H \sqrt{T_4}$	670.82 rpm·K$^{-1\,2}$ (500 rpm·°R$^{-1\,2}$)
$(P\,P)_{FID}$	3	$\dot{w}_{2.1}$	90.716 kg sec (200 lbm sec)	$N_H(\dot{w}_p)HT$	1461.9 kg-K-cm²-sec^{-1}rpm^{-1}·K$^{-1\,2}$_rpm (4000 lbm-°R-psia^{-1}rpm^{-1}_sec^{-1})
$P_{2.1}$	82.738 N cm² (120 psia)	$\dot{w}_{BL7}$	5.4431 kg sec (12 lbm sec)	$N_H(hp)_{NT}$	2.0792×10⁷ J-kg^{-1}-K$^{-1\,2}$_rpm (6667 Btu-lbm^{-1}°R$^{-1\,2}$_rpm^{-1})
$(P\,P)_{LC}$	5	$\dot{w}_{2.2}$	90.718 kg sec (200 lbm sec)	$N_L \sqrt{T_{4.1}}$	536.66 rpm·K$^{-1\,2}$ (400 rpm·°R$^{-1\,2}$)
$P_{2.2}$	103.42 N cm² (150 psia)	$\dot{w}_{BL12}$	2.2680 kg sec (5 lbm sec)	$N_L(\dot{w}_p)LT$	1.4619·10⁴ kg-K-cm²-sec^{-1}-rpm^{-1}-N^{-1} (4×10⁴ lbm-°R-psia^{-1}-rpm^{-1}-sec^{-1})
$P_{s.2.2}$	103.42 N cm² (150 psia)	$\dot{w}_3$	90.718 kg sec (200 lbm sec)	$N_L(hp)_{LT}$	6.2374·10⁷ J-kg^{-1}-K$^{-1\,2}$-rpm^{-1} (2·10⁴ Btu-lbm^{-1}°R$^{-1\,2}$-rpm^{-1})
$(P\,P)_{HC}$	5	$\dot{w}_{F4}$	1.3608 kg sec (3 lbm sec)	$\dot{w}_{2.1}\sqrt{2.1}/\varepsilon_{2.1}$	34.019 kg sec (75 lbm sec)
P_3	275.79 N cm² (400 psia)	$\dot{w}_4$	90.718 kg sec (200 lbm sec)	$\dot{w}_{2.2}\sqrt{2.2}/\varepsilon_{2.2}$	18.144 kg sec (40 lbm sec)
$P_{s.3}$	275.79 N cm² (400 psia)	$\dot{w}_{BLHT}$	4.5359 kg sec (10 lbm sec)	$(\Delta h)_{HT}$	3.4868·10⁵ J kg (150 Btu lbm)
P_4	275.79 N cm² (400 psia)	$\dot{w}_{4.1}$	90.718 kg sec (200 lbm sec)	$(\Delta h)_{LT}$	4.6471·10⁵ J kg (200 Btu lbm)
$P_{4.1}$	103.42 N cm² (150 psia)	$\dot{w}_{BLLT}$	2.2680 kg sec (5 lbm sec)	XPL7	1
$P_{4.1} P_4$	1	$\dot{w}_6$	90.718 kg sec (200 lbm sec)	XPI.12	1
P_5	55.158 N cm² (80 psia)	$\dot{w}_{F7}$	2.7215 kg sec (6 lbm sec)	PLA	150°
$P_5 P_{4.1}$	1	$\dot{w}_7$	90.718 kg sec (200 lbm sec)	$\dot{w}_{FZ1}$	2.2679 kg, sec (5 lbm sec)
P_6	55.158 N cm² (80 psia)	$\dot{w}_2-\dot{w}_{2.1}$	136.08 kg sec (300 lbm sec)	$\dot{w}_{FZ2}$	→
P_7	55.	$\dot{w}_{1.3}$	136.08 kg sec (300 lbm sec)	$\dot{w}_{FZ3}$	
$P_{1.6}$	555.55 K (1000° R)	$\dot{w}_{1.6}$	136.08 kg sec (300 lbm sec)	$\dot{w}_{FZ4}$	
$P_{1.7}$		$\dot{w}_{F1.7}$	3.6787 kg sec (8 lbm sec)	$\dot{w}_{FZ5}$	
T_2	2	$\dot{w}_{1.7}$	136.08 kg sec (300 lbm sec)	A_N	1.0322 m² (1600 in.²)
$(T\,T)_{FOD}$	2	$W_{2.2}$	13.608 kg (30 lbm)	$C_{d,N}A_N$	1.0322 m² (1600 in.²)
$(T\,T)_{FID}$	2	W_3	0.90718 kg (2 lbm)	$(P\,P)_{CN}$	1
$T_{2.1}$	1111.1 K (2000° R)	W_4	0.90718 kg (2 lbm)	FN7	3.6
$(T\,T)_{1C}$	833.33 K (1500° R)	$W_{4.1}$	11.340 kg (25 lbm)	$C_{d.8}P_7$ FN7	19.154 N cm² (27.78 psia)
$T_{2.2}$	2	$W_{1.3}$	3.6287 kg (8 lbm)	$(P\,P)_{DN}$	1
$(T\,T)_{HC}$	2	$W_{1.6}$	3.6787 kg (8 lbm)	FN17	3.6
T_3	1666.7 K (3000° R)	$W_{1.7}$	68.038 kg (150 lbm)	$C_{d.1.8}P_{1.7}$ FN17	19.154 N cm² (27.78 psia)
T_3	1111.1 K (2000° R)	$(WT)_4$	1259.9 kg-K (5000 lbm-°R)	$A_{1.8}$	0.51613 m² (800 in.²)
T_4	2222.2 K (4000° R)	$(WT)_{4.1}$	25.199 kg-K (100 lbm-°R)	$N_L(Q_{LT}-Q_{FOD}-Q_{FID}+IC)$	4.5192·10¹⁰ N-cm-rpm (4·10⁹ in.-lbf-rpm)
$T_{4.1}$	1388.9 K (2500° R)	$(WT)_{1.3}$	1511.9 kg-K (6000 lbm-°R)	$N_H(Q_{NT}-Q_{HC})$	2.2596·10¹⁰ N-cm-rpm (2·10⁹ in.-lbf-rpm)
T_5	1111.1 K (2000° R)	$(WT)_{1.7}$	2.5199·10⁴ kg-K (1·10⁵ lbm-°R)		
T_6	1111.1 K (2000° R)	N_1	2·10⁴ rpm		
T_7	2777.8 K (5000° R)	$N_1 \sqrt{T_1}$	2×10⁴ rpm		

TABLE XVI. - DIGITAL-TO-ANALOG

MULTIPLIER UTILIZATION

FOR TF30-P-3

DAC channel		DAM chan-nel (analog output)	DAM variable
Digital input[a]	Analog input[b]		
7	19	7	$P_2(\dot{w}_c)_{FAN}$
8	20	8	$N_H(\dot{w}_p)_{HT}$
9	21	9	$N_H(hp)_{HT}$
10	22	10	$N_L(\dot{w}_p)_{LT}$
11	23	11	$N_L(hp)_{LT}$

[a]See table III for list of digital input variables.
[b]See figure 18 for source of analog input variables.
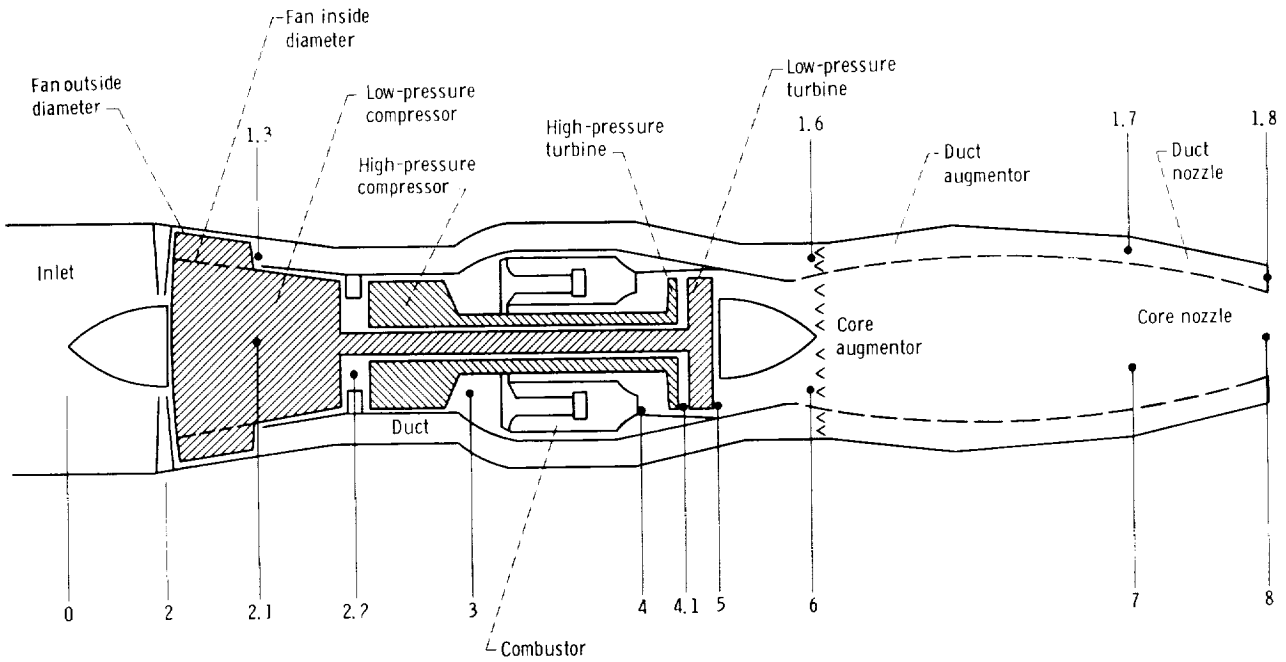
Figure 1. - Schematic of TF30-P-3 engine.
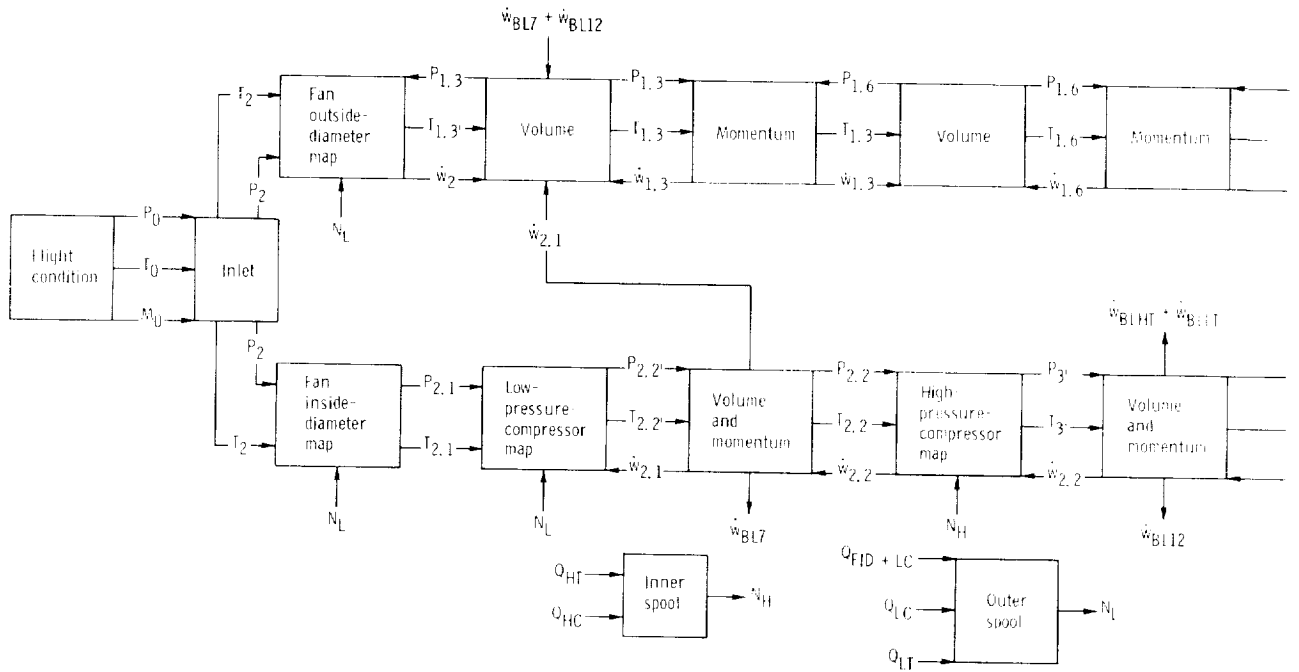
Figure 2. Real-time simulation

68
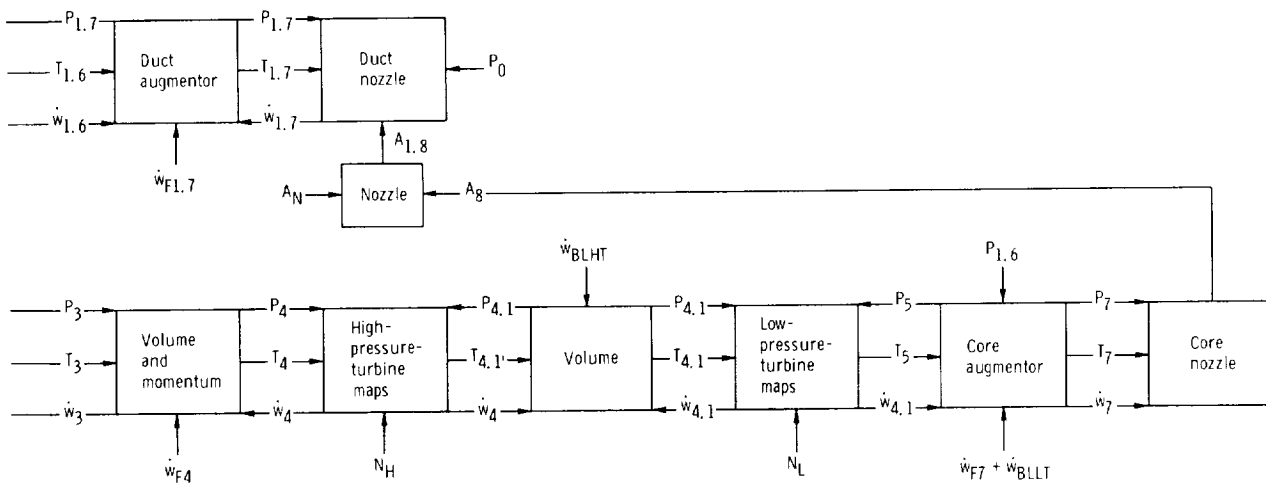
flow diagram for TF30-P-3.
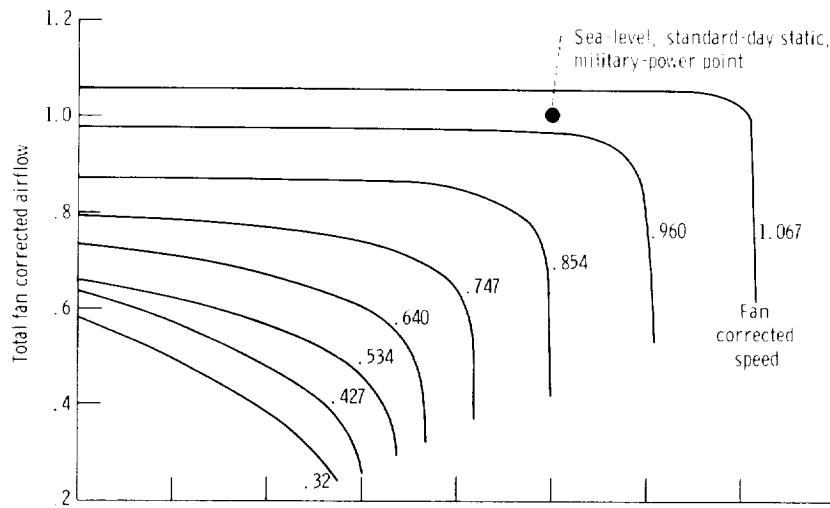
(a) Fan corrected airflow map (normalized).
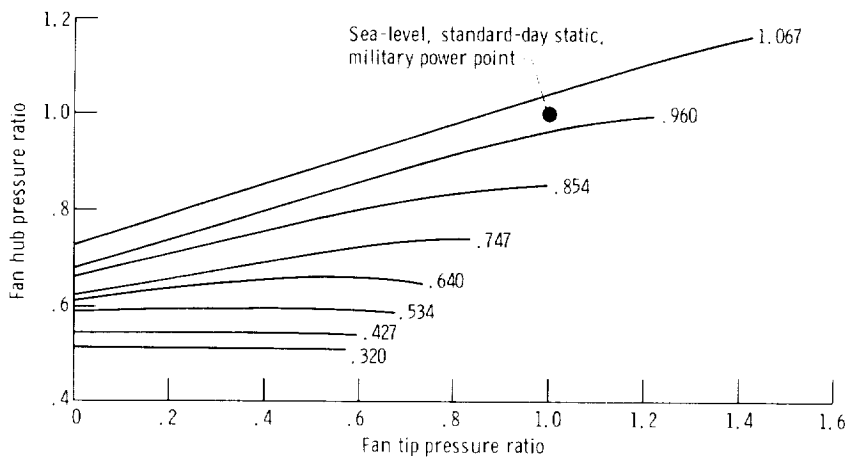
(b) Fan hub pressure ratio map (normalized).

Figure 3. - Bivariate functions representing performance of fan.

70
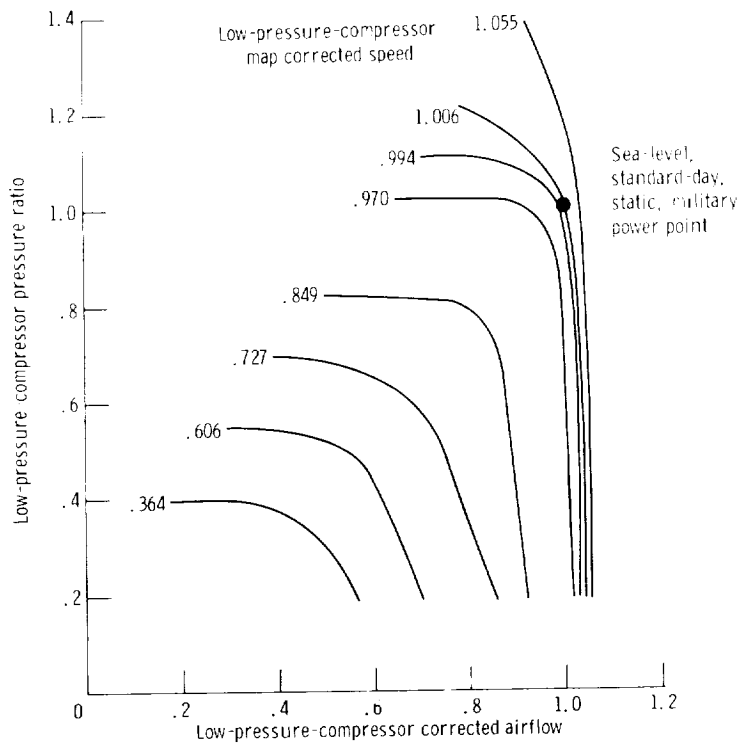
(a) Low-pressure-compressor pressure ratio map (normalized).
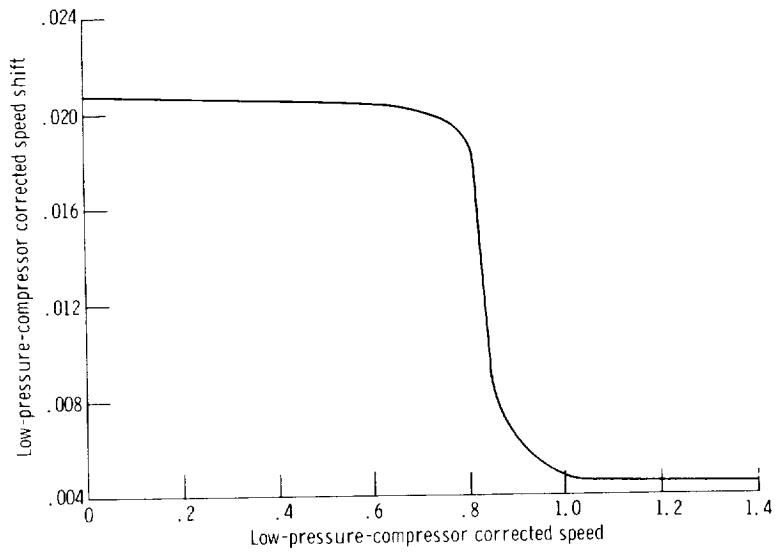
(b) Shift in low-pressure-compressor map corrected speed due to seventh-stage bleed (normalized by sea-level, standard-day, static, military power value of corrected speed).

Figure 4. - Bivariate functions representing performance of low-pressure compressor.

71
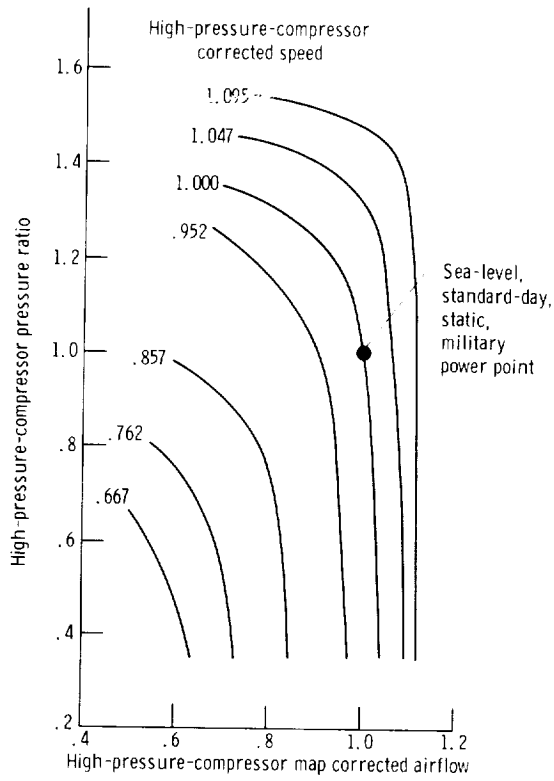
(a) High-pressure-compressor pressure ratio
map (normalized).
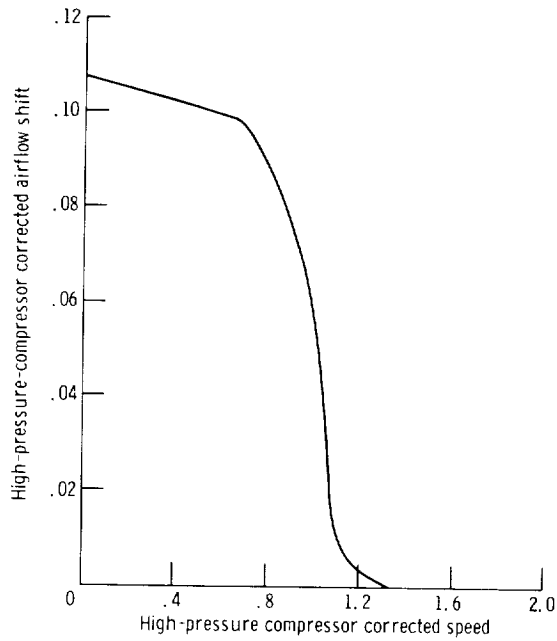
(b) Shift in high-pressure-compressor map corrected
airflow due to 12th-stage bleed (normalized by sea-
level, standard-day, static, military power values of
corrected airflow and speed).

Figure 5. – Bivariate functions representing high-
pressure-compressor performance.

(a) High-pressure-turbine flow parameter map (normalized).

(b) High-pressure-turbine enthalpy drop parameter map (normalized).
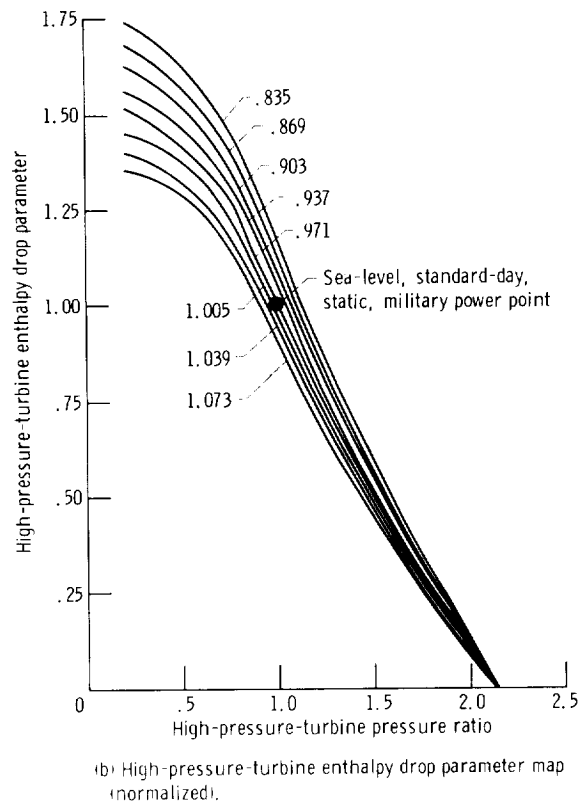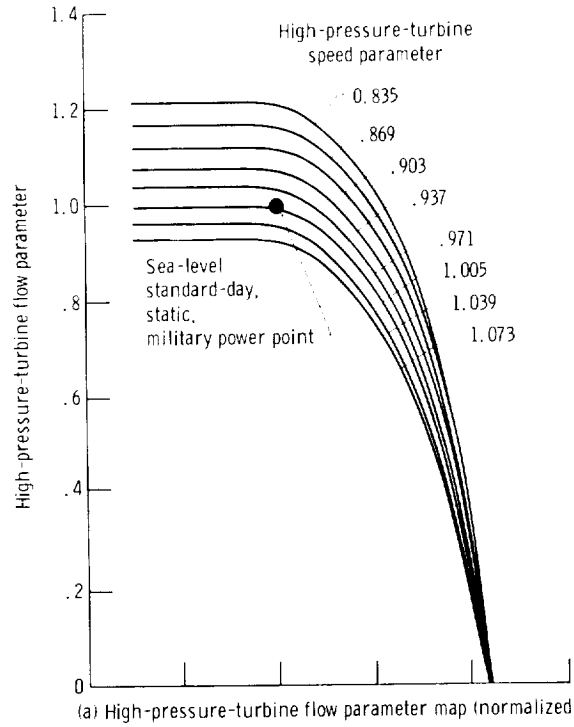
Figure 6. - Bivariate functions representing high-pressure-turbine performance.

(a) Low-pressure-turbine flow parameter map (normalized).

(b) Low-pressure-turbine enthalpy drop parameter map (normalized).
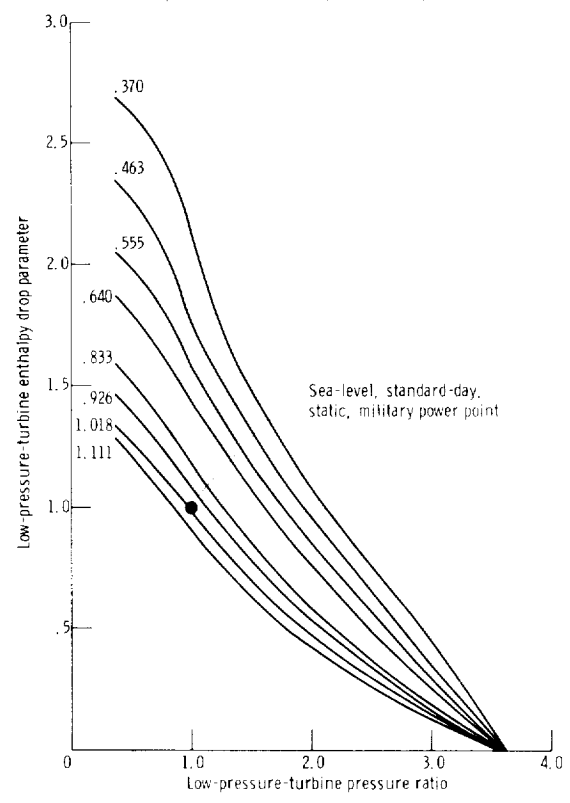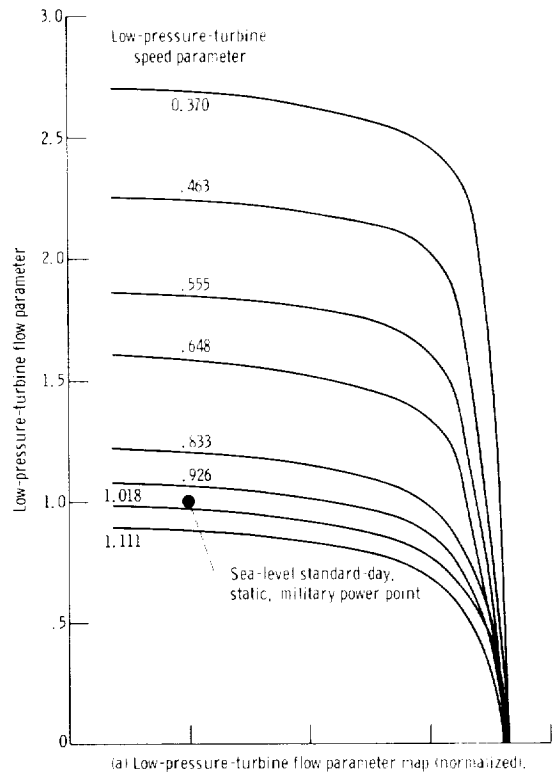
Figure 7. - Bivariate functions representing low-pressure-turbine performance.

74

EAI 640 digital	EAI 680 analog

Function generation for -
  Fan
  Low-pressure
    compressor
  High-pressure
    compressor
  Turbines
	Fan input calculations
	Low-pressure-compressor
	  input calculations
	High-pressure-compressor
	  input calculations
	640-680 Interface
	Control interface

EAI 690 hybrid

SEL 810B digital

Control

Central patching

EAI 231-R analog

Duct
Duct augmentor
Duct nozzle

EAI 231-R analog

Combustor
Turbine input calculations
Core augmentor
Core nozzle
Rotor dynamics

Figure 8. - Split of TF30-P-3 simulation computation load.
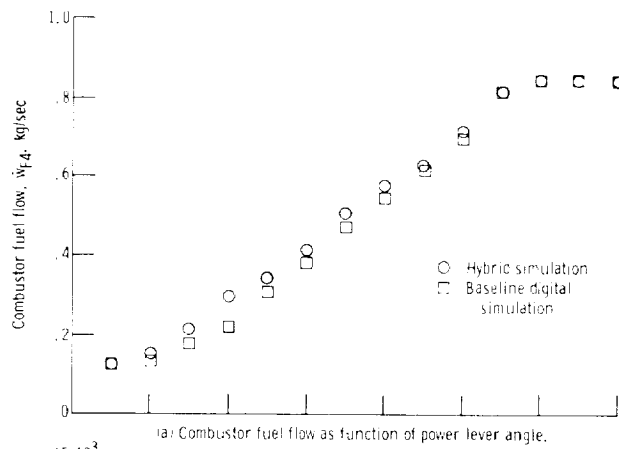
(a) Combustor fuel flow as function of power lever angle.
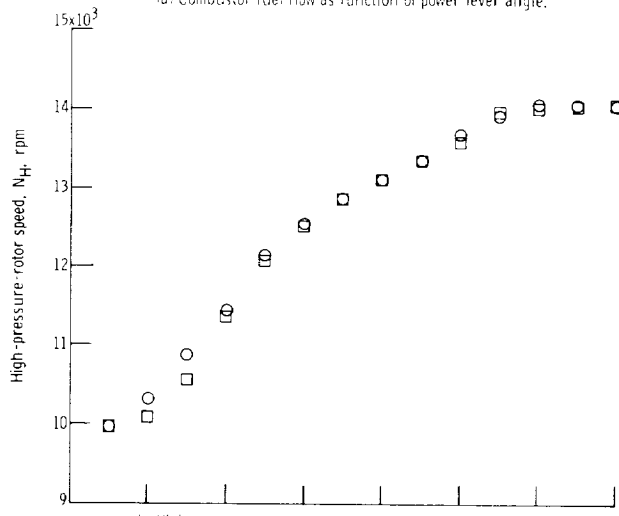
(b) High-pressure-rotor speed as function of power lever angle.
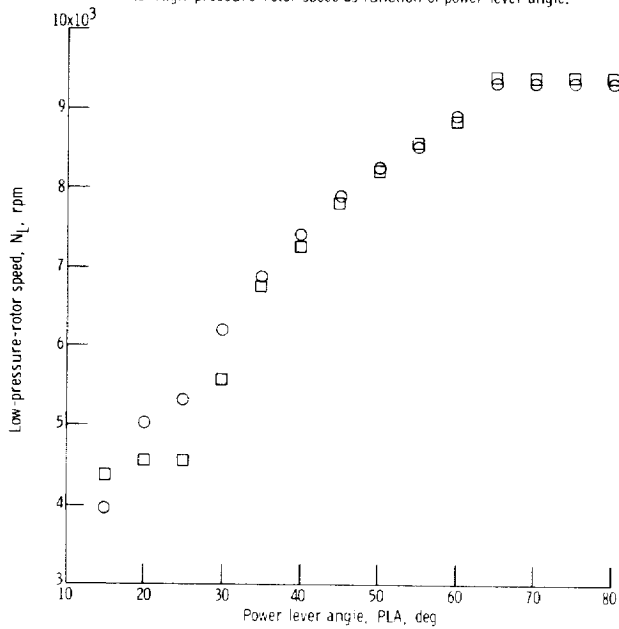
(c) Low-pressure-rotor speed as function of power lever angle.
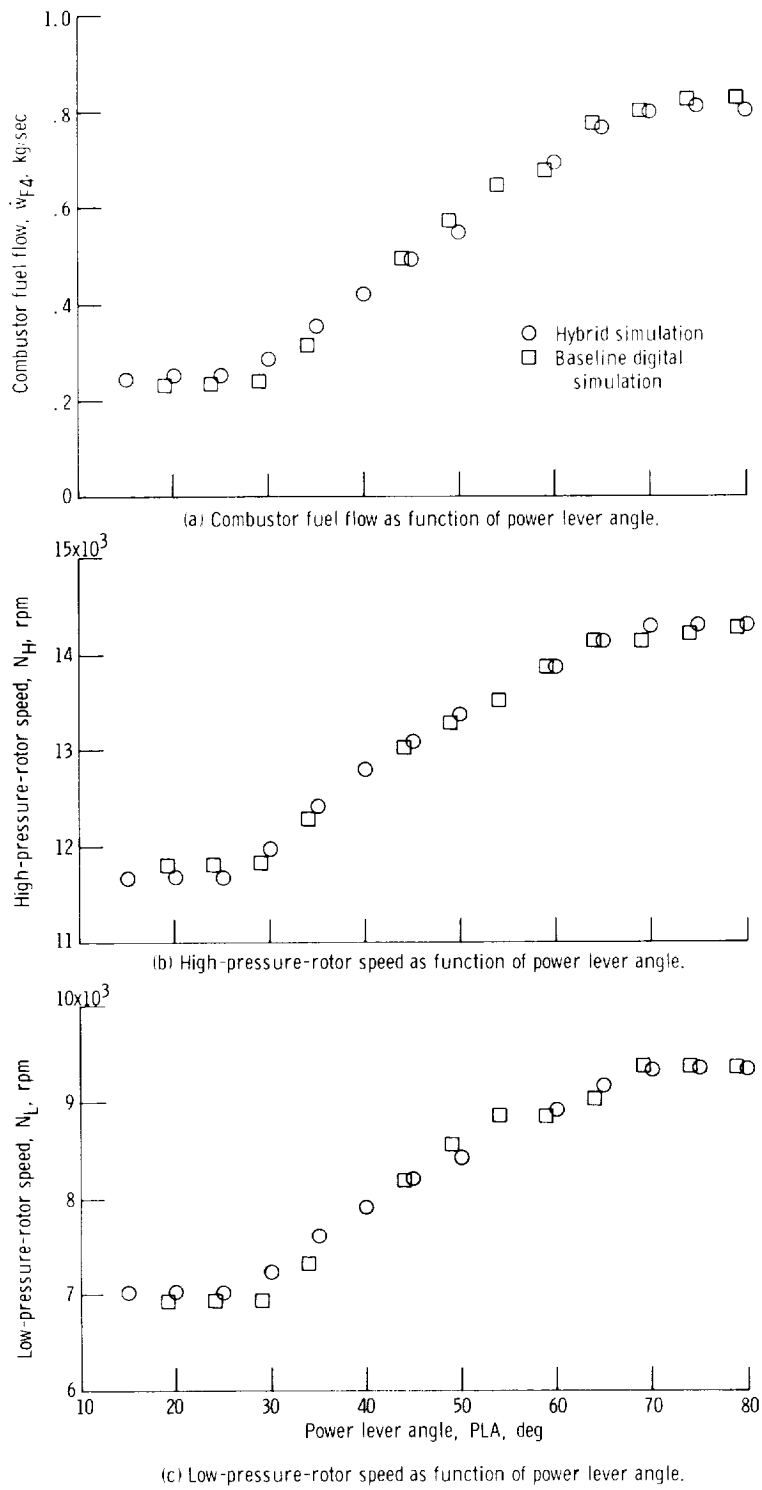
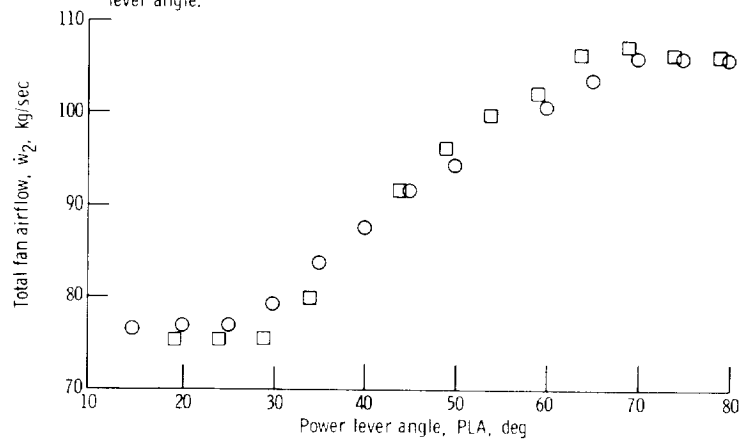Figure 9. - Comparison of hybrid and baseline digital results for sea-level, standard-day static conditions.
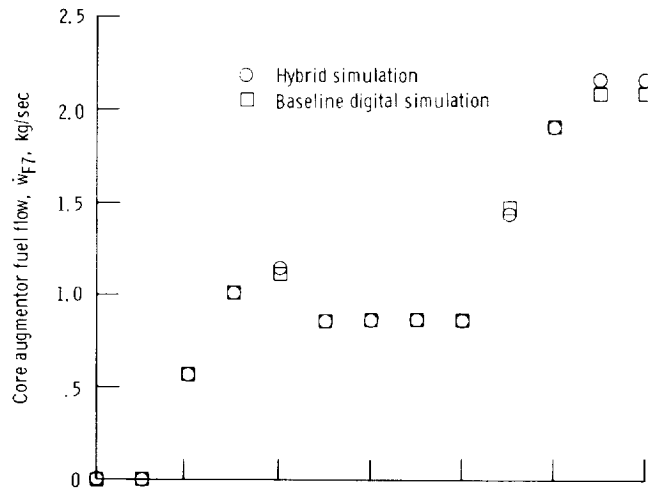
76

High-pressure-turbine inlet temperature, T_4, K

○ Hybrid simulation
□ Baseline digital simulation

(d) High-pressure-turbine inlet temperature as function of power lever angle.

High-pressure-compressor discharge static pressure, $P_{s,3}$, N/cm^2

(e) High-pressure-compressor discharge static pressure as function of power lever angle.

Total fan airflow, w_2, kg/sec

Power lever angle, PLA, deg

(f) Total fan airflow as function of power lever angle.

Figure 9. - Continued.

(g) Core augmentor fuel flow as function of power lever angle.
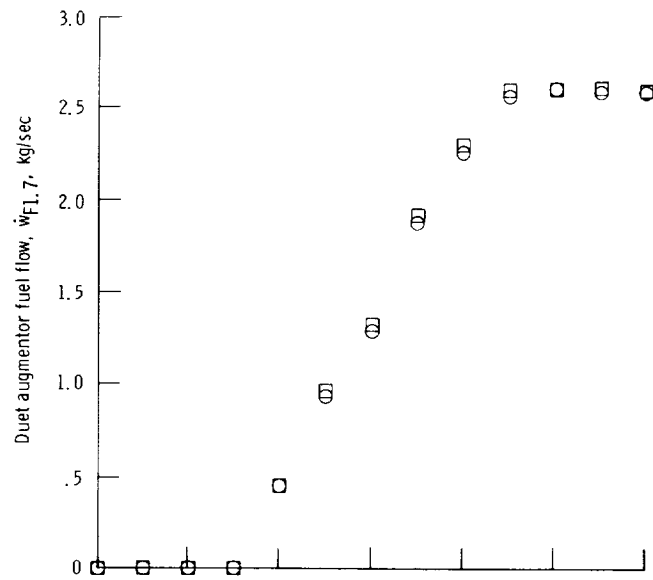
(h) Duct augmentor fuel flow as function of power lever angle.
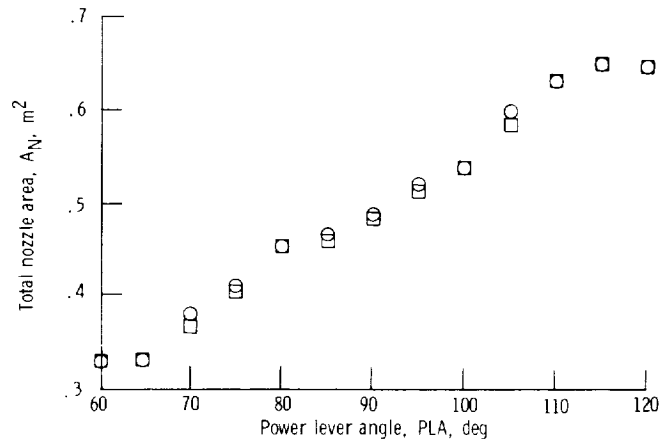
(i) Total nozzle area as function of power lever angle.

Figure 9. – Concluded.

78

(a) Combustor fuel flow as function of power lever angle.

(b) High-pressure-rotor speed as function of power lever angle.

(c) Low-pressure-rotor speed as function of power lever angle.

Figure 10. - Comparison of hybrid and baseline digital results for 6.096-kilometer (20 000-ft) simulated altitude, Mach 1.2 flight condition.
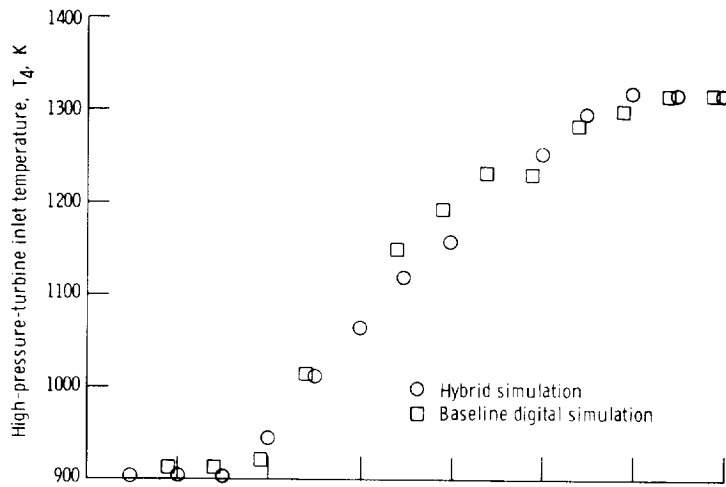
(d) High-pressure-turbine inlet temperature as function of power lever angle.
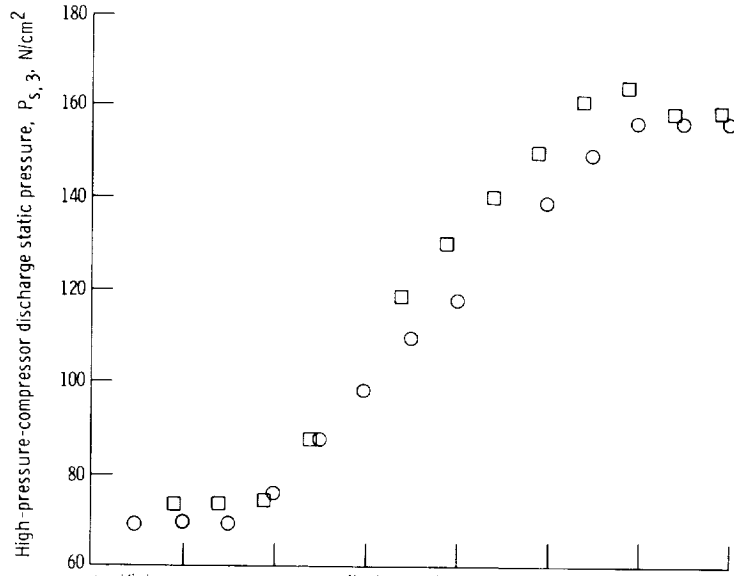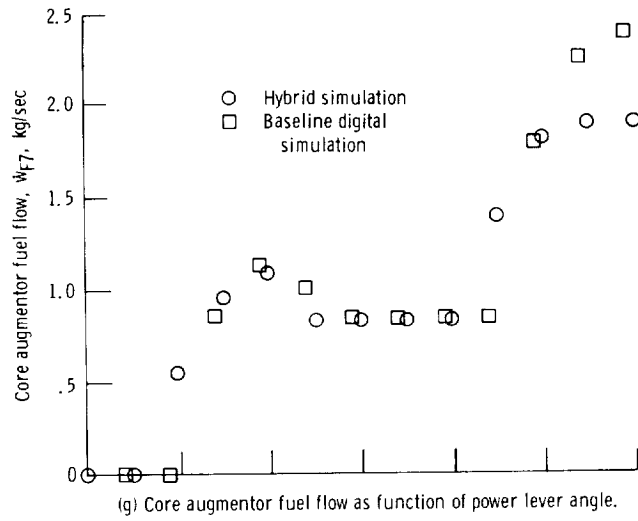
(e) High-pressure-compressor discharge static pressure as function of power lever angle.

(f) Total fan airflow as function of power lever angle.

Figure 10. - Continued.

80

(g) Core augmentor fuel flow as function of power lever angle.

(h) Duct augmentor fuel flow as function of power lever angle.
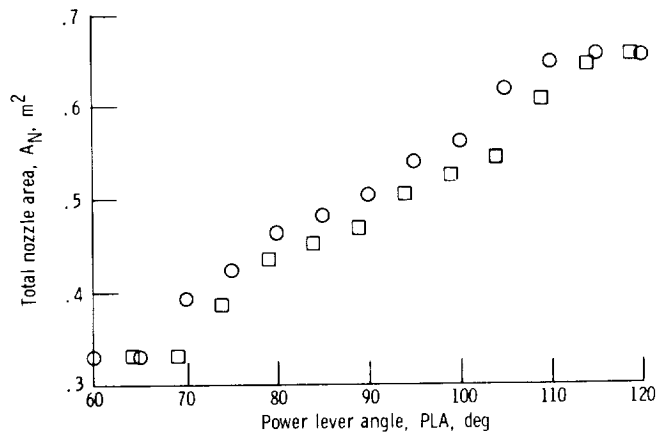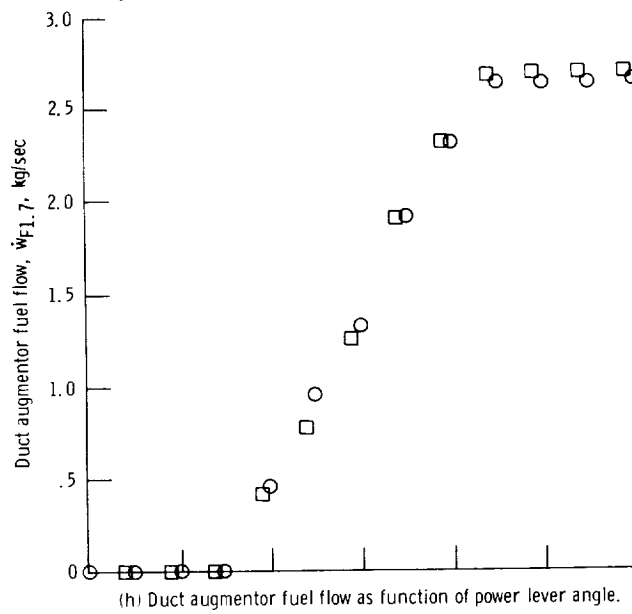
(i) Total nozzle area as function of power lever angle.
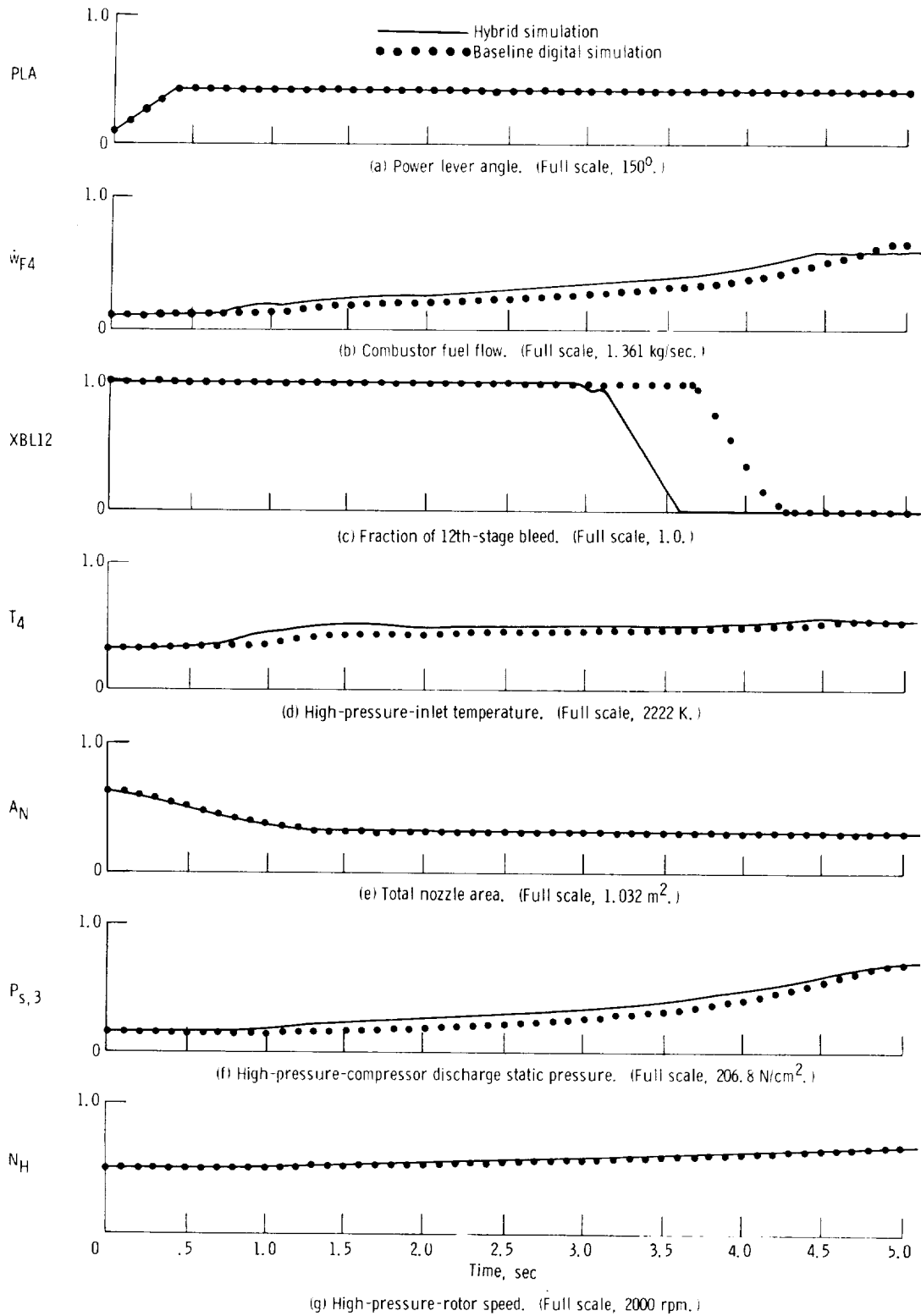
Figure 10. - Concluded.

Figure 11. - Comparison of hybrid and baseline digital simulation responses to throttle slam from power lever angle of 15° to 67° at 125 degrees per second.
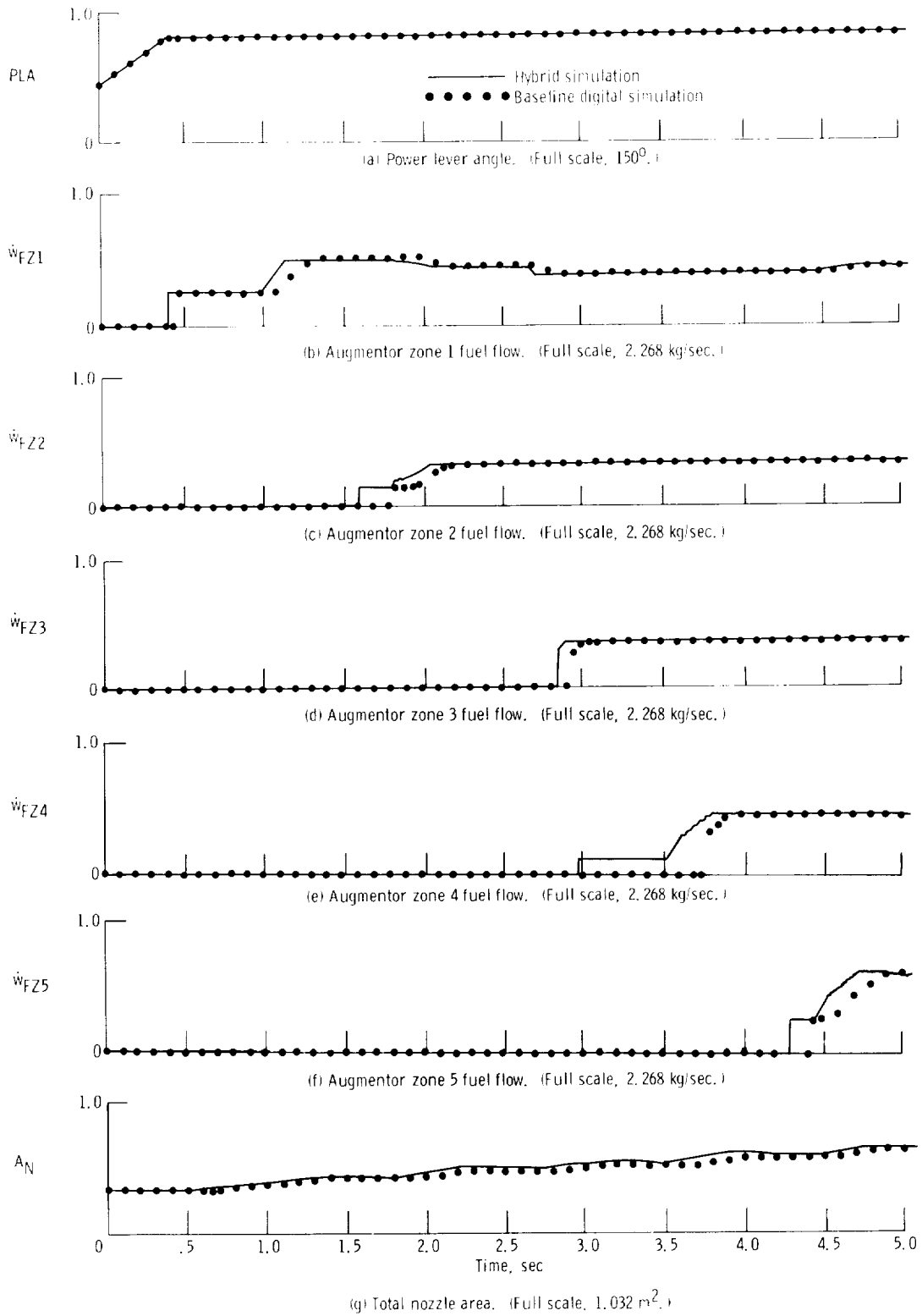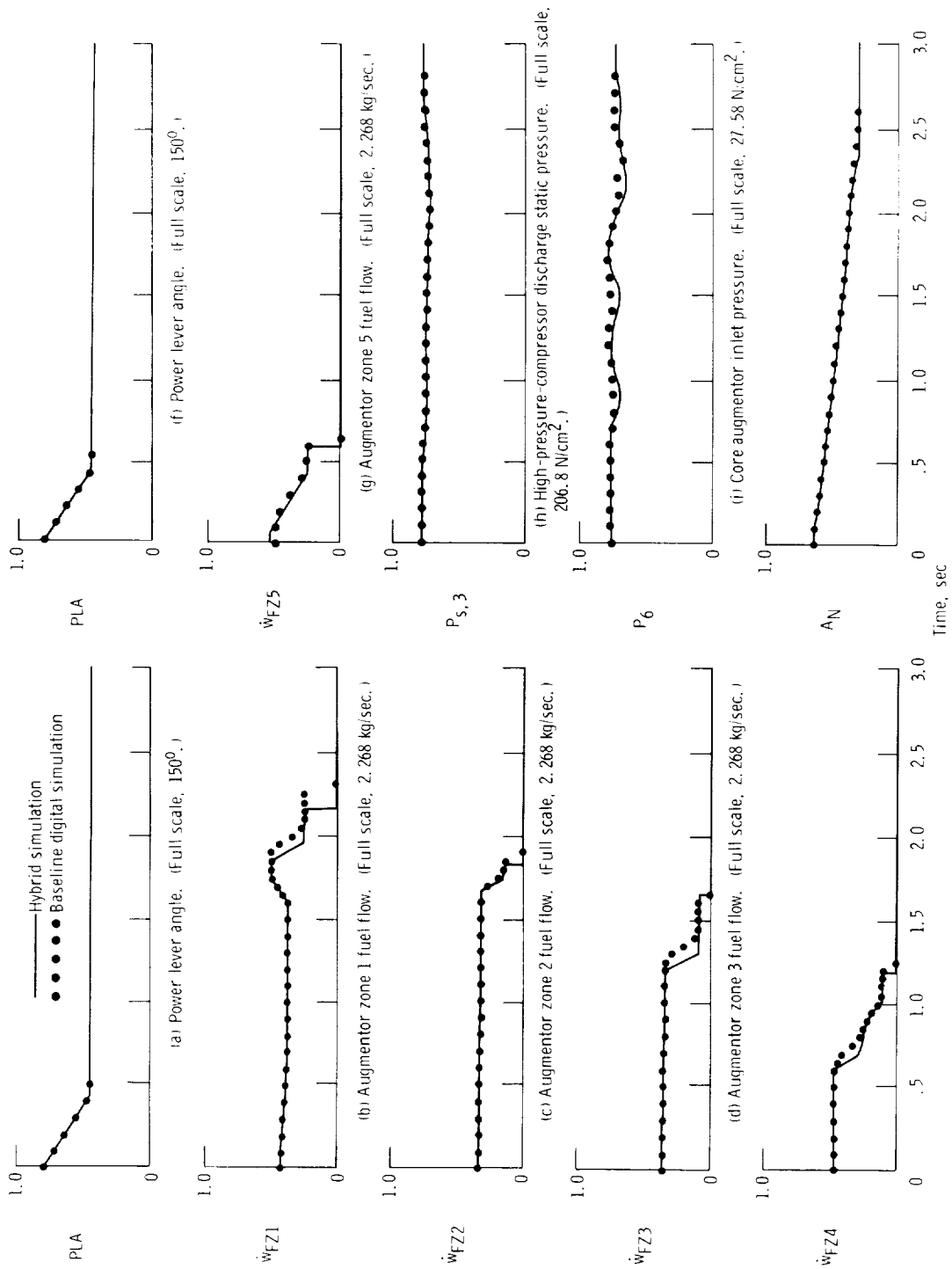
82

(a) Power lever angle. (Full scale, 150°.)

(b) Augmentor zone 1 fuel flow. (Full scale, 2.268 kg/sec.)

(c) Augmentor zone 2 fuel flow. (Full scale, 2.268 kg/sec.)

(d) Augmentor zone 3 fuel flow. (Full scale, 2.268 kg/sec.)

(e) Augmentor zone 4 fuel flow. (Full scale, 2.268 kg/sec.)

(f) Augmentor zone 5 fuel flow. (Full scale, 2.268 kg/sec.)
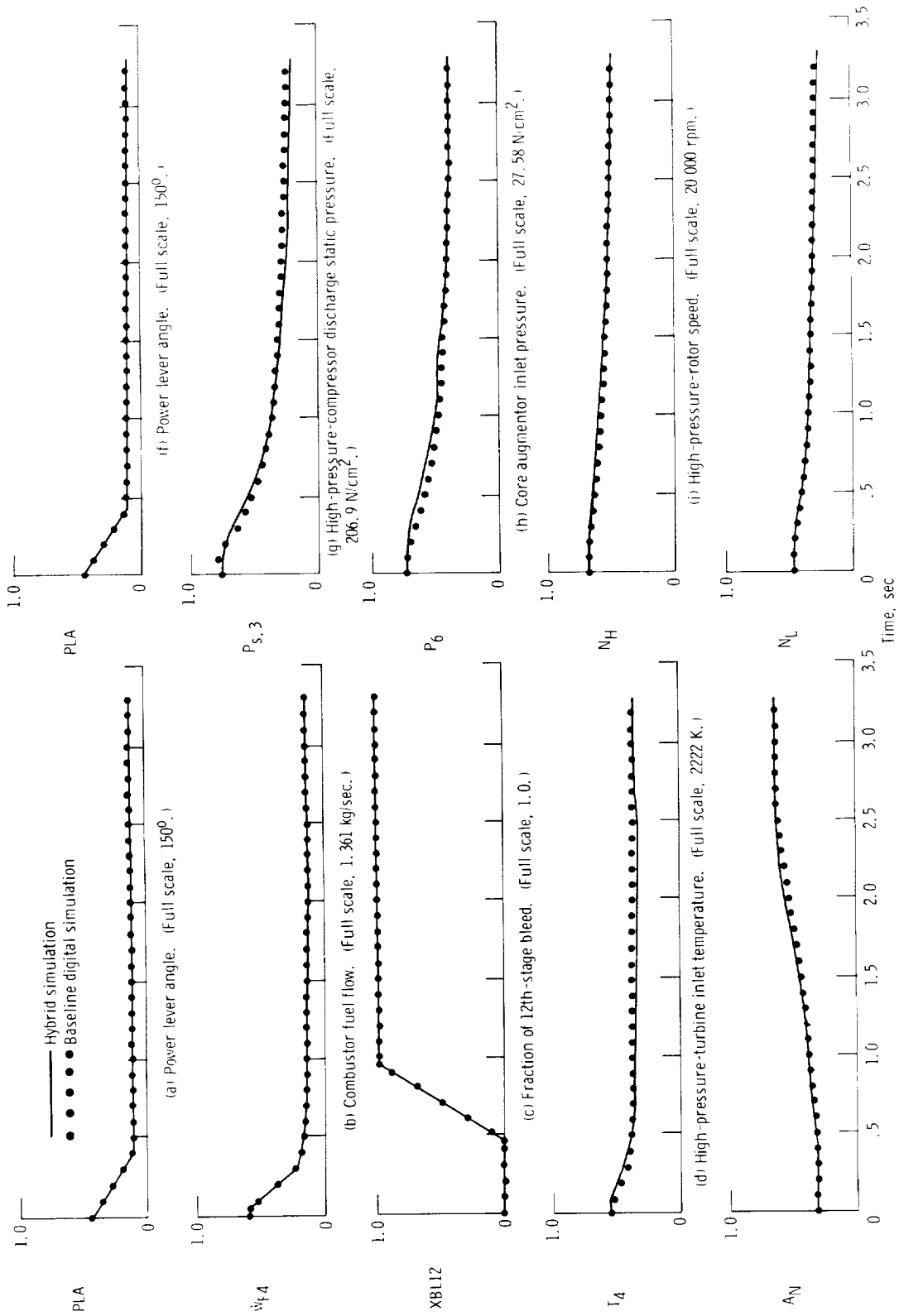
(g) Total nozzle area. (Full scale, 1.032 m².)

Figure 12. - Comparison of hybrid and baseline digital simulation responses to throttle slam from power lever angle of 67° to 120° at 125 degrees per second.

83

Figure 13. - Comparison of hybrid and baseline digital simulation responses to throttle chop from power lever angle of 120^0 to 67^0 at 125 degrees per second.

(a) Power lever angle. (Full scale, 150^0.)

(b) Augmentor zone 1 fuel flow. (Full scale, 2. 268 kg/sec.)

(c) Augmentor zone 2 fuel flow. (Full scale, 2. 268 kg/sec.)

(d) Augmentor zone 3 fuel flow. (Full scale, 2. 268 kg/sec.)

(e) Augmentor zone 4 fuel flow. (Full scale, 2. 268 kg/sec.)

(f) Power lever angle. (Full scale, 150^0.)

(g) Augmentor zone 5 fuel flow. (Full scale, 2. 268 kg/sec.)

(h) High-pressure-compressor discharge static pressure. (Full scale, 206.8 N/cm^2.)

(i) Core augmentor inlet pressure. (Full scale, 27.58 N.cm^2.)

(j) Total nozzle area. (Full scale, 1.032 m^2.)

Hybrid simulation

● ● ● ● ● Baseline digital simulation

— Hybrid simulation
•••• Baseline digital simulation

(a) Power lever angle. (Full scale, 150°.)

(b) Combustor fuel flow. (Full scale, 1.361 kg/sec.)

(c) Fraction of 12th-stage bleed. (Full scale, 1.0.)

(d) High-pressure-turbine inlet temperature. (Full scale, 2222 K.)

(e) Total nozzle area. (Full scale, 1.032 m².)

(f) Power lever angle. (Full scale, 150°.)

(g) High-pressure-compressor discharge static pressure. (Full scale, 206.9 N/cm².)

(h) Core augmentor inlet pressure. (Full scale, 27.58 N/cm².)

(i) High-pressure-rotor speed. (Full scale, 20 000 rpm.)

(j) Low-pressure-rotor speed. (Full scale, 20 000 rpm.)

Figure 14. - Comparison of hybrid and baseline digital simulation responses to throttle chop from power lever angle of 67° to 15° at 125 degrees per second.

85
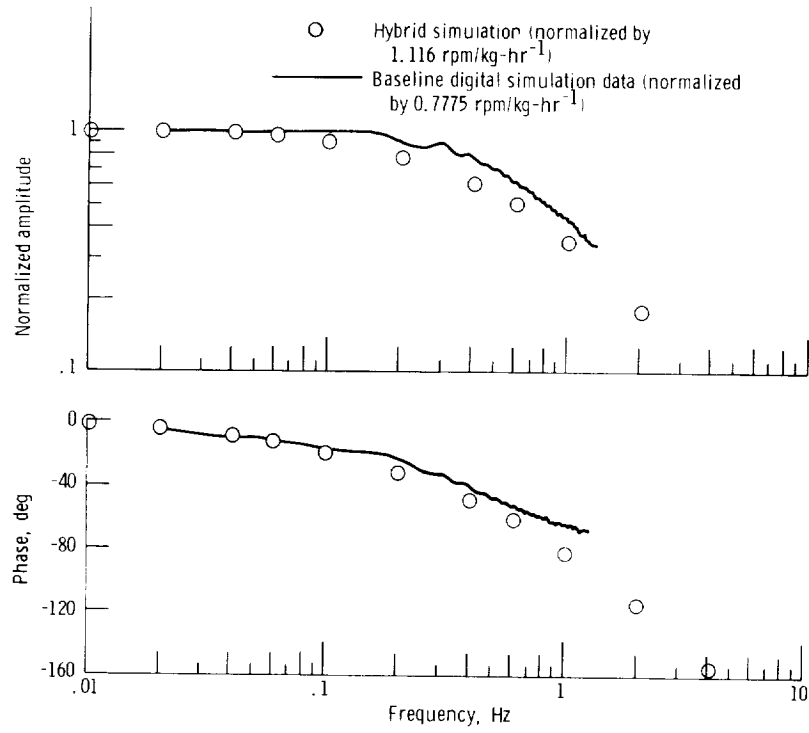
Figure 15. - Comparison of hybrid and baseline digital frequency responses of high-pressure-rotor speed to fuel flow oscillations. Sea-level, standard-day, static conditions; power lever angle, 50°.
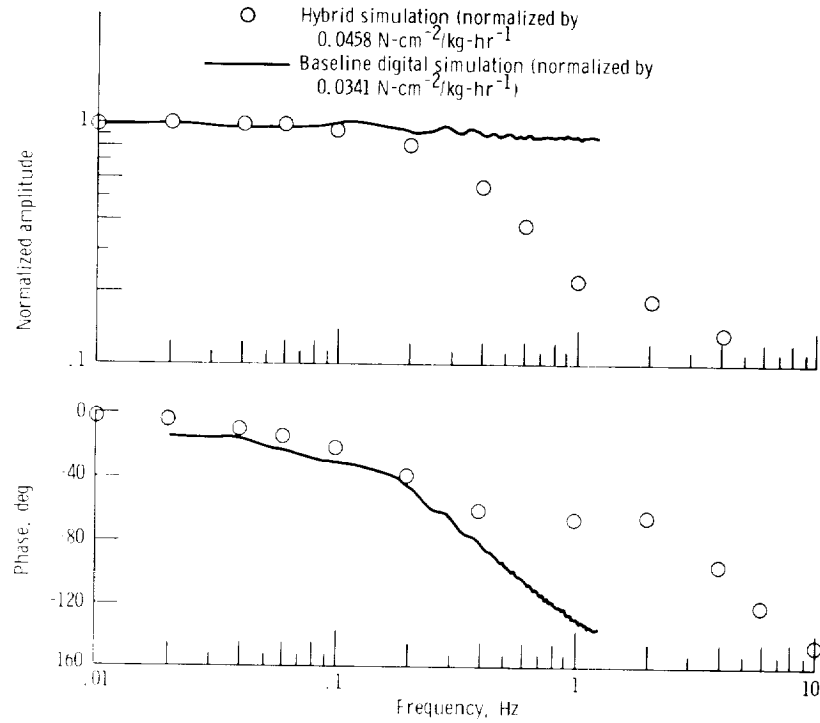
Figure 16. - Comparison of hybrid and baseline digital frequency responses of high-pressure-compressor discharge static pressure to fuel flow oscillations. Sea-level, standard-day, static conditions; power lever angle, 50°.
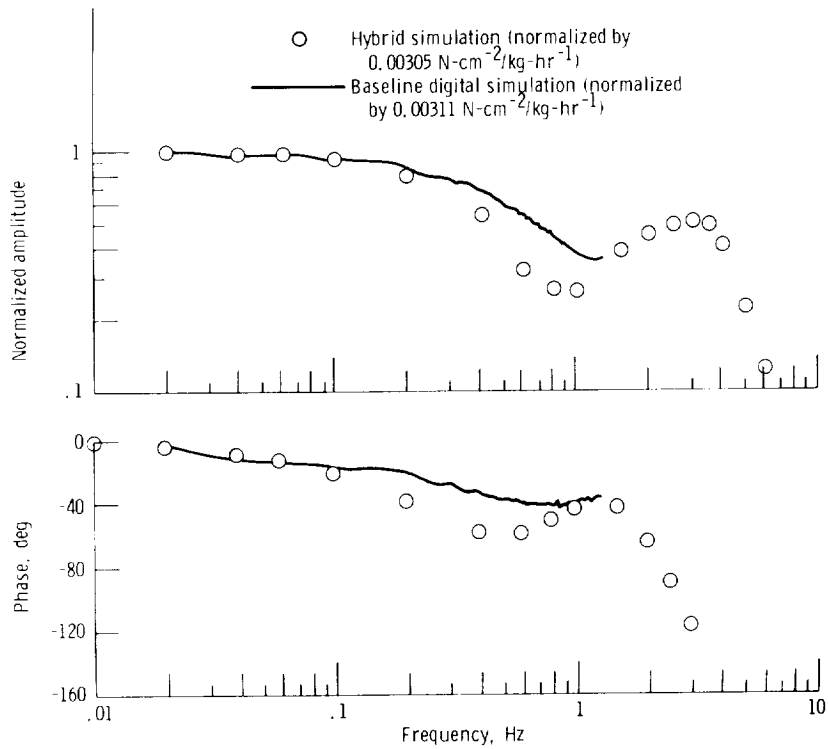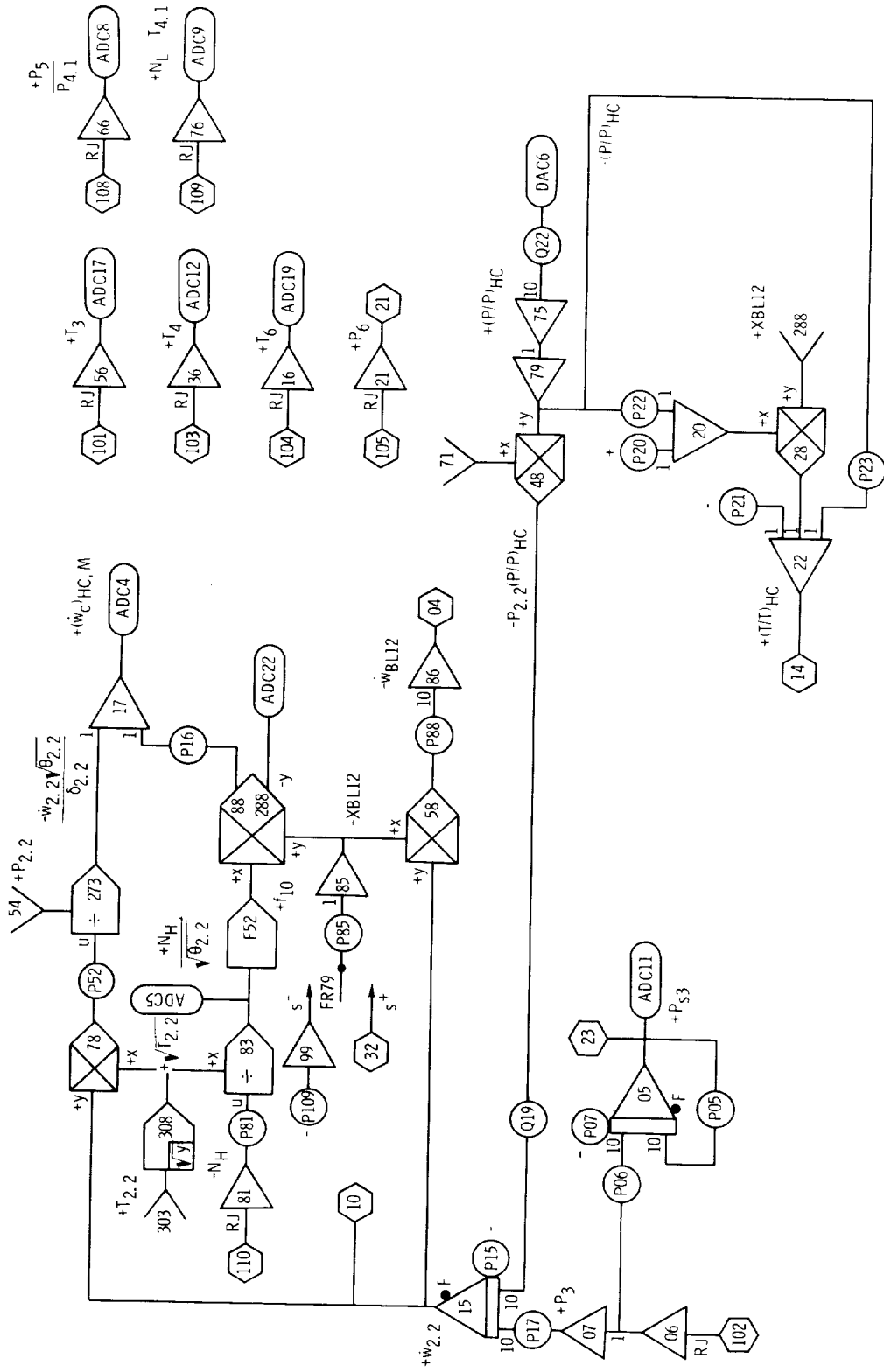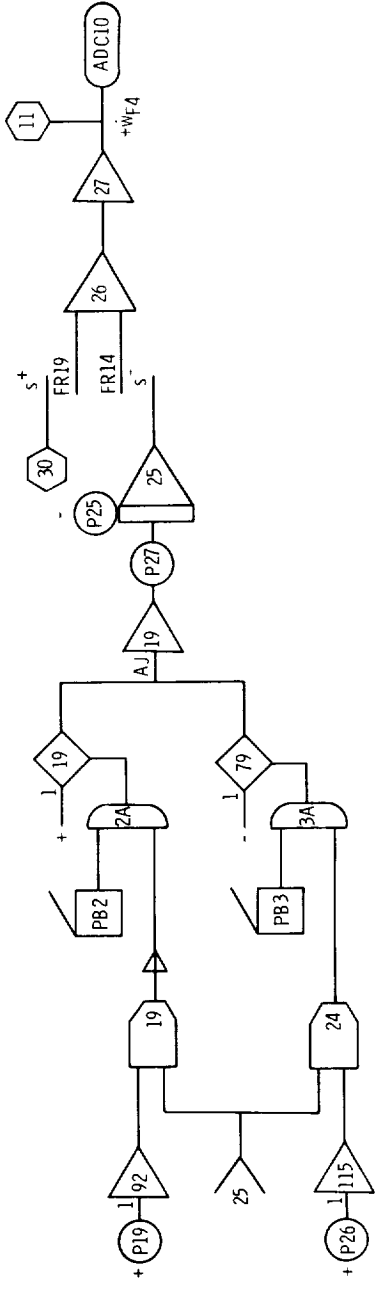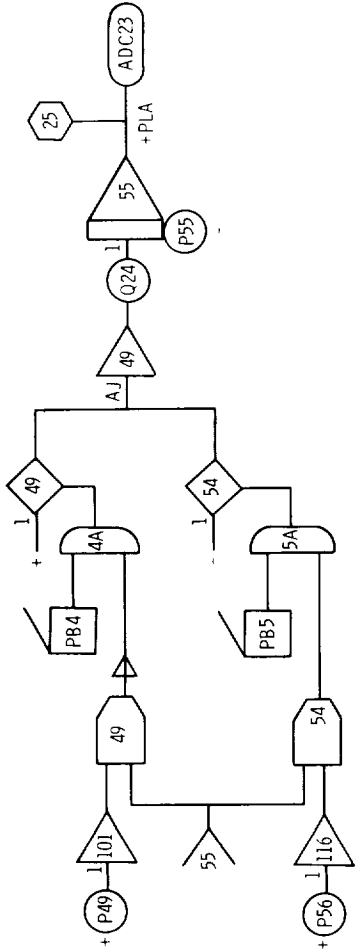
86

Figure 17. – Comparison of hybrid and baseline digital frequency responses of core augmentor inlet pressure to fuel flow oscillations. Sea-level, standard-day, static conditions; power lever angle, 50°.
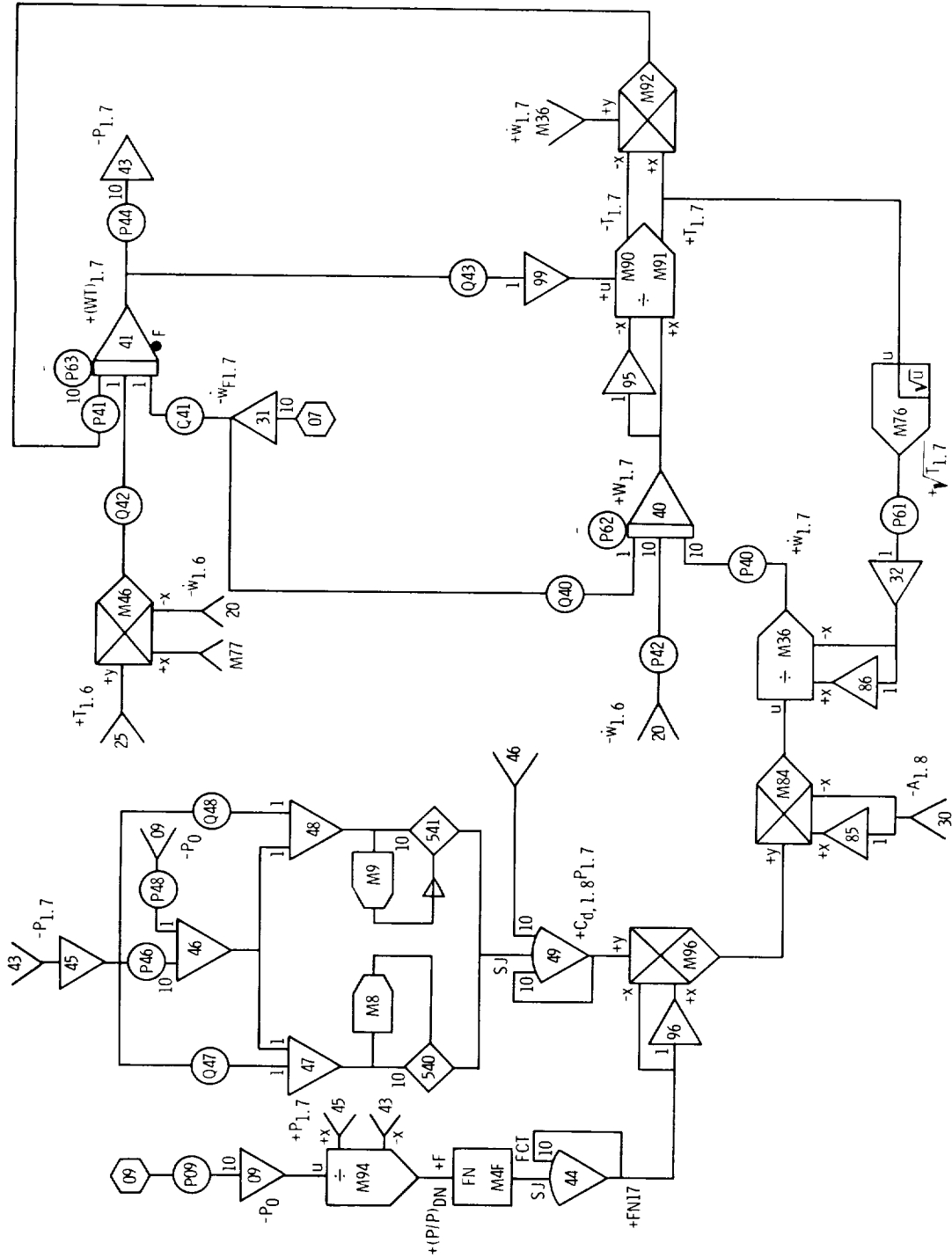
Figure 18. - Patching diagrams for EAI 680 Analog Computer.

(a) Fan interface.

(b) Low-pressure compressor.

Figure 18. - Continued.

89

(c) High-pressure-compressor interface.

Figure 18. - Continued.

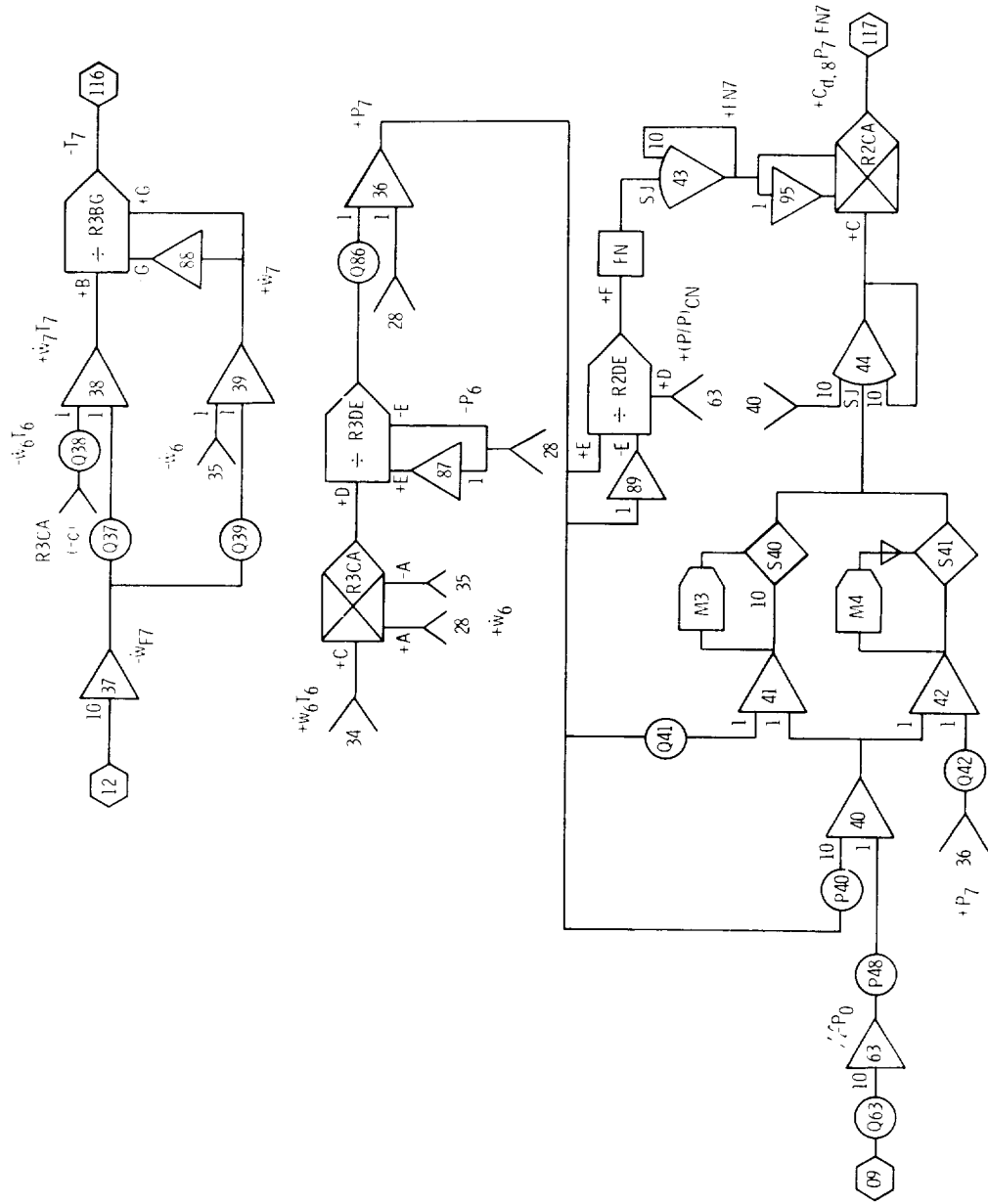(d) Power-lever-angle - fuel-flow-ramp generators.

Figure 18. – Continued.

(e) Control outputs.

Figure 18. - Concluded.

92

Figure 19. – Patching diagrams for EAI 231-4 Analog Computer.

(a) Duct inlet.

93

(b) Duct exit.

Figure l9. - Continued.

94

(c) Duct augmentor.

Figure 19. - Continued.

95
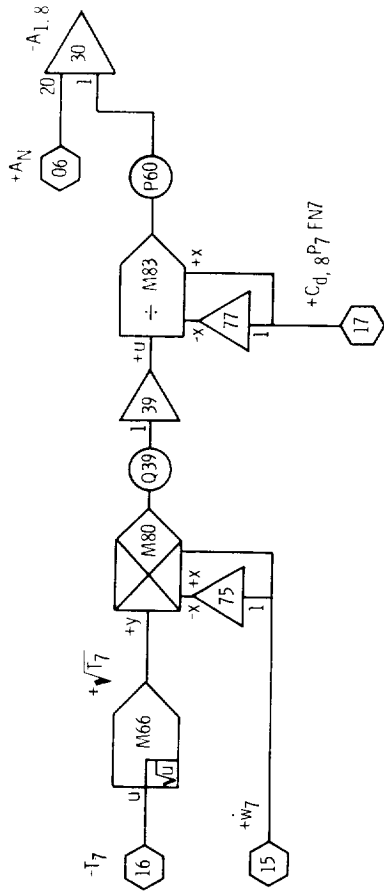
(d) Duct nozzle area.

Figure 19. – Concluded.

96

Figure 20. - Patching diagrams for EAI 231-5 Analog Computer.

(a) Combustor.

97

(b) High-pressure turbine.

Figure 20. - Continued.

(c) Low-pressure turbine.

Figure 20. - Continued.

99

(d) Core augmentor and nozzle.

Figure 20. - Continued.

100

(e) Rotor dynamics.

Figure 20. - Concluded.